

TOPICAL REVIEW

Recoil-ion momentum spectroscopy

J Ullrich^{†§}, R Moshhammer[‡], R Dörner[‡], O Jagutzki[‡], V Mergel[‡],
H Schmidt-Böcking[‡] and L Spielberger[‡]

[†] Gesellschaft für Schwerionenforschung mbH, Planckstraße 1, D-64291 Darmstadt, Germany

[‡] Institut für Kernphysik, Universität Frankfurt, August-Euler Straße 6, D-60486 Frankfurt, Germany

Received 10 February 1997

Abstract. High-resolution recoil-ion momentum spectroscopy (RIMS) is a novel technique to determine the charge state and the complete final momentum vector \mathbf{P}_R of a recoiling target ion emerging from an ionizing collision of an atom with any kind of radiation. It offers a unique combination of superior momentum resolution in all three spatial directions of $\Delta P_R = 0.07$ au with a large detection solid angle of $\Delta\Omega_R/4\pi \geq 98\%$. Recently, low-energy electron analysers based on rigorously new concepts and reaching similar specifications were successfully integrated into RIM spectrometers yielding so-called ‘reaction microscopes’.

Exploiting these techniques, a large variety of atomic reactions for ion, electron, photon and antiproton impact have been explored in unprecedented detail and completeness. Among them kinematically complete experiments on electron capture, single and double ionization in ion–atom collisions at projectile energies between 5 keV and 1.4 GeV have been carried out. Double photoionization of He has been investigated at energies E_γ close to the threshold ($E_\gamma = 80$ eV) up to $E_\gamma = 58$ keV. At $E_\gamma > 8$ keV the contributions to double ionization after photoabsorption and Compton scattering were separated kinematically for the first time. These and many other results will be reviewed in this paper. In addition, the experimental technique is described in some detail and emphasis is given to envisaging the rich future potential of the method in various fields of atomic collision physics with atoms, molecules and clusters.

1. Introduction

The investigation of the stationary structure of atoms or ions has traditionally been central to research activities in atomic physics over many decades up to the present day. Experimentally, precise information on the binding energies of electrons and, thus, on the atomic structure is obtained by measuring the discrete energy of one emerging photon or electron as well as by exciting one electron using advanced laser or maser techniques. Sophisticated high-resolution spectrometers have been developed and a profound theoretical understanding on the electronic, muonic or antiprotonic level structure has been achieved, including contributions due to relativistic, quantum electrodynamic, electroweak, nuclear-size or even quantum chromodynamic effects (see, for example, Kinoshita 1990, Mohr and Soff 1993, Stöhlker *et al* 1993, Werth 1987, Weitz *et al* 1994).

In contrast, one still faces basic problems in the experimental investigation as well as theoretical description of even the most fundamental dynamical situations in atomic scattering reactions like the single ionization of hydrogen or helium atoms by low-energy charged particle or antiparticle impact (see, for example, Ermolaev 1990, Toshima 1993,

§ Author to whom correspondence should be addressed. E-mail address: J.Ullrich@gsi.de

Knudsen *et al* 1995, Ovchinnikov and Macek 1995, Schultz *et al* 1996). Severe difficulties arise for reactions involving two active electrons such as for double ionization of helium in collisions with photons, ions or electrons (for a recent review see McGuire 1995). The *ab initio* quantum mechanical description of the correlated dynamics of true many-electron systems (more than two active electrons) as well as kinematically complete experiments for these reactions have been beyond present capabilities. In essence, so far such experiments have been restricted to photon and electron-impact ionization with not more than two electrons in the final continuum states; i.e. single ionization after electron impact (for a review see, e.g., Lahmam-Bennani (1991)) or double ionization as a result of the absorption of a photon (Schwarzkopf *et al* 1993, Huetz *et al* 1994, Lablanquie *et al* 1995, Dawber *et al* 1995).

The reason for the lack of experimental data is twofold. First, the momentum vectors of at least two reaction products have to be measured simultaneously in order to completely determine the kinematics of the simplest three-particle reactions (single ionization of hydrogen by charged-particle impact or double photoionization of helium). Secondly, these particles are usually emitted into a broad continuum of final momenta corresponding to energies ranging from meV to more than keV. Thus, for example, traditional electron spectrometers, optimized to determine discrete energies of Auger electrons with high resolution but small detection solid angle are badly adapted to the situation in an atomic scattering experiment. If two electrons are to be detected, two conventional spectrometers are needed with a typical product solid angle of $\Delta\Omega_{ee}/4\pi \approx 10^{-4}$ – 10^{-7} . Therefore, systematic studies scanning all relative emission angles and energies are very time consuming and investigations have been limited to processes where the cross sections are not ‘too small’. The simultaneous detection of three electrons yields extremely small coincidence rates and only two pioneering experiments for favourable kinematics have been reported in the literature to the best of our knowledge (see, e.g., Lahmam-Bennani *et al* 1989).

For ion impact another problem arises. Since the final momenta of all reaction products in an ion–atom collision (electrons, photons, recoiling target ion) are typically small, on the order of a few atomic units and below (1 au is the momentum of a 13.6 eV electron), the relative momentum change of the fast projectile $\Delta P_P/P_P$ is usually undetectably tiny, ranging between $10^{-9} \leq \Delta P_P/P_P \leq 10^{-4}$. Only a few ion-beam facilities (Park 1978) or storage rings (Bosch 1993) provide beams with a momentum spread as small as $\Delta P_P/P_P \approx 10^{-5}$. Thus, the best techniques developed to measure the energy loss or gain as well as the angular scattering of the ionic projectiles are limited to this level of precision. Up to now, such an accuracy has only been achieved (at very small solid angle $\Delta\Omega_P/4\pi \approx 10^{-4}$) for slow collisions with proton projectiles at energies below 400 keV (Park 1978, Htwe *et al* 1994, see also, e.g., Mann *et al* 1982, Cederquist *et al* 1989, Roncin *et al* 1991, Lebius and Huber 1992). Consequently, no kinematically complete experiment on single ionization in an ion–atom collision has been performed until the advent of recoil-ion momentum spectroscopy.

Recoil-ion momentum spectroscopy (RIMS) has been developed over more than a decade in order to overcome these basic experimental problems on a principle level and to provide an efficient and precise experimental tool to explore the correlated dynamics of collision-induced atomic many-particle reactions. Apart from early measurements (see, e.g., Federenko and Afrosimov 1956, Everhart and Kessel 1965, Kessel and Everhart 1966, McConkey *et al* 1972) the recoiling target ion momentum has practically not been accessed by the experimentalists for a long time, the reason being the extremely small energies transferred to the target nucleus during most of the atomic reactions for charged particle or

photon impact (Puckett and Martin 1976). Due to the large mass of the nucleus compared with the electron mass recoil energies, E_R are typically well below 1 eV ranging into the μeV and even sub- μeV regime for a majority of atomic reactions. In the late 1980s a few groups reported successful attempts to detect such ions and obtained information on their mean energies (Levin *et al* 1987, Olson *et al* 1987, Grandin *et al* 1988). At the same time Ullrich and Schmidt-Böcking in Frankfurt were the first to actually measure the recoil-ion momenta (Ullrich 1987, Ullrich and Schmidt-Böcking 1987, Ullrich *et al* 1988b) using static, spatially extended targets at room temperature with a resolution limited by the thermal motion at 300 K ($\Delta E_R \approx 40$ meV). Later, in an improved version, a static 30 K target was developed with $\Delta E_R \approx 4$ meV (Dörner *et al* 1989, Ullrich *et al* 1991). Recoil-ion momenta transverse to the incoming projectile momentum were measurable with these concepts, where the ions drifted in a field-free environment and solid angles of up to a few per cent of 4π were obtained. By exploiting inverse kinematics, scattering angles of heavy projectiles in the μrad regime became indirectly accessible and first experimental investigations of transverse momentum exchanges for ionization, electron capture and transfer ionization reactions were performed (Ullrich *et al* 1988a, b, 1989, 1993a, Olson *et al* 1987, 1989b, Dörner *et al* 1989, 1991, 1993, Forberich *et al* 1991, Gensmantel *et al* 1992, Lencinas *et al* 1993).

Rapid progress was initialized by implementing localized gas-jet targets in connection with ion-projection techniques. Recoil ions created in the interaction volume between the localized gas target and the ion beam were extracted by an electrostatic field and projected onto position-sensitive detectors (Ali *et al* 1992, Frohne *et al* 1993, 1996, Jardin *et al* 1993, Jagutzki 1995). By measuring the times of flight and the impact positions of the ions on the detector, their trajectories can be reconstructed in an unambiguous way and the complete initial momentum vectors can be calculated. A tremendous increase in solid angle to values of nearly 100% of 4π was realized using this concept and a similar resolution to that of cooled static targets was obtained using ‘warm’ effusive jets. Internally cold supersonic atomic jets paved the way to a dramatic increase in momentum resolution corresponding to energy resolutions far below 1 meV (Jardin *et al* 1993, 1996, Jagutzki 1995). Precooling of the target gas before the supersonic expansion pushed the resolution to $\Delta E_R \approx \pm 30$ μeV for helium ions and was termed cold-target recoil-ion momentum spectroscopy (COLTRIMS) (Mergel 1994, Mergel *et al* 1995a, Ullrich *et al* 1994a). Using a focusing geometry and electrostatic extraction fields (for details see the next section) the development recently culminated in a superior resolution of $\Delta E_R \approx \pm 1.2$ μeV for He^+ ions with a solid angle of 4π for the detection of momenta below 5 au (Mergel *et al* 1995b, Mergel 1996, Dörner *et al* 1995b). At a larger momentum acceptance of up to 160 au and an energy resolution of ± 7 μeV was reported (Moshhammer *et al* 1994).

With these spectrometers for the first time the complete momentum vector of one reaction product, the target ion, emerging from an atomic collision was measurable with a resolution of a few per cent of an atomic unit and a solid angle of nearly 100% of 4π . Experiments became feasible where contributions to the projectile ionization due to the electron–nucleus or electron–electron interaction were kinematically separated (Dörner *et al* 1994, Wu *et al* 1994a). State-selective scattering-angle-dependent studies of single- and double-electron capture into different shells of the projectile at medium velocities were performed (Mergel 1994, Mergel *et al* 1995a, b, Wu *et al* 1994a, b, 1995, Kambara *et al* 1995, Abdallah *et al* 1997, Cassimi *et al* 1996). ‘Transfer ionization’ in proton–helium collisions (one helium electron is captured by the projectile and the other one is emitted) was investigated in kinematically complete experiments (Mergel *et al* 1995c, Mergel 1997). The contributions of photoabsorption and Compton scattering to He double ionization at high photon energies became separable (Spielberger *et al* 1995, 1996).

The latest and most important improvement of the instruments was marked by the combination of a high-resolution recoil-ion momentum spectrometer with a novel low-energy electron analyser where the basic principles of recoil-ion detection were now applied in addition to the electrons: they were efficiently projected onto a position-sensitive detector by a combination of electrostatic and solenoidal magnetic fields (Moshhammer *et al* 1994, 1996b, c, Ullrich *et al* 1995). In the most recent arrangements the complete momentum vectors of up to three electrons with energies below 50 eV can be determined simultaneously (in addition to the recoil ion) using three independent electron detectors (Kollmus *et al* 1996, Ullrich *et al* 1996). A momentum resolution for the electrons of $\Delta P_e \approx \pm 0.01$ au has been achieved corresponding to an electron energy resolution at zero electron energy of $\Delta E_e \approx \pm 5$ meV. Using these or similar ‘reaction microscopes’ kinematically complete experiments have been performed for single and double ionization of helium after ion impact (Moshhammer *et al* 1994, 1996a, b, 1997a, Dörner *et al* 1996a) as well as for He double photoionization close to the threshold (Dörner *et al* 1996c, d).

This review deals with ‘recoil-ion momentum spectroscopy’ as far as (pre-cooled) supersonic jet targets were used and RIMS was combined with the spectroscopy of electrons, since these techniques benchmark the decisive breakthrough compared with earlier methods. Previous results using static or effusive targets have been summarized by Ullrich (1994) and have been partly reviewed by Cocke and Olson (1991). After an outline of the general concepts of RIMS and some technical details in section 2 a short introduction into the kinematics of recoil-ion production with illustrating examples is given in section 3. The main emphasis is put on section 4 providing an extended overview on the manifold results on collision-induced atomic reactions achieved with RIMS for ion, photon and electron impact. A limited level of detail had to be accepted in order to cover the broad scope of different processes investigated up to now. This is followed by a short summary of the current state of the field in section 5.

2. Experimental technique

The experimental part concentrates on reviewing high-resolution RIM spectrometers, i.e. devices based on (pre-cooled) supersonic jet targets. Technical information on the various former concepts are found for warm static targets in Ullrich (1987), Ullrich *et al* (1987, 1988b), for effusive targets in Levin *et al* (1987), Grandin *et al* (1988), for cooled static targets in Ullrich *et al* (1991), Ullrich (1994), Dörner *et al* (1991) and for effusive gas jet targets in Ali *et al* (1992), Frohne *et al* (1993, 1996), Wu *et al* (1994a, b, 1995) (see also the reviews by Cocke and Olson (1991) and Ullrich (1994)).

2.1. General concept

High-resolution recoil-ion momentum spectrometers as well as ‘reaction microscopes’ (coincident with electrons) are both based on well localized inherently cold atomic targets ensuring a ‘perfect’ preparation of the initial target momentum. Providing a cold target is essential for the recoil-ion momentum resolution, since the momenta to be measured are of the order of or even below the typical thermal momentum spread of atoms at room temperature. In all existing devices (at the University of Frankfurt; CIRIL, Caen; GSI, Darmstadt; Kansas State University, Manhattan, KS; RIKEN, Wako, Saitama; LBNL, Berkeley, CA; University of Missouri, Rolla, MO), these targets are realized by supersonic expansion forming a cold atomic beam which is crossed by any projectile beam in the presence of well defined electrostatic and, in some designs, magnetic fields.

In this way, ions (and electrons or ionic fragments) created during the collision are guided efficiently onto position-sensitive detectors and large detection solid angles are achieved. From the final positions and their times of flight (TOF) in the apparatus, the trajectories of ions (and electrons) are reconstructed and their initial momenta are calculated.

2.2. Recoil-ion spectrometers based on supersonic jet targets

2.2.1. Supersonic expansion. In these spectrometers a well localized atomic or molecular (Moshhammer *et al* 1996c) target is generated exploiting the features of quasistatic adiabatic (i.e. isentropic) supersonic expansion of the target gas. For monoatomic ideal gases the free enthalpy H of $\frac{5}{2}kT_0$ (k is the Boltzmann constant and T_0 the temperature) can be converted into directed kinetic energy (Buchenau *et al* 1990). After the expansion, atoms of mass M_R move in a jet with a momentum of $P_{\text{jet}} = (5kT_0M_R)^{1/2}$ which is about 5.9 au for helium at $T_0 = 300$ K ($E_{\text{jet}} = 64$ meV) and 1.9 au at $T_0 = 30$ K. In practice, the actual quality of the jet is expressed by its speed ratio $S = (5T_0/2T)^{1/2}$ where T is the leftover internal jet temperature after the expansion, which approaches zero in the ideal case. In the various RIM spectrometers the gas expands through a small nozzle (typical diameters 5–75 μm) at pressures prior to the expansion of between 0.2 and 30 bar and temperatures of the gas reservoir between 14 and 300 K. The quality of the jet, its inherent temperature, depends strongly on the expansion parameters and different values might be ideal for different experimental situations and targets. The optimum momentum resolution is achieved by pre-cooling the gas and simultaneously using high pressures before the expansion. Depending on the gas to be used the ultimate limit is reached if the gas starts to form dimers, trimers or clusters during expansion (various groups plan to investigate reactions with cluster targets in the near future). The expanding gas is then skimmed in one (Mergel 1994, 1997, Moshhammer *et al* 1994, 1996c, Jagutzki 1995), two (Jardin *et al* 1993, 1996, Moshhammer 1996a, d) or even four stages (Schmidt *et al* 1997) in order to form a well defined atomic beam and to guarantee good vacuum conditions in the interaction chamber.

For example, the COLTRIMS set-up developed by Mergel (1994), presently providing the best momentum resolution, is shown in figure 1. Here, the rare gas (He, Ne, Ar, etc) is pre-cooled to a temperature of approximately 15 K (for He) at a pressure between 200 and 1000 mbar using a cryogenic cold head. The gas then expands through a 30 μm hole forming a supersonic jet. The inner jet fraction passes through a 0.3 mm skimmer into the scattering chamber, yielding an atomic beam with a diameter of about 1 mm at the intersection point with the projectile beam. The internal momentum spread of the target in the direction of the gas jet is determined by the parameters of the expansion and is typically below ± 0.05 au. In the direction transverse to the jet expansion an even smaller momentum spread of between ± 0.015 and ± 0.035 au is achieved by skimming of the atomic beam. The momentum resolutions finally obtained in the two directions transverse to the jet expansion (x -, y -directions) depend on the x -, y -extensions of the interaction volume (the interaction volume will be defined as the geometrical overlap volume between the atomic and the projectile beams with a line density of typically up to 10^{12} atoms/cm²; for details see Moshhammer *et al* (1996c)). Using brilliant photon beams from third-generation light sources with diameters as small as 50 μm extremely small x -, y -extensions are realized and momentum resolutions of the order of $\pm 10^{-3}$ au have been estimated (Ullrich *et al* 1996) in the direction transverse to the expansion.

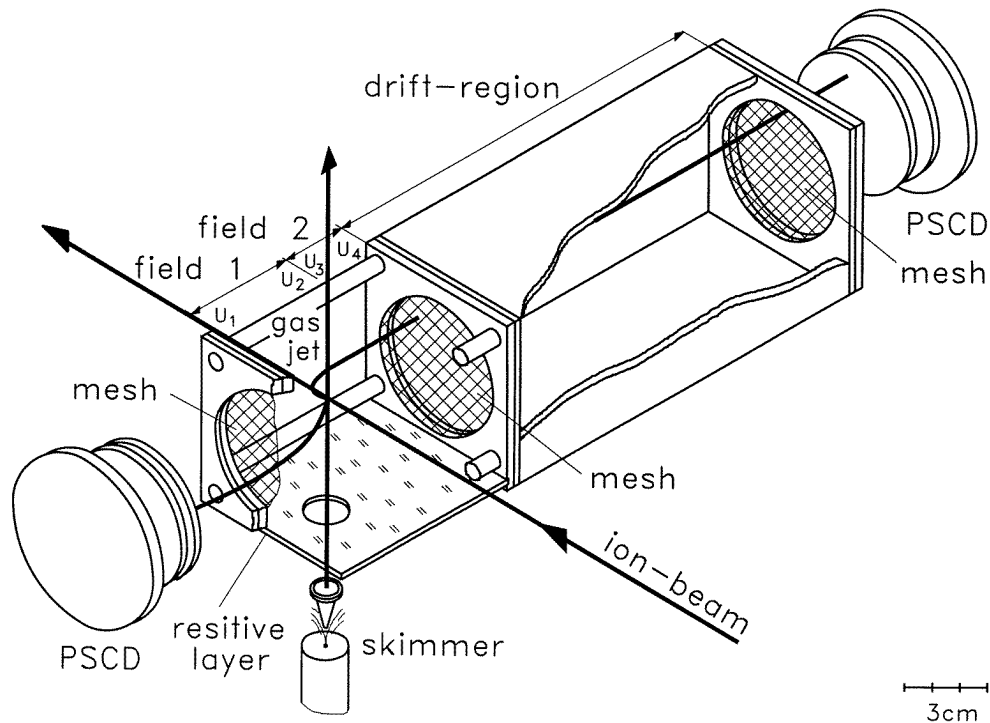


Figure 1. Recoil-ion momentum spectrometer developed by Mergel (1997) (see also Mergel *et al* 1995a). The gas nozzle is cooled to 15–30 K, the supersonic gas jet has a diameter of 1.1 mm at the intersection with the projectile beam. The extraction field is homogeneously divided down by a resistor chain between U_1 and U_2 (field 1) as well as between U_3 and U_4 (field 2). A step in the potential between U_2 and U_3 generates a simple electrostatic lens focusing all ions with identical momenta but different starting positions in the plane defined by the ion and atomic beam directions to the same position on the detector. The geometry has been optimized such that different starting positions of ions with identical momenta along the extraction field lead to the same time of flight on the ion detector ('three-dimensional focusing'). The electron detector is located on the left-hand side (PSCD: position sensitive channel plate detector).

2.2.2. Extraction of the recoil ions. The atomic beam is intersected by a projectile beam and target ions are produced in different atomic reactions. Depending on the actual reaction under investigation an appropriate electrostatic field is applied at the interaction region (see figure 1) such that all recoil ions with the momenta of interest are projected onto a multichannel-plate (MCP) detector with a two-dimensional position-sensitive (2DPS) readout (Martin *et al* 1981). Different methods of creating precisely controlled electrostatic extraction fields have been described in the literature. Initially, homogeneous fields transverse to the projectile beam were used (Jagutzki 1995, Jardin *et al* 1993), carefully shielded from external potentials. Mergel *et al* (1995a) wound a 10 m long $7 \mu\text{m}$ diameter carbon fibre around four supporting germanium-coated isolator screws homogeneously dividing the extraction voltage to ground potential according to the electrostatic resistance of the fibre. Recently, non-homogeneous, lens-like extraction fields E_{ex} have been developed. They guide ions which emerge with identical momenta from different positions in the two-dimensional plane transverse to the extraction field within the interaction volume to the same position on the channel plate (Cocke 1994). Thus, the momentum resolution in the

two dimensions perpendicular to the extraction is no longer restricted by the uncertainty of the starting positions. In all spectrometers a drift region follows the extraction field (see figure 1). Its length is adapted to the length and form of E_{ex} in such a way that the ions created at different positions along the field within the interaction volume focus to first order in time of flight at the detector. Combining both concepts, spectrometers which focus in all three spatial dimensions have become feasible (Mergel 1997) and the momentum uncertainty due to the finite size of the interaction volume becomes negligibly small.

In another set-up the ions are likewise extracted into the longitudinal direction (along the projectile beam) generating the extraction field between two ceramic plates (see figure 2). Each ceramic is plated with two burned-in resistive layers of different resistances in such a way that any direction of the electrostatic field vector can be generated (in the transverse or longitudinal or any other direction; details are given in Moshammer *et al* (1996c)). Voltages can be applied such that position-focusing electrostatic fields are generated for the transverse momentum components. The longitudinal momentum component containing the most important information for ion impact (the inelasticity, see section 3) is time focused. This concept is extremely versatile and turned out to be essential for the combination of a RIM spectrometer with the magnetic large solid angle electron spectrometer (see the next section). In addition, the dimensions of this spectrometer are about twice as large as in other set-ups resulting in a factor of 30 increased dynamic range in the direction of the

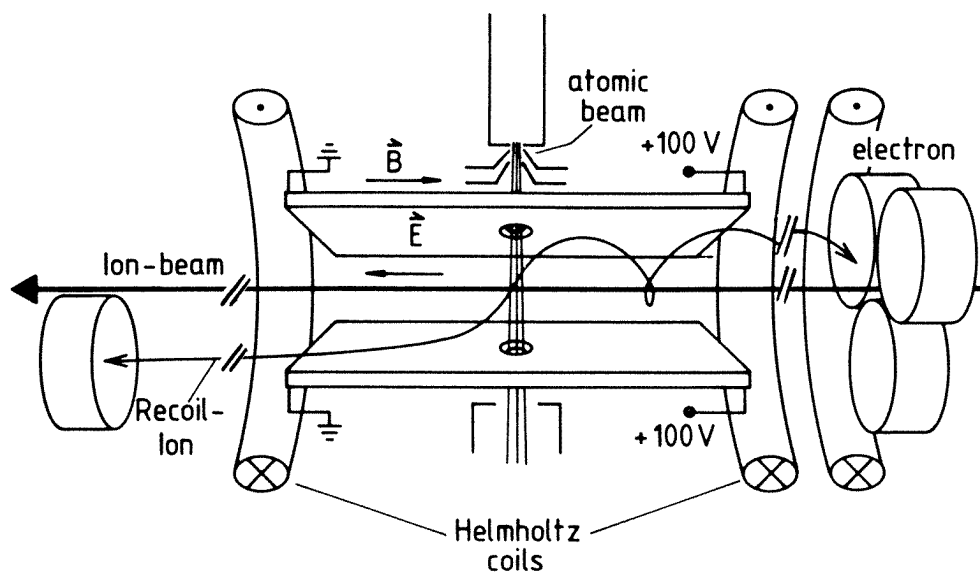


Figure 2. ‘Reaction microscope’ developed by Ullrich *et al* (1995) and Moshammer *et al* (1996c) (see also Kollmus *et al* 1997). The two-stage supersonic gas jet can be cooled before expansion and has a diameter of 2.2 mm at the intersection with the projectile beam. Ions and electrons can be extracted in any direction (see text) and longitudinal extraction is illustrated in the figure. Three (in some set-ups two) 1.5 m diameter Helmholtz coils generate a homogeneous magnetic field of up to 100 G with its field vector approximately parallel to the electric field and the projectile propagation. The recoil-ion detector as well as the three independent electron detectors are positioned in a time-focusing geometry. In this way uncertainties in the measurement of the longitudinal momenta of ions and electrons resulting from the unknown starting position within the interaction volume, as defined in the text, can be eliminated to first order.

extraction (recoil-ion longitudinal momenta of up to $P_{R\parallel} \leq 150$ au are accepted) at very good momentum resolution in all directions of $\Delta P_R \approx \pm 0.05$ au. This instrument, designed to be implemented in storage rings, was the first one without potential grids separating the acceleration from the drift region. In this way, defocusing small-size variations of the electrostatic field at the meshes of the grid are avoided.

The suitable direction of extraction (transverse or longitudinal) is determined by the details of the reaction to be investigated, the recoil-ion momenta to be expected and the resolution required in the different momentum components. As a general rule extraction should be along the symmetry axis of the collision, i.e. in the longitudinal direction for charged particle impact (axial symmetry along the beam direction) and in the transverse direction for linearly polarized photon impact (symmetry along the polarization direction transverse to the photon beam).

2.3. Coincidences with scattered projectiles

A series of experiments have been reported where the transverse momentum change of the projectile was measured in coincidence with the transverse momentum of the recoil ion using RIM spectrometers with static, pre-cooled gas cells (Dörner *et al* 1989, Forberich *et al* 1991, Gensmantel *et al* 1992, Lencinas *et al* 1993). In this way important information on the transverse many-particle momentum balance for single and multiple ionization was obtained. Only one such coincidence experiment has been performed up to now using a high-resolution spectrometer with a supersonic gas jet to investigate transfer ionization (Mergel *et al* 1995c, d, Mergel 1997). Since five momentum components were accessible experimentally, the full final momentum vector of the emitted electron could be calculated by exploiting conservation laws (see the next section) and kinematically the reaction was completely determined. Typical resolutions reached in the projectile deflection angle ϑ_p are around 0.1 mrad, the best values achievable might be a factor of 10 better. Due to the large incoming longitudinal momentum of the projectile $P_p = M_p v_p$ (M_p, v_p are the projectile mass and velocity, respectively) a sufficient absolute transverse momentum resolution $\Delta P_{p\perp} = \Delta \vartheta_p P_p \leq 1$ au can only be obtained at small v_p , restricting the regime where this technique is reasonably applicable to velocities below 1 MeV u^{-1} and to light projectiles.

2.4. Coincidences with emitted electrons: ‘reaction microscopes’

The particular strengths of RIMS, the open geometry of most spectrometers and the large recoil-ion detection solid angle makes this technique ideally suited to performing coincidences with other reaction products, i.e. electrons or photons. The invention of an extremely efficient and precise new method for the detection of electrons with energies $E_e < 1$ keV and its successful implementation into high-resolution RIM spectrometers (Moshhammer *et al* 1994) has led to a decisive extension of the applicability and future potential of RIMS. These instruments, which have been termed ‘reaction microscopes’ open completely new windows to explore atomic many-particle reactions and therefore shall be reviewed in some detail.

In the most recent set-up described by Kollmus *et al* (1997) (figure 2) longitudinal extraction of the recoil ions in the backward direction was applied with a total extraction voltage of up to +100 V. Thus, all electrons with longitudinal backwards energies of $E_{e\parallel} \leq 50$ eV (potential at the point of interaction of +50 V) were accelerated downstream hitting one out of three 2DPS microchannel plates. The detectors were placed in the forward

direction in the time-focusing geometry at a total flight path of 33 cm (using the same principle as described above for the ions). By applying a weak solenoidal magnetic field (12 G) with its axis approximately along the beam axis all electrons with non-zero transverse energies $E_{e\perp}$ were forced onto spiral trajectories and projected onto the detectors with a 4π solid angle for $E_{e\perp} \leq 50$ eV. The electron longitudinal momenta were obtained from the times of flight (TOF), measured in coincidence between each of the electrons, the projectile and the recoil ion. The position contains information on the transverse momentum and on the azimuthal emission angle. Thus, the complete momentum vectors of up to three electrons has been determined simultaneously and a solid angle close to 4π was reached for all electrons with $E_e \leq 50$ eV. By applying larger magnetic fields of up to 100 G (Kollmus *et al* 1997) electrons with $E_{e\parallel}, E_{e\perp} \leq 1$ keV can be projected onto the detectors. The energy resolution of the most recent apparatus has been discussed by Kollmus and a resolution of $\Delta E_e = \pm 1.4$ meV corresponding to a momentum resolution of $\Delta P_e = \pm 1 \times 10^{-2}$ au for low-energy electrons ($E_e \leq 5$ eV) has been estimated. Very recently, it has been reported (Ullrich *et al* 1996) that one of the detectors was equipped with a fast position-sensitive delay-line readout (Sobottka and Williams 1988, Nüttgens 1994) and the signals were recorded using a multi-hit time-to-amplitude converter (TDC). Electronically, up to 16 electrons emerging from one single collision can be accepted using this technique and for each of them the complete momentum vector can be calculated.

It has been emphasized by Kollmus *et al* (1997) that unprecedented values for the electron momentum resolution are achievable in such spectrometers for low-energy electrons. Due to the smaller mass of the electrons their initial-state momentum uncertainty resulting from the internal temperature of the supersonic jet is only 7×10^{-6} au ($\Delta E_e = 6 \times 10^{-10}$ eV). The focusing geometry and extraction fields can and have been used to minimize the uncertainty due to the finite interaction volume and realistic resolutions as small as 10^{-4} au or energy resolutions below $1 \mu\text{eV}$ have been envisaged.

Another concept, well adapted to detecting low-energy electrons ($E_e < 10$ eV) in combination with high-resolution RIMS was used by Dörner *et al* (1996a, d) placing a position-sensitive detector for the emitted electrons in the direct vicinity of the interaction volume opposite to the recoil-ion detector (figure 1). Without a magnetic field a 4π detection solid angle has been achieved only for electrons with momenta transverse to the extraction field below 0.9 au. In one of the experiments (Dörner *et al* 1996a) no resolution has been obtained along the direction of the electrostatic field due to the missing explicit time-of-flight measurement for the electrons (recoil-ion–electron coincidence). Assuming a constant TOF for all the low-energy electrons in the short distance between the interaction volume and the detector a 6% momentum resolution has been reported for electrons with momenta along the extraction field below 0.1 au. Performing a recoil-ion–electron-pulse coincidence in experiments on double photoionization all three electron momentum components have been determined with this spectrometer (Dörner *et al* 1996d).

3. Kinematics

In this section a short summary on the kinematics of the recoiling target ion and the information which is contained in the recoil momentum will be given which is helpful for the interpretation and understanding of the experimental results reviewed in section 4. Details can be found in previous publications (Ullrich *et al* 1988b, Schmidt-Böcking *et al* 1990, Mergel 1994, 1997, Rodríguez *et al* 1995a, see also Fastrup 1980). Since recoil-ion momentum spectroscopy has mainly been used in fast ion–atom collisions, emphasis is given to this specific subject. Throughout this paper atomic units are used where the

electron mass m_e , the electron charge e and Planck's constant \hbar are taken to be equal to unity ($m_e = e = \hbar = 1$).

3.1. Distant ion–atom collisions

For the overwhelming part of all atomic reactions in ion–atom collisions little momentum, energy and mass compared to the initial momentum (P_p), energy (E_p) and mass (M_p) of the incoming projectile are transferred during the encounter. This is true even for small projectile masses (protons, and in many cases, even for electrons) as well as for comparably violent collisions where the target atom is multiply ionized in an encounter with a highly charged ion. Also, the momenta of emitted photons are typically small and can be neglected in the present discussion. Under these conditions the longitudinal and transverse momentum balances are decoupled (Ullrich *et al* 1988b), contain different information on the collision and can be calculated separately on the basis of non-relativistic energy and momentum conservation (relativistic recoil-ion kinematics was discussed by Mergel 1997).

3.1.1. Transverse momentum balance. In the transverse direction one obtains for the final momenta of the recoil-ion ($\mathbf{P}_{R\perp}$), the projectile ($\mathbf{P}_{p\perp}$) and the electrons ($\sum \mathbf{P}_{e\perp}^i$) in the laboratory frame (bold denotes vectors):

$$\mathbf{P}_{R\perp} = -(\mathbf{P}_{p\perp} + \sum \mathbf{P}_{e\perp}^i). \quad (1)$$

The length of the vector $\mathbf{P}_{R\perp}$ (for all vectors the convention $P_\perp = |\mathbf{P}_\perp|$ is used) is given by

$$P_{R\perp} = \sqrt{(P_{p\perp})^2 + (\sum P_{e\perp}^i)^2 - 2P_{p\perp} \sum P_{e\perp}^i \cos \varphi} \quad (1a)$$

where φ is the angle between the vectors of the projectile momentum and the electron sum-momentum in the plane perpendicular to the beam. For reactions with no electrons in the continuum (pure electron capture) or those where $\sum P_{e\perp}^i$ is small compared with the heavy particle momenta (i.e. at small impact parameters or for collisions at small projectile energies), one obtains $P_{R\perp} \approx P_{p\perp}$. In this case the transverse recoil-ion momentum results from the repulsive inter-nuclear scattering and an impact parameter can be calculated for a given deflection potential (Ullrich *et al* 1988a, 1989, Gensmantel *et al* 1992, Dörner *et al* 1996a). For ionization reactions at medium and high projectile velocities the transverse momenta of all reaction products are usually of the same order of magnitude so that full many-body momentum exchange has to be considered.

Recently, the full recoil-ion and electron momentum vectors were measured in coincidence for single ionization of He in collisions with $3.6 \text{ MeV u}^{-1} \text{ Se}^{28+}$ (Moshhammer *et al* 1994, 1996a, 1997a). In this way projectile scattering angles $\vartheta_p = P_{p\perp}/P_p$ of $0.12 \mu\text{rad}$ were indirectly resolved ($\mathbf{P}_{p\perp} = -\mathbf{P}_{R\perp} - \mathbf{P}_{e\perp}$), i.e. projectile deflections of 1.2 mm on a distance of 10 km became observable. In another experiment (Mergel *et al* 1995d) at lower projectile energies (0.2–0.4 MeV p on He) the proton transverse deflection (two momentum components) was measured directly in coincidence with \mathbf{P}_R (three momentum components) for transfer ionization (one target electron is captured and the other is emitted). A resolution of $\Delta P_{p\perp}/P_p = \pm 7 \times 10^{-5}$ was achieved and the electron momentum vector was completely determined (for the transverse direction via $\mathbf{P}_{e\perp} = -(\mathbf{P}_{R\perp} - \mathbf{P}_{p\perp})$ with a resolution of $\Delta P_{e\perp} \approx \pm 0.5 \text{ au}$).

3.1.2. *Longitudinal momentum balance.* In the longitudinal direction one obtains

$$P_{R\parallel} = -\left(\Delta P_{P\parallel} + \sum_{i=1}^{n_P+n_T} P_{e\parallel}^i\right) \quad (2)$$

where

$$\Delta P_{P\parallel} = \Delta E_P/v_P = -Q/v_P + \frac{1}{2}(n_C n_P)v_P - \sum_{i=1}^{n_P+n_T} E_c^i/v_P \quad (2a)$$

denotes the momentum change of the projectile in the longitudinal direction which can be related to the energy change of the projectile ΔE_P at an initial velocity v_P . n_P, n_T and n_C are the numbers of electrons emitted from the projectile, the target and those transferred from the target to the projectile, respectively. Q denotes the change in internal energy of the projectile and the target, i.e. the energy difference between final and initial bound electronic states $Q = E_f^{\text{bind}} - E_i^{\text{bind}}$ (exothermic reactions yield negative Q -values). E_c^i is the continuum energy of the i th electron in the laboratory frame.

Thus, the energy balance of the collision is completely contained in the longitudinal momentum components and information on the Q -value of the reaction as well as on the mass transfer can be obtained by measuring these components alone.

3.1.3. *Examples.* For illustration, two examples for simple reactions are given below:

Electron transfer from the target to the projectile (electron capture). If there are no electrons in final continuum states equation (2a) reduces to

$$P_{R\parallel} = Q/v_P - \frac{1}{2}n_C v_P = -\Delta P_{P\parallel} \quad (3)$$

and the final longitudinal recoil-ion momentum directly reflects the Q -value of the reaction, i.e. the difference in the binding energies of the electrons in the initial and final state. In this way electron capture cross sections from He targets have been investigated as a function of the final state of the captured electron(s). Thus, state-selective cross sections have been accessible for the first time at large projectile velocities where traditional energy gain or loss techniques are hardly applicable (Ali *et al* 1992, Mergel *et al* 1995a). In addition, $P_{R\perp} = P_{P\perp}$ is fulfilled exactly since only two particles are in final continuum states and the projectile scattering is accessible with high accuracy. Also, it was discussed recently (Moshhammer *et al* 1996c) that precise energy gain measurements via inverse kinematics can be used to absolutely determine the 1s binding energy E^{1s} (or higher levels) of heavy one-electron ions from the measured recoil-ion longitudinal momentum, the well known beam velocity and the first ionization potential U^{He} of helium: $E^{1s} = U^{\text{He}} + v_P P_{R\parallel} + \frac{1}{2}v_P^2$.

Ionization of the target. For pure target ionization, in the longitudinal direction one obtains

$$P_{R\parallel} = Q/v_P + \sum E_c^i/v_P - \sum P_{e\parallel}^i. \quad (4)$$

The Q -value is given by the sum of the well known sequential ionization potentials of the emitted electrons U_i and the excitation energies of the remaining target (and projectile) electrons E_i^{exc} (if non-bare ionic projectiles are used). So, Q/v_P is fixed for a given beam velocity and final target (and projectile) excitation and the recoil-ion longitudinal momentum only depends on the energies and longitudinal momenta of the emitted electrons (for details see Rodríguez *et al* (1995a), Wang *et al* (1996a)). Thus, RIMS has been considered as an alternative ‘electron spectroscopy’ which is especially well suited to

investigating the emission of very low-energy electrons and is a unique tool to obtain information on the collective behaviour of ejected electrons in the case of multiple-target ionization. Both are extremely difficult to investigate using traditional techniques. For low-energy continuum electrons at large projectile velocities v_p , the first two terms on the right-hand side of equation (4) are small. Then, the recoil-ion longitudinal momentum distribution mirrors the sum-momentum distribution of the emitted electrons along the beam direction $P_{R\parallel} \approx -\sum P_{e\parallel}^i$. Moshhammer *et al* (1996a) have pointed out that equation (4) describes the longitudinal momentum balance for photoionization in the relativistic limit where v_p approaches the velocity of light $v_p \rightarrow c$. Neglecting the momentum of the

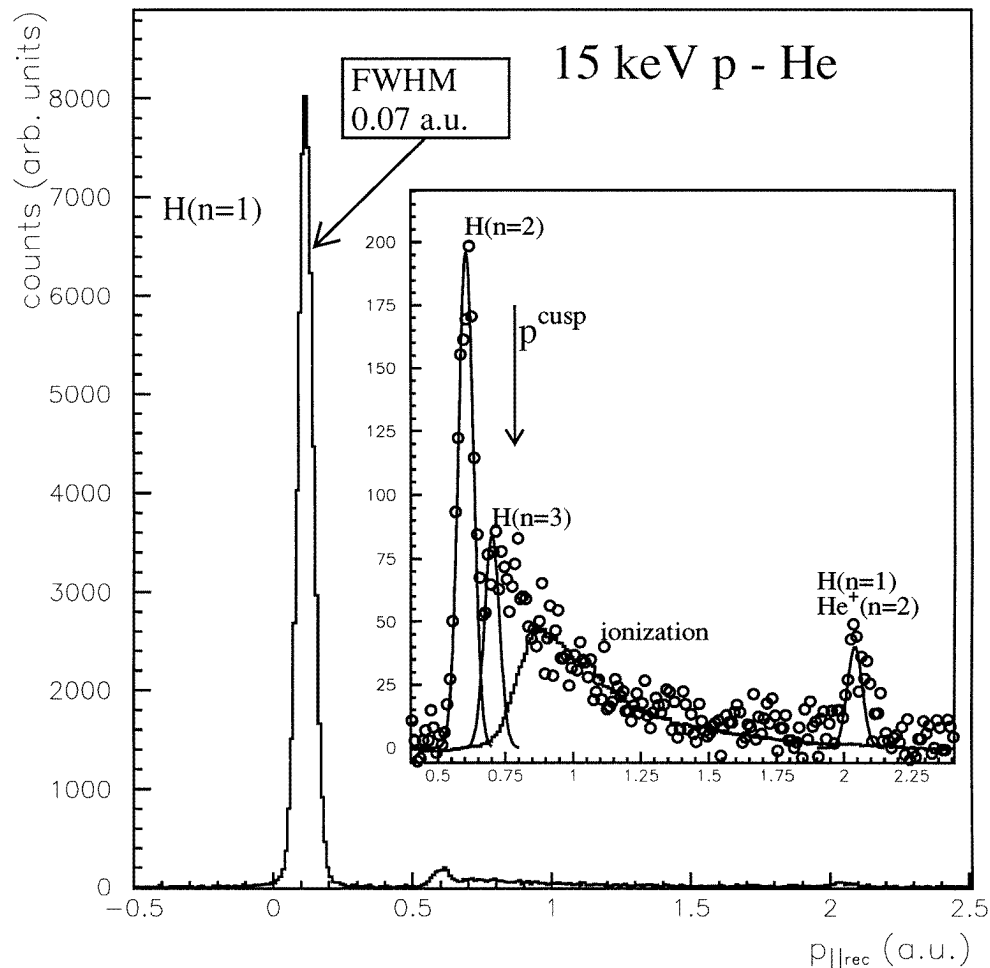


Figure 3. Longitudinal momentum distribution of He^+ ions from 15 keV proton impact (Dörner *et al* 1995b). The dominant peak is due to the capture to the projectile ground state. The arrow indicates the position of the capture to the projectile continuum. The full curve to the right of the arrow shows the momentum distribution for ionization only which has been measured separately by detecting an electron in coincidence with the recoil ion. The momentum resolution is ± 0.035 au, equivalent to a resolution in energy gain of ± 0.7 eV or in recoil-ion energy of ± 4.5 μeV .

photon ($p_\gamma = E_\gamma/c$, see the next section) the corresponding photon energy E_γ would be $E_\gamma = \sum (U_i + E_e^i + E_i^{\text{exc}})$.

Both reaction channels, electron capture as well as target ionization, can be observed simultaneously as demonstrated in figure 3 (taken from Dörner *et al* (1995b)), showing the $P_{R\parallel}$ distribution of He^+ ions created in collisions with 15 keV protons ($v_p = 0.77$ au). First, single-electron transfer into different final states of the proton is observed as sharp lines (the width being given by the experimental resolution of ± 0.035 au). They were resolved until $n = 2$ and unfolded until $n = 3$. The series limit for single-electron capture into the continuum (so-called cusp electrons) is reached at $P_{R\parallel} = U^{\text{He}}/v_p - v_p$ indicated in the figure as P^{cusp} . At the same time, this is the minimum $P_{R\parallel}$ reachable for single-target ionization. Thus, the broad continuous distribution on the right-hand side of P^{cusp} is due to He single ionization and reflects a mixture of the emitted electron continuum energy and longitudinal momentum distribution $P_{R\parallel} \propto E_e/v_p - P_{e\parallel}$. The additional line at $P_{R\parallel} = 2.06$ au is due to capture of one electron into the hydrogen ground state and simultaneous excitation of the remaining He electron to $n = 2$. A small contribution of ionization plus excitation of the target would result in a continuous distribution above 2.7 au.

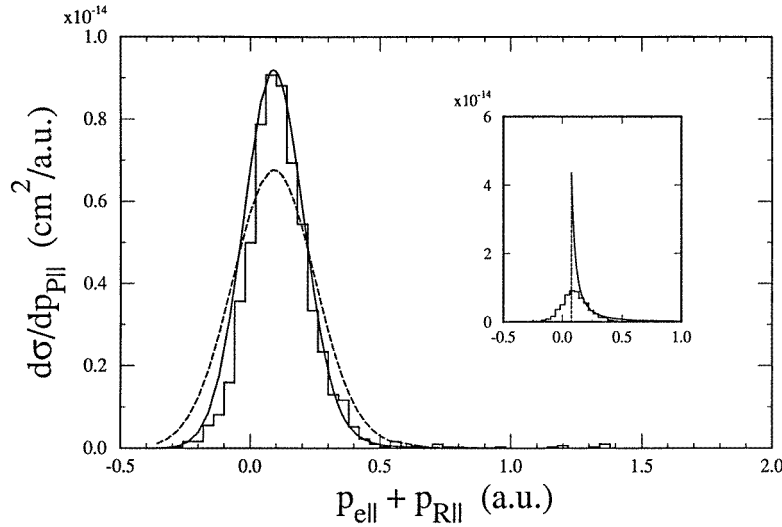


Figure 4. Measured (histogram, Moshammer *et al* (1994)) and calculated (curves, Rodríguez *et al* (1995b)) longitudinal sum-momentum distribution $P_{e\parallel} + P_{R\parallel} = -\Delta P_p$ for single ionization of He by $3.6 \text{ MeV u}^{-1} \text{ Ni}^{24+}$. Full (broken) curve, convolution of the theoretical CDW-EIS results (full curve in the inset) to a Gaussian distribution of width 0.22 au (0.16 au). See also the comparison with the unfolded theoretical results of CTMC calculations (figure 2 in Moshammer *et al* (1994)).

Coincidences with other reaction products. Since $\Delta P_{p\parallel} = -\sum (U_i + E_i^{\text{exc}} + E_e^i)/v_p$ for a reaction without mass transfer from or to the projectile the projectile momentum (energy) change can be simply obtained by measuring the longitudinal momentum components of the emitted electrons and of the recoil ion alone: $\Delta P_{p\parallel} = -(P_{R\parallel} + \sum P_{e\parallel}^i)$. In figure 4 the longitudinal sum-momentum $P_{R\parallel} + P_{e\parallel}$ is plotted for helium single ionization by $3.6 \text{ MeV u}^{-1} \text{ Ni}^{24+}$ impact along with calculations using the CDW-EIS method by Rodríguez *et al* (1995b) (continuum distorted wave–eikonal initial state). Excellent agreement with the experimental data was observed by folding the theoretical result (see

inset) with a Gaussian distribution with a width of 0.16 au (full curve) to account for the experimental resolution. This corresponds to an unprecedented resolution in the projectile momentum change of $\Delta P_P/P_P \approx \pm 6 \times 10^{-8}$. In an earlier publication (Moshhammer *et al* 1994) the experimental results have been compared to the results of classical trajectory Monte Carlo (CTMC) calculations. (For an early description of this theoretical method see, for example, Gryzinski (1959), Abrines and Percival (1966) or Olson and Salop (1977). Later two-electron atoms were modelled in various ways, the implementation of the dynamical screening ‘dCTMC’ by Montemayor and Schiwietz (1989) being the most frequently used presently. Finally, the method was extended to the case of n -electron atoms termed ‘ n CTMC’ by Olson *et al* (1989a)).

In the above-mentioned experiment on transfer ionization by Mergel and co-workers (Mergel *et al* 1995b, Mergel 1997) the transverse projectile momentum was measured in coincidence with P_R , yielding the full momentum vector of the emitted electron. Exploiting momentum conservation one obtains for the longitudinal direction (the transverse direction was discussed above)

$$P_{e\parallel} = v_P \pm \sqrt{2v_P^2 + 2Q - P_{e\perp}^2 + v_P P_{R\parallel}}. \quad (5)$$

3.2. Collisions with photons

Only the gross features of the kinematics of photon–atom collisions are given here. Details have been given by Vogt (1996).

3.2.1. Absorption of a photon. If a photon is absorbed by an atom practically its entire energy is deposited into the target electron shell. Thus, for single photoionization, one electron emerges with an energy of $E_e = E_\gamma - E^{\text{bind}} - E^{\text{exc}}$ and a momentum of $P_e = \sqrt{2E_e}$ (the energy of the remaining ion E_R is negligibly small due to its large mass $E_R/E_e = \mu$, where μ being the reduced mass of the electron and the ion). This momentum is compensated by the recoiling target ion resulting in P_R distributions on spheres in momentum space with radii $P_R = P_e$ in the centre-of-mass system depending on the incident photon energy and the excitation energy of the remaining target electrons. In the laboratory frame the sphere for the ion is shifted along the photon beam direction by $P_{R\parallel} = P_\gamma = E_\gamma/c$ (the momentum of the incoming photon is mainly transferred to the ion and the electron momentum sphere is only shifted by $P_{e\parallel} = \mu P_\gamma$). The intensity distribution on these spheres mirror the angular emission characteristics of the emitted photoelectron.

In figure 5 the two-dimensional transverse momentum distribution of recoiling He^+ ions measured by Dörner *et al* (1997) is shown for an incident photon energy of $E_\gamma = 80.1$ eV integrated over $-0.1 \text{ au} \leq P_{R\parallel} \leq +0.1 \text{ au}$ (note that the whole momentum sphere was measured simultaneously and only an illustrative subset is shown in figure 5). The longitudinal shift due to the photon momentum of $P_\gamma = 0.022 \text{ au}$ is negligibly small. The various kinematic rings observed are due to different final states of the remaining He^+ ion (outer ring, ground state; second ring, first excited state, etc). Since linearly polarized light (along the x -axis) has been used in this experiment, the intensity distribution on the outer ring is given by the dipole emission characteristics of the emerging photoelectron (ion). If the second electron is left in an excited state (via ionization plus excitation or double excitation in the vicinity of a resonance followed by autoionization), the emitted electron (recoiling target ion) does not display dipole characteristics which can be efficiently explored using RIMS.

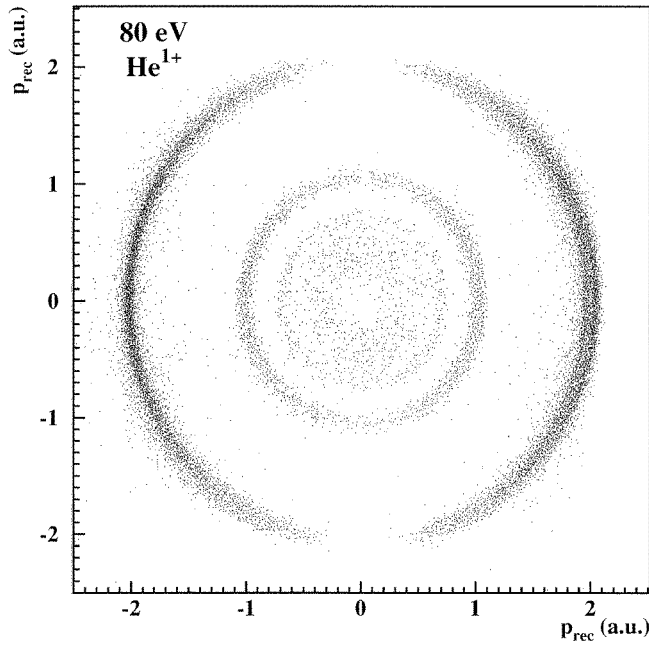


Figure 5. Momentum distribution of He^+ ions produced by 80.1 eV photons (Dörner *et al* (1997); note that a different notation for the recoil-ion momenta was used in this paper $P_R = P_{\text{rec}}$). The x -axis is the direction of the electric field vector of the linearly polarized light. The y -axis is the direction of the gas jet. The data are integrated over a momentum range of ± 0.1 au in the z -direction, which is the direction of the photon beam.

3.2.2. Compton scattering of a photon. For Compton scattering of the photon dominating the photoabsorption cross section at large E_γ the recoil-ion kinematics is very different from that for photoabsorption. Whereas only a bound electron can absorb a photon (the target nucleus has to compensate the emitted electron momentum) the scattering of a photon can occur by free electrons (Compton scattering) where energy and momentum conservation is fulfilled by the photon and the electron alone ($\mathbf{P}_e = \mathbf{P}_\gamma - \mathbf{P}_{\gamma'}$ and $E_e = E_\gamma - E_{\gamma'}$ for an electron initially at rest in the laboratory system). If the electron is initially in a bound state, the three-body momentum balance has to be considered. For large momentum transfers by the photon the impulse approximation can be applied assuming the bound electron to be quasi-free with an initial momentum distribution given by its momentum distribution in the atom (\mathbf{P}_e^{in} with $E_e^{\text{in}} = \frac{1}{2}(\mathbf{P}_e^{\text{in}})^2$), i.e. its ‘Compton profile’. This yields $\mathbf{P}_e = \mathbf{P}_\gamma - \mathbf{P}_{\gamma'} + \mathbf{P}_e^{\text{in}}$ and from momentum conservation one obtains for single ionization by Compton scattering,

$$\mathbf{P}_\gamma + \mathbf{P}_{\text{He}} = \mathbf{P}_{\gamma'} + \mathbf{P}_R + \mathbf{P}_e \quad (6)$$

or

$$\mathbf{P}_R = -\mathbf{P}_e^{\text{in}} \quad (6a)$$

in the approximation that no momentum exchange with the target nucleus occurs in the exit channel and that the initial momentum of the helium atom $\mathbf{P}_{\text{He}} \approx 0$ (both approximations are usually well fulfilled). Then, for ionization as a result of Compton scattering the target-ion recoil momentum is a broad distribution even for monoenergetic photon impact and mirrors the electron initial-state momentum distribution.

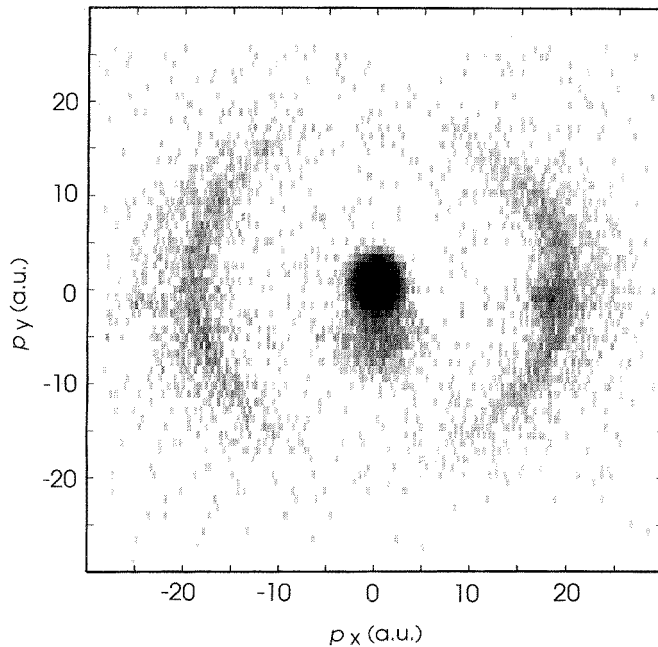


Figure 6. Momentum distribution of He^+ ions produced by 8.8 keV photons (Spielberger *et al* (1995); note that a different notation for the recoil-ion momenta was used in this publication $P_{R_{x,y}} = p_{x,y}$). The x -axis is the direction of the electric field vector of the linearly polarized light. The y -axis is the direction of the gas jet. The data are integrated over the full momentum range of ± 30 au in the z -direction, which is the direction of the photon beam.

Discriminating between ions of small and large momenta, Samson *et al* (1994) have exploited the difference in recoil-ion kinematics for Compton scattering and photoabsorption to measure the photon energy dependence of He single ionization for Compton scattering. The He^+ - and He^{2+} -ion momentum distributions for 8.8 keV photon impact were measured directly for the first time by Spielberger *et al* (1995). In addition to the kinematic sphere for photoabsorption with a radius of about 30 au, a narrow recoil-ion momentum distribution was observed centred around $\mathbf{P}_R = 0$ au with a width of the distribution of about 1 au resulting from Compton scattering of the photons (figure 6 for He single ionization). In this way, the contributions of both processes to helium single and double ionization have been separated in recent experiments (Spielberger 1995, 1996).

Only a few simple examples have been chosen in this section providing an idea of the wealth of information contained in the final state momentum of a recoiling target ion after collision-induced atomic reactions.

4. Results

In addition to the unique features offered by RIMS, as the large solid angle with simultaneously excellent momentum resolution as well as the open geometry of the spectrometers which is ideal for implementing other detection devices, one further advantage makes this technique extremely versatile: this is its applicability for all projectile species at any impact energy as well as the nearly complete independence of the achievable resolution from the projectile beam energy spread and angular divergence (see also section 2.2.2). This

is fundamentally different from the situation one faces in conventional (e, 2e) experiments or projectile energy-loss–gain measurements and has prompted experiments extending over the whole variety of projectiles and collision energies available. Thus, in this section results are reviewed for ion–atom collisions with ions from H^+ to U^{65+} at energies between 5 keV and 1.4 GeV. They are followed by data for photon impact at energies between 80 eV and 58 keV and by first results for electron impact. Recently, measurements have been performed with antiproton beams and for ion impact at up to TeV energies.

4.1. Ion–atom collisions

Historically, RIMS has been designed with the intention of exploring many-particle momentum transfers in the field of ion–atom collisions. Therefore, most of the existing data deal with ions as projectiles. Three basically different reactions might be distinguished: first the transition of one or more electrons from bound states of the target to bound states of the projectile (*electron capture*; electron transfer from the projectile to the target is small in most cases). Second, the promotion of target or projectile electrons to excited energy levels (*excitation*) and third, the transfer of bound target or projectile electrons into the continuum (*ionization*). All of these reactions and combinations have been observed in different experiments using RIMS. Since RIMS is based on the detection of a target ion, most data, however, have been collected for electron capture and target ionization (reviewed in the next two subsections). The ionization of the projectile (for simultaneous target ionization) has been investigated in detail and therefore is summarized separately. Excitation of the target or the projectile in combination with target ionization has been observed in RIMS experiments (see, for example, figure 3) but has not yet been discussed in the literature.

4.1.1. Electron capture. The capture of a target electron might proceed ‘kinematically’ (the target nucleus is needed to satisfy the conservation laws), radiatively under the emission of a photon (REC, ‘radiative electron capture’ which is the time-reversed photoeffect) or in an energy-resonant process (RTE, ‘resonant transfer and excitation’ which is the time-reversed Auger effect). Experimental information about the final electronic state populated in the projectile after a capture reaction can be obtained by detecting either the decay products of excited states (electrons, photons) or by analysing the Q -value of the reaction.

Zero-degree Auger spectroscopy yields superior energy resolution and many experimental investigations have been devoted to the investigation of kinematic capture into doubly excited states (see, e.g., Stolterfoht (1987), Stolterfoht *et al* (1990), for new electron detection techniques see Kravis *et al* (1996)) and to RTE processes (for a recent review see Zouros (1996)). Using traditional electron spectroscopy the electron capture to the continuum (ECC) leading to a sharp, cusp-shaped peak in the electron spectra under forward emission angles, has been explored in numerous studies (for details see, for example, Breinig *et al* (1982)). The coincident detection of an Auger electron with the polar and azimuthal projectile scattering angle of the projectile allows us to access the relative phases of doubly excited populated states (Khemliche *et al* 1995). Stöhlker *et al* (1997) were able to extract state-selective electron capture cross sections using x-ray–projectile coincidence techniques. Similar information has been obtained recently by measuring the scattered projectile in coincidence with the polarization or angular distribution of emitted photons (see, e.g., Hoekstra *et al* 1989, Roncin *et al* 1994).

The Q -value of a capture reaction is accessible by observing the longitudinal momentum change of the projectile (translational spectroscopy). The simultaneous determination of the

projectile deflection and of the projectile energy change ΔE_P yields angle-dependent state-selective scattering cross sections. Using this method numerous experiments have been performed which were limited, however, to the regime of low projectile energies (see, e.g., Mann *et al* 1982, Ohtani *et al* 1982, Schmeisser *et al* 1984, Cederquist *et al* 1989, 1995, Roncin *et al* 1991, Barat *et al* 1992, Lebius and Huber 1992). This limitation results from the restricted achievable resolution in the determination of the projectile energy change of $\Delta E_P/E_P \approx 10^{-4}$ and scattering angle of $\Delta\vartheta_P \approx 10^{-4}$ rad (Park *et al* 1978, Schuch *et al* 1988, Htwe *et al* 1994).

For the case where no target electrons are in final continuum states (see the discussion in section 3.1) or if the final momenta of such electrons are measured, e.g. by using reaction microscopes, RIMS opens the unique possibility to extend Q -value measurements to even the highest E_P and to the study of REC or RTE. High-resolution RIM spectrometers are even competitive with translational spectroscopy at small velocities (Dörner *et al* 1995b, Cassimi *et al* 1996). Until now, kinematic electron capture and 'transfer ionization' (one target electron is captured, the other is ionized) have been explored by this technique. Experiments to investigate REC and RTE are under preparation at storage rings.

Pioneering experiments on the longitudinal momentum transfer to recoil ions after kinematic electron capture were performed for low-energy highly charged ion impact (Ali *et al* 1992, Wu *et al* 1993, 1994b, Raphaelian *et al* 1995) as well as at larger projectile velocities (Frohne *et al* 1993, Wu *et al* 1994a, 1995). With a resolution of the pinhole-collimated effusive jet of ± 11 au in the directions transverse to the atomic beam propagation Frohne and co-workers were able for the first time to observe the backward scattering of the recoil ion as a function of the number of captured electrons n_C following from the electron translation factor $\frac{1}{2}n_C v_P$ (equation (3)). The Q -value of the reaction was not accessible in this experiment due to the uncontrolled momenta of the emitted electrons but has been investigated later for single capture and transfer ionization collisions with a helium target (Wu *et al* 1994a, 1995). Using an improved experimental arrangement with a resolution of about ± 0.75 au, Wu and co-workers were able to separate capture into the projectile K from L and higher shells. Due to the limited scope of this review, these first experiments cannot be described in detail and emphasis will be given to recent high-resolution studies. Also, results on electron capture reactions obtained with the above-mentioned traditional techniques cannot be reviewed and the reader has to be referred to the references given above.

Single-electron capture at different velocities. With the implementation of supersonic jets into RIM spectrometers, high-resolution state-selective scattering angle-dependent studies became feasible and were first reported for fast He^{2+} on He collisions (Mergel *et al* 1995a, b) reaching a resolution of $\Delta P_{R\parallel} = \pm 0.13$ au and $\Delta P_{R\perp} = \pm 0.02$ au. At 1 MeV and no electron in a final continuum state ($\Delta P_{R\perp} = P_{P\perp}$) this corresponds to $\Delta E_P/E_P = \pm 2.2 \times 10^{-5}$ ($\Delta E_P = 22$ eV) and $\Delta\vartheta_P \approx \Delta P_{R\perp}/P_P = \pm 1 \times 10^{-6}$ rad which is hardly achievable with translational spectroscopy. In figure 7 the $P_{R\parallel}$ distributions are shown for single-electron capture at two different projectile velocities. According to equation (3) the recoil-ion longitudinal momentum can be decomposed into the mass transfer term ($\frac{1}{2}v_P$, full arrow in the figure) and into a contribution depending on the inelasticity of the reaction (Q/v_P , broken arrows). Different peaks are resolved corresponding to capture into the K- and L-shells of the projectile. As in translational spectroscopy for symmetric collision systems, the experiment cannot distinguish whether the projectile or the target is in a final excited state (final target, projectile states are indicated by the first and second number in parentheses).

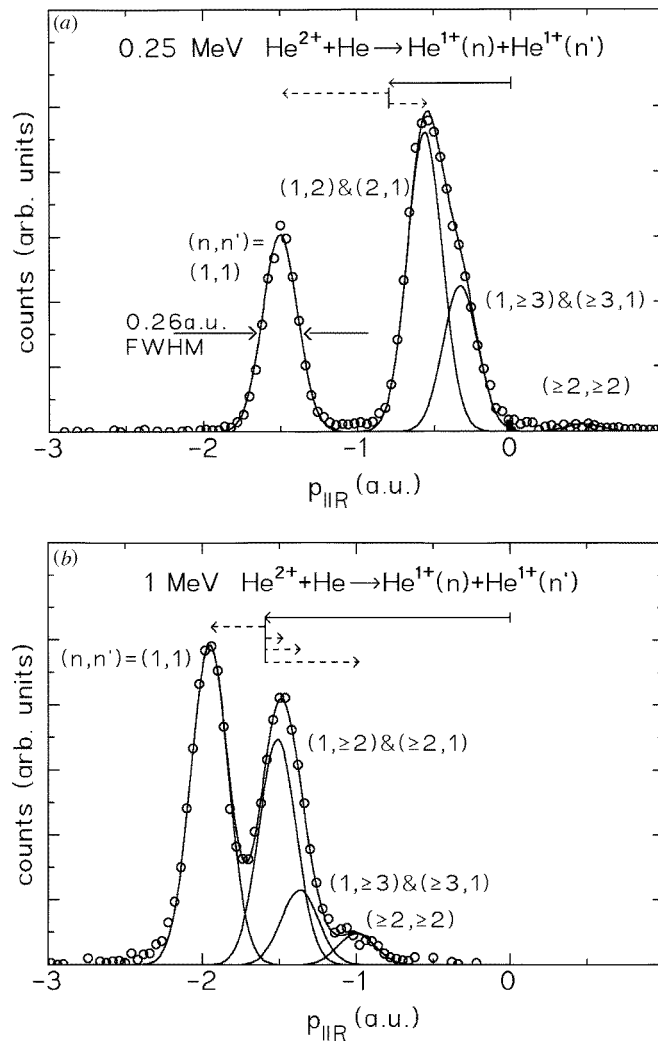


Figure 7. Recoil-ion longitudinal momentum distributions for single-electron capture by 0.25 MeV and 1 MeV He^{2+} impact on helium (Mergel *et al* 1995a). The peaks correspond to the different states of the projectile and target as indicated in the figure (see text).

Summation over all final states and integration over all transverse momenta yielded total electron capture cross sections as a function of the projectile energy. The RIMS results were found to be in good agreement with earlier experimental data (Shah and Gilbody 1985, Pivovar *et al* 1982, DuBois 1987) and were reasonably reproduced by several theoretical models as continuum distorted-wave (CDW, Belkic and Gayet 1977), coupled-channel (Gramlich *et al* 1989, Shingal and Lin 1991), molecular-orbital (Kimura 1988) and eikonal distorted-wave calculations (Deco *et al* 1984). However, experimental state-selective cross sections had not been reported until that time and quantum mechanical calculations which are partly in good agreement with the total capture data were only available for ground-state capture. Recent dCTMC calculations ('dynamical screening CTMC'; Meng *et al* (1993)) are found to describe the cross sections for all final states reasonably. In the

dCTMC model the mutual dynamical screening of the two electrons is considered, in that the strength of the helium nuclear potential for each electron depends on the position of the second electron during the encounter (see also Montemayor and Schiwietz 1989). Scattering angle (ϑ) dependent state-selective capture cross sections for the same collision system at different energies have been measured by Mergel *et al* (1995b) using RIMS. It was found that the maximum in the ϑ dependence of ground- and excited-state capture occurred at $\vartheta \approx 40 \mu\text{rad}$. In addition, oscillations were observed in the ratios between capture into the ground state and into excited states as a function of the recoil-ion transverse momentum (projectile scattering angle) which has been identified as being due to resonant K–K transfer processes. Single-electron capture by 200–400 keV protons in collisions with He has been investigated by Mergel (1994).

At larger projectile charge states and still moderate energies, only one measurement has been reported in the literature so far (Kambara *et al* 1995, 1997) using high-resolution RIMS where the capture into various final states was observed for 8.7 MeV O^{7+} on helium collisions (similar experiments have been performed by Abdallah *et al* (1997) for 1–1.5 MeV u^{-1} F^{9+} on He). Two complications arise at higher velocities v_p and high projectile charge states Z_p . First, the cross sections σ_{cap} decrease strongly with increasing v_p ($\sigma_{\text{cap}} \propto v_p^{-12}$ in the high-energy limit) and the capture takes place at smaller impact parameters. In particular, for large Z_p this results in large transverse recoil-ion momenta $P_{R\perp}$. These are hard to handle with present set-ups if the longitudinal momentum transfers are small at the same time and if a good $P_{R\parallel}$ resolution is required (see the discussion in Moshhammer *et al* (1996c)). Secondly, for the same $P_{R\parallel}$ resolution of a spectrometer the Q -value resolution decreases linearly with the velocity (equation (3)). As illustrated in figure 8, the resolution achieved in that experiment of ± 0.5 au (only slightly better than the one reported by Wu *et al* (1994a, 1995)) was not sufficient to separate capture into

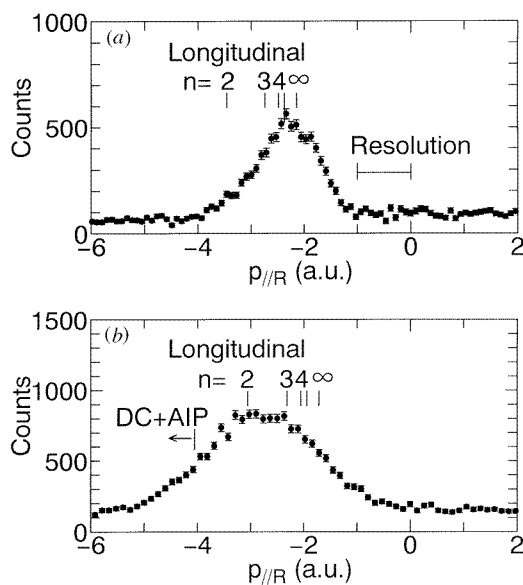


Figure 8. Recoil-ion longitudinal momentum distributions for pure single-electron capture (a) and for transfer ionization (b) by 8.7 MeV O^{7+} impact on helium (Kambara *et al* 1995). Principal quantum numbers are indicated in the figures. DC + AIP denotes double-electron capture plus autoionization of the projectile.

different shells of the projectile. It was reported that pure single-electron capture dominantly populated $n = 4$ and higher states which was found to be in agreement with the prediction of the simple classical overbarrier (COB) charge-exchange model (Ryufuku *et al* 1980). Single capture accompanied by the ionization of the target electron (transfer ionization), however, mainly proceeded into $n = 2-4$ states. This has also been explained by the authors within the COB model, assuming the ionization and capture processes to be independent and the ionization to precede the capture of the electron. Then, the second electron in singly charged He^+ is more tightly bound yielding a lower potential barrier so that an n -value of about three was predicted by the COB model. The experimental data were also compared with semiclassical close-coupling calculations (Kimura and Lane 1989).

Earlier experiments for single-electron capture have been performed by Wu *et al* (1994a, 1995) and are shown on the left-hand side of figure 20 for different projectile energies ranging from 20–40 MeV O^{7+} on helium. At these higher velocities capture is observed to proceed mainly into the L and higher shells at 20 MeV and significant indications for K-shell capture are only found for collision energies of 36 and 40 MeV.

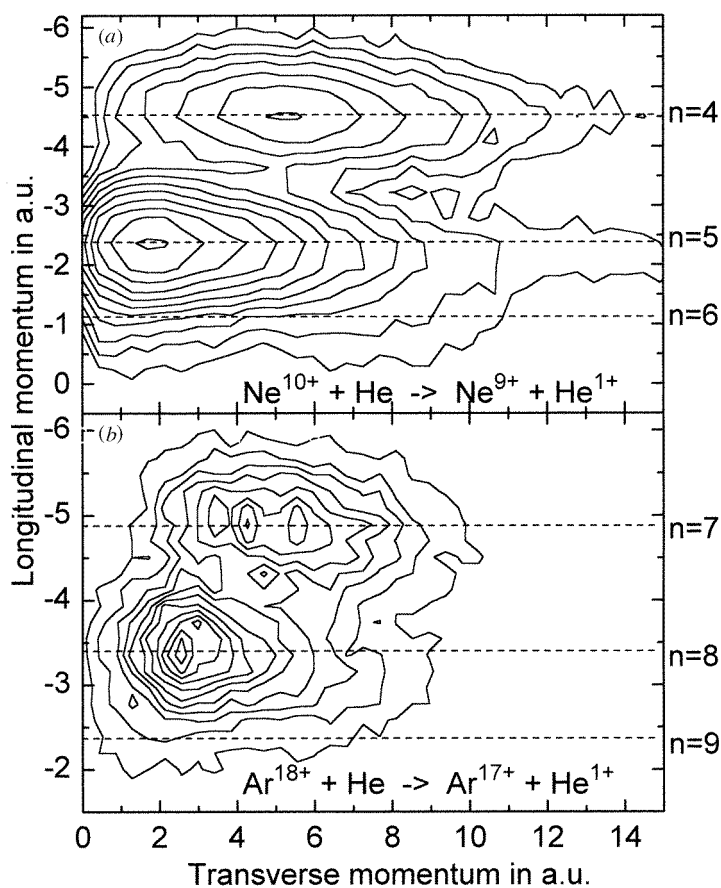


Figure 9. Experimental recoil-ion momentum distributions of longitudinal versus transverse momenta for the single-capture reaction from He by (a) $6.82 \text{ keV u}^{-1} \text{ Ne}^{10+}$ and (b) $6.75 \text{ keV u}^{-1} \text{ Ar}^{18+}$. Broken lines, calculated position of electron capture to specific n -levels (Cassimi *et al* 1996).

Superior energy-gain resolutions, ΔE_p , of the order of a few eV or even lower ($\Delta E_p = \pm 0.7$ eV, see figure 3) as well as ϑ -resolutions of a few μrad have been achieved at low projectile velocities (Dörner *et al* 1995b, Cassimi *et al* 1996). For highly charged ion-impact capture into final principal number quantum states of $n = 4, 5, 6$ and $n = 6, 7, 8, 9$ have been identified for $6.82 \text{ keV u}^{-1} \text{ Ne}^{10+}$ and $6.75 \text{ keV u}^{-1} \text{ Ar}^{18+}$ on He collisions, respectively, by Cassimi *et al* (1996). In figure 9 the recoil-ion transverse momentum is plotted versus the longitudinal momentum, in essence representing the scattering angle-dependent ($\propto P_{R\perp}$) state-selective ($\propto P_{R\parallel}$) cross sections for both collision systems. Two features are obvious: first, capture into higher n -states occurs at smaller transverse momentum transfers $P_{R\perp}$. Using $n\text{CTMC}$ (' n -body CTMC'; see, e.g., Olson *et al* (1989a)) calculations it was shown that a close correspondence between $P_{R\perp}$ and the impact parameter is obtained at these low velocities and typical impact parameters extracted from the transverse momenta were found to be consistent with curve-crossing arguments. In the $n\text{CTMC}$ model all n target electrons are modelled in the atom's initial state in such a way that the individual electrons are bound with the sequential ionization potentials of the atom. Thus, the total electronic binding energy of the 'classical atom' is correct and part of the electron-electron interaction is considered in the ground state. However, the electrons are not indistinguishable and the dynamical electron-electron interaction is not implemented as in the $d\text{CTMC}$ approximation. Secondly, one observes that $P_{R\parallel}$ is independent of the transverse momentum transfer for given inelasticity (Q -value) of the reaction. Thus, the momentum components are decoupled and yield completely different information, as has been discussed in section 3.

Double-electron capture. At collision velocities between 0.06 and 0.19 MeV u^{-1} state-selective scattering angle-dependent double-electron capture cross sections were measured by Dörner *et al* (1996b) for He^{2+} on He collisions (experimental data are unpublished up to now). In agreement with recent theoretical results (Tökési and Hock 1996) it was found that the resonant ground-state capture is the dominant channel and capture into non-autoionizing excited states only contributes up to 17%. Thus, RIMS provides the unique possibility to investigate capture into the ground state of the projectile which might even be neutral in the exit channel. In previous experiments the ($4 \rightarrow 3$) line emission (Folkerts *et al* 1993) or Auger decay of doubly excited states (Zouros *et al* 1987) of the projectile was investigated making only excited final states observable.

Transfer excitation and ionization. The capture of one target electron by the projectile and the simultaneous ionization of a second one has been investigated using an effusive gas jet by Wu *et al* (1995) for $20\text{--}66 \text{ MeV F}^{8+}$ and O^{7+} on helium collisions. Capture plus excitation of a target electron as well as transfer ionization has recently been observed in high-resolution RIMS experiments (see figure 3 for transfer excitation (Dörner *et al* 1995b)). Mergel *et al* (1995c, d) briefly reported on the first kinematically complete experiments on transfer ionization for $0.15\text{--}1.4 \text{ MeV}$ proton on helium collisions which were performed with the goal of identifying different mechanisms contributing to transfer ionization (all the experimental results have been published very recently by Mergel 1997). Since three particles are in final continuum states (nine final momentum components) five have to be determined in order to control the reaction kinematics completely (the remaining four momentum components can be deduced from momentum and energy conservation). Experimentally this was accomplished by measuring all three momentum components of the recoiling target ion in addition to the transverse scattering of the projectile (see section 3). Two different reaction

mechanisms showing different kinematic signatures were observed for 1 MeV proton impact (figure 10) by projecting the nine-dimensional momentum space onto the $(P_{Rz}-P_{Rx})$ plane for fixed projectile deflection into the x -direction of $0.45 \text{ mrad} < \vartheta < 0.65 \text{ mrad}$ (the incoming beam direction is along the positive z -axis). One is the first-order kinematic capture of one target electron leading to $P_{Rz} = P_{R\parallel} = 2.8 \text{ au}$ according to equation (3) accompanied by the simultaneous but independent emission of the second target electron (see the lower peak on the dashed line in figure 10). The other mechanism is a second-order process pioneered experimentally by Horsdal *et al* (1986) and Pálinkás *et al* (1989) and predicted by Thomas (1927) on the basis of classical arguments to be the dominant contribution at large velocities. Here, in a first projectile–electron interaction one target electron is scattered under 45° leading to a projectile deflection for protons of 0.55 mrad independent of the projectile energy. This electron, having a velocity of $\sqrt{2} v_p$ hits the second target electron such that it is emitted under 90° in the laboratory frame whereas the first one emerges with $v_e = v_p$ and subsequently can be captured by the projectile. In this reaction, momentum and energy conservation are fulfilled by the projectile and the electrons alone. The doubly ionized He target is left as a spectator without momentum transfer leading to a final momentum distribution centred around $P_{Rz} = P_{Rx} \approx 0$ which is broadened by the two-electron initial-state Compton profile (see the upper peak in figure 10).

As mentioned at the beginning of this subsection RIMS has only started to be used as an instrument to explore various electron capture mechanisms at a few laboratories and the experiments reviewed give a flavour of what will be possible in the near future. With the implementation of RIM spectrometers into storage rings scheduled for 1997 (ESR; CRYRING, Schmidt *et al* (1997)), the improvement of the transverse momentum acceptance of present devices and the implementation of large solid-angle high-resolution electron spectrometers, kinematically complete investigations of REC, RTE and various higher-order kinematic capture mechanisms as well as coincidences with emitted photons should become feasible.

4.1.2. Ionization of the target. Over a long time the experimental investigation of target single or multiple ionization by fast ion impact has been limited to total charge production measurements and to the determination of total cross sections as a function of the final target and projectile charge (for a review see Cocke and Olson (1991)). A huge amount of systematic experimental data on double-differential cross sections for the electron emission (differential in the emission angle and energy of one outgoing electron) has been reported over more than three decades revealing detailed information on the various ionization processes (for reviews see, e.g., Rudd and Macek (1972), Rudd *et al* (1976, 1992), Stolterfoht (1978), Stolterfoht *et al* (1997)). Subsequently, experiments were performed which were differential in the transverse momentum change $\Delta P_{p\perp}$ of the projectile (see, e.g., Giese and Horsdal 1988, Kamber *et al* 1988, Kelbch *et al* 1988, 1989, Schuch *et al* 1988, Kristensen and Horsdal-Pedersen 1990) or as a function of the transverse momentum transfer $P_{p\perp}$ to the recoil ion (see, e.g., Ullrich and Schmidt-Böcking 1987, Ullrich *et al* 1988a, 1989, Frohne *et al* 1993, 1996). The energy loss of low-energy light projectiles and their scattering angle distribution was investigated by Htwe *et al* (1994) and Schiwietz *et al* (1994a). Few coincidence experiments have been performed where only one of the reaction products was momentum analysed: these were double-differential electron-emission cross sections (Schiwietz *et al* 1994b) or energy loss spectra of the projectile (Schuch *et al* 1988) as a function of the target-ion charge state. A new insight into the ionization collision dynamics was provided by coincidence experiments

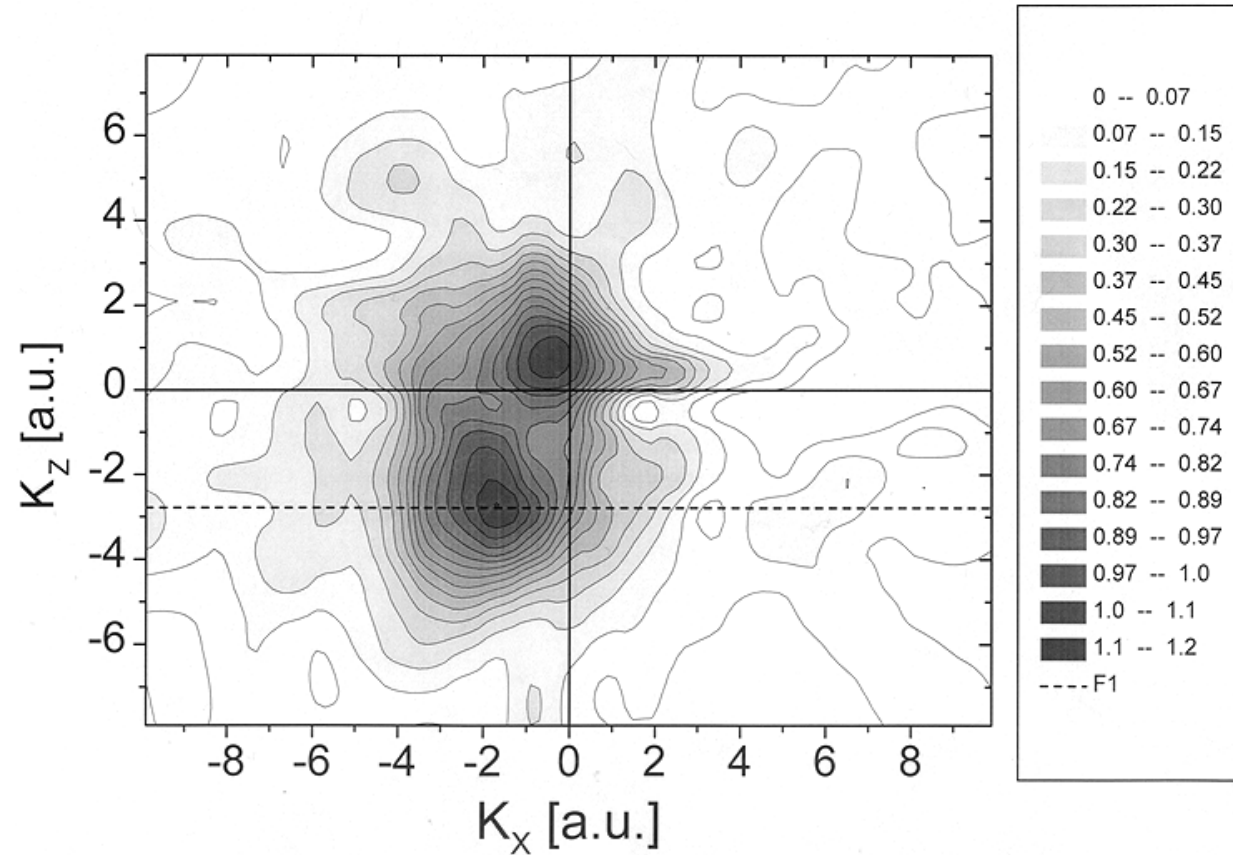


Figure 10. Recoil-ion momentum distribution for transfer ionization in 1 MeV p on He collisions (Mergel *et al* 1995c, 1997) at projectile scattering angles of $0.45 \text{ mrad} < \vartheta < 0.65 \text{ mrad}$. Events are projected onto the scattering plane, which is defined by the incoming projectile direction along the positive z -axis and the scattered projectile transverse direction along the positive x -axis. A binary collision between the nuclei would lead to a transverse recoil-ion momentum of $K_x = -6.3 \text{ au}$ for a projectile being scattered to $\vartheta = 0.55 \text{ mrad}$. The linearly spaced contour lines and greyscales between them represent counts on an arbitrary scale.

accessing differential information on two reaction partners: double-differential cross sections for the emission of an electron were recorded as a function of the polar projectile scattering angle (see, e.g., Schiwietz 1988, Schiwietz *et al* 1987, 1988) and transverse recoil-ion momenta were measured for defined polar and azimuthal projectile deflections (Dörner *et al* 1989, 1991, Forberich *et al* 1991, Gensmantel *et al* 1992, Lencinas *et al* 1993). Many of these measurements, however, suffered from a limited momentum resolution for the heavy collision partners (projectile and recoil ion), prohibiting the investigation of the ionization collision dynamics at very small momentum transfers on the order of a few atomic units or below, where the majority of ionizing reactions take place. Most importantly, no kinematically complete experiment for even single ionization of the target by ion impact that would be comparable to (e, 2e) investigations had been performed until recently.

With the design of high-resolution RIM spectrometers and especially with the development of ‘reaction microscopes’ the simultaneous determination of the complete momentum vectors of up to four reaction products (the recoil ion and three emitted electrons) became feasible for the first time. Achieving a resolution of the order of 0.1 au at a 4π solid angle for all of the particles (see section 2.4) a new generation of experiments on target single, double and multiple ionization by ion impact, which are unprecedented in resolution and completeness have been performed and are reviewed in this subsection.

Single ionization of the target at different collision velocities. A pioneering kinematically complete experiment on target single ionization in an ion–atom collision was reported for $3.6 \text{ MeV u}^{-1} \text{ Ni}^{24+}$ on helium collisions (Moshhammer *et al* 1994, Ullrich *et al* 1995). Using a ‘reaction microscope’ (Moshhammer *et al* (1996c), Ullrich *et al* (1996) and section 2.4) the recoil-ion and electron momentum vectors were measured in coincidence and, thus, the nine-dimensional final state momentum space (exploiting energy and momentum conservation) was determined. A momentum acceptance for both spectrometers of $0 \text{ au} \leq P_{\text{R,e}} \leq 2 \text{ au}$ enabled the simultaneous detection of more than 90% of all the ejected ions and electrons. At the same time a superior momentum resolution in the longitudinal direction of $\Delta P_{\text{R}\parallel} = \pm 0.08 \text{ au}$ for the recoil ion and of $\Delta P_{\text{e}\parallel} = \pm 0.1 \text{ au}$ for the electron was achieved corresponding to a recoil-ion energy resolution of $\Delta E_{\text{R}\parallel} = \pm 12 \mu\text{eV}$ and an electron energy resolution of $\Delta E_{\text{e}\parallel} = \pm 130 \text{ meV}$ at zero energies, respectively. The electron energy resolution in the transverse direction was a function of the electron time of flight with an optimum resolution of $\Delta E_{\text{e}\perp} = [(0.13 \text{ eV})/E_{\text{e}\perp}]^{1/2}$ and a mean total energy resolution of $\Delta E_{\text{e}} \leq 400 \text{ meV}$ was achieved. Thus, the complete electron-emission characteristics was accessible for all low-energy electrons, including those with zero emission velocities as a function of the measured recoil-ion momenta and final charge states of the projectile and of the target.

In figure 11 the single-differential electron-emission cross sections (integrated over all electron-emission angles and all recoil-ion momenta) for helium single ionization are shown (full circles) in comparison with recent results of CDW-EIS (‘continuum distorted wave–eikonal initial state’) calculations (chain curve, Rodríguez *et al* (1995b)) and results obtained from a first Born approximation (broken curve). The experimental data were found to be in good agreement with the CDW-EIS results whereas the first Born approximation is not applicable in this regime of strong perturbations ($q/v_{\text{p}} = 2$) as expected. *n*CTMC calculations (full curve, Moshhammer *et al* (1994)) underestimate the total cross section by about a factor of 1.6 which in essence is a result of the initialization where the electrons are distinguishable and bound with the sequential ionization potentials. The shape of

the single-differential electron-emission cross sections is well reproduced. The complete electron-emission characteristics integrated over all final recoil-ion momenta is shown in figure 12 in a $P_{e\perp}$ versus $P_{e\parallel}$ representation (Moshhammer *et al* 1996b) demonstrating that about 93% of all low-energy electrons were emitted into the forward hemisphere (positive longitudinal electron momenta) with mean energies in this direction of about 2.5 eV. The forward emission of the electrons was found to be well reproduced by n CTMC calculations (right-hand part of figure 12). The width of the electron momentum distribution differed, however, in that the longitudinal momentum distribution was observed to be smaller and the transverse wider than the experimental one.

It has been pointed out by Suárez *et al* (1993) that such cross sections are extremely difficult to obtain by applying conventional detection techniques and that large discrepancies have been found between different measurements for electron energies below 20 eV (Suárez *et al* (1993) and references therein). In fact, the data shown in figures 11–13 were the first absolute single- and double-differential electron-emission spectra from ion–atom collisions reported in the literature where all soft electrons have been detected for controlled final charge states of the heavy particles. One other study on absolute $d\sigma/dE_e$ has been published for low-energy proton impact without control of the final target charge state and without information on the double-differential cross sections (Pieksma *et al* 1994). Very recently, Kravis and co-workers (Kravis *et al* 1996) reported single-differential cross sections $d\sigma^+/dP_{e\parallel}$ for low-energy electrons for defined final charge states of the target and the projectile (see also Wang *et al* 1996a). In this experiment all soft electrons were projected onto a 2DPS MCP by a strong electrostatic field. Two momentum components were accessible with this technique but no electron energy distributions ($d\sigma^+/dE_e$) were obtained due to the missing third electron momentum component.

Projecting the two-dimensional distribution (figure 12) onto the $P_{e\parallel}$ -axis the strong forward–backward asymmetry of the soft electron ejection by the highly charged projectile

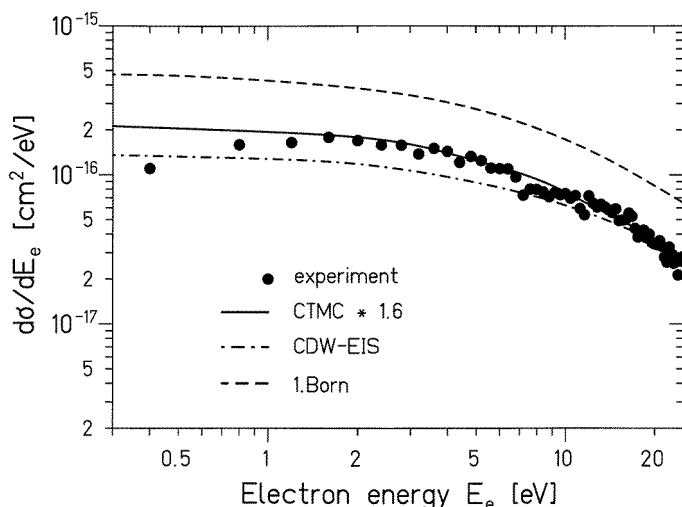


Figure 11. Single-differential cross section for the emission of an electron as a function of the electron energy E_e for single ionization of He by $3.6 \text{ MeV u}^{-1} \text{ Ni}^{24+}$ impact. Experimental points (full circles) are from Moshhammer *et al* (1994). Theory, n CTMC (full curve, Moshhammer *et al* (1994)) multiplied by a factor of 1.6 (see text); first Born approximation (broken curve, Rodríguez *et al* (1995b)); CDW-EIS (chain curve, Rodríguez *et al* (1995b)).

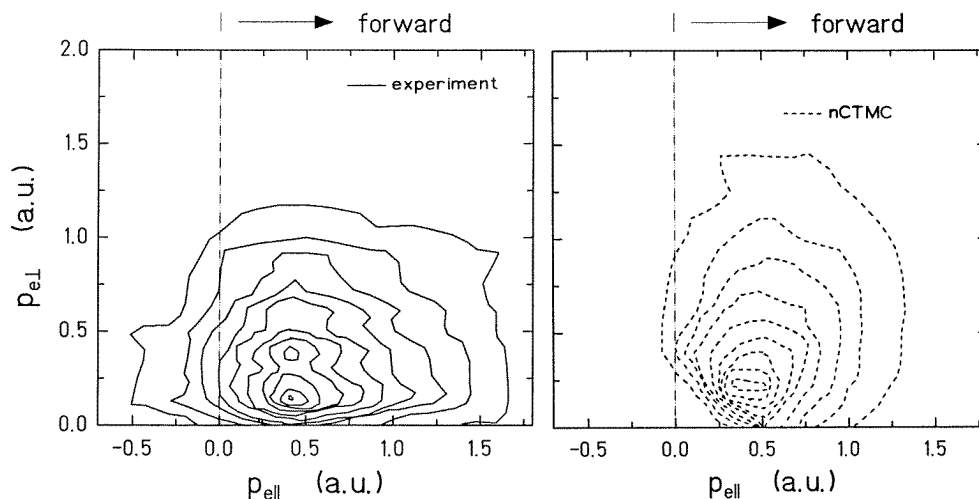


Figure 12. Doubly differential cross sections $d\sigma^+/dp_{e\perp}dp_{e\parallel}$ for the emission of an electron for single ionization of He by $3.6 \text{ MeV u}^{-1} \text{ Ni}^{24+}$ impact (Moshammer *et al* 1996b). The linearly spaced contour lines represent the counts. Left-hand side, experiment; right-hand side, *n*CTMC.

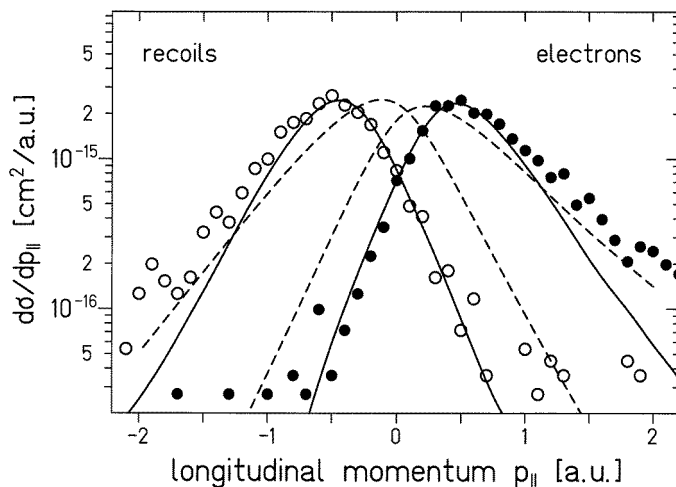


Figure 13. Longitudinal momentum distributions (single-differential cross sections $d\sigma^+/dp_{\parallel}$) of the electron (full circles) and of the recoil ion (open circles) for single ionization of He by $3.6 \text{ MeV u}^{-1} \text{ Ni}^{24+}$ impact (Moshammer *et al* 1994). Theory, *n*CTMC (full curves, Moshammer *et al* (1994)) multiplied by a factor of 1.6 (see figure 11); CDW-EIS (broken curves, Rodríguez *et al* (1995b)). For theory also see O'Rourke and Crothers (1997a, b).

was made more evident in figure 13. The asymmetry as well as the width of the $P_{e\parallel}$ distribution was well reproduced by *n*CTMC and CDW-EIS calculations. The forward emission of the electrons was interpreted as being due to the post-collision interaction (PCI) of the emerging highly charged projectile with the low-energy electron in essence 'pulling' it behind. This interpretation was supported by recent calculations in the dCTMC approach with 100 keV antiprotons as projectiles (Wood and Olson 1996) yielding backward emission of the electrons in the repulsive potential of the emerging antiproton. At the same

time forward ejection of the recoil ions was observed. Forward emission of soft electrons for single-target ionization has also been observed recently in 30–140 keV p and C⁶⁺ on He collisions (Kravis *et al* 1996, Wang *et al* 1996a).

The interaction of continuum (and Auger) electrons with the nuclear charges of the projectile and of the target has been investigated in many experimental as well as theoretical studies under the synonyms ‘two-centre phenomena’ or ‘post-collision interaction’, respectively (for recent overviews on the field see, for example, Fainstein *et al* (1991), Stolterfoht *et al* (1997) and references therein). Up to now, mostly energetic electrons were considered in the region of the electron capture to the continuum. Enhanced forward emission of soft electrons was observed early on (see, e.g., Platten *et al* 1987, Pedersen *et al* 1990 and references therein) as well as more recently (see, e.g., Suárez *et al* (1993) and Stolterfoht *et al* (1995), for a recent theoretical discussion see e.g. Colavecchia *et al* (1995) and references therein).

Investigating the complete three-body longitudinal momentum transfer for the Ni²⁴⁺ on the He collision system (figure 13) it was found that $P_{e\parallel}$ is not balanced by the projectile (see figure 4) but by the recoiling target ion which is scattered into the backward direction (see also Moshhammer *et al* 1996a). The projectile momentum transfer, calculated for each single collision from the measured final longitudinal momenta of the electron and of the recoil-ion $\Delta P_{P\parallel} = -(P_{R\parallel} + P_{e\parallel}) = -(Q/v_p + E_e/v_p)$ was observed to be extremely small. Formally, this is evident from the above equation (see also equation (4)) for small Q -values and small emitted electron energies E_e at large projectile velocities v_p . In the limit of projectile velocities approaching the speed of light the longitudinal momentum transfer of the highly charged projectile becomes as small as the momentum transfer by a photon of equivalent energy. Therefore, the fast highly charged projectile was interpreted recently (Moshhammer *et al* 1996a, 1997a, Kollmus *et al* 1997) to act like an ultra-short, intense and broadband virtual photon field, dissociating the atom. It has been pointed out (Moshhammer *et al* 1994) that the simultaneous measurement of $P_{e\parallel}$ and $P_{R\parallel}$ allows one to determine the energy loss of the 0.2 GeV Ni²⁴⁺ projectile experimentally in a single collision with an accuracy of $\Delta E_P/E_P = 3.4 \times 10^{-7}$ which is orders of magnitude better than that achievable in any energy gain or loss measurement using conventional techniques. Since the electron energy was measured simultaneously, the Q -value, i.e. the He ionization potential was directly accessible. It was emphasized that this method, i.e. the direct measurement of the inelasticity of a collision by performing a kinematically complete experiment, might be applicable to determine absolute binding energies of heavy few-electron systems (U⁹¹⁺, Pb⁸¹⁺, etc) circulating in the GSI heavy ion storage ring (ESR) with a resolution of 10 eV (FWHM).

In a recent study, the longitudinal and transverse recoil-ion momentum distributions were measured for 0.25–1 MeV proton on helium singly ionizing collisions and compared with theoretical calculations in the n CTMC (n -body CTMC; Dörner *et al* (1995a)) and CDW-EIS approach (Wang *et al* 1996a). Inspecting equation (4) it is obvious that the recoil-ion longitudinal momentum distribution only depends on the energies and longitudinal momenta of the emitted electrons and therefore can be deduced from doubly differential electron-emission cross sections. Thus, RIMS has been considered as being complementary to the conventional electron spectroscopy (Rodríguez *et al* 1995a) well suited to explore low-energy electrons and the ionization collision dynamics. In figure 14 the $P_{R\parallel}$ -distribution is shown for 0.25–1 MeV p on He single ionization. In these collision systems the perturbation is about one order of magnitude smaller ($q/v_p \leq 0.32$) than for the previous Ni collisions. Therefore, the PCI has been found to be strongly reduced, the distribution was nearly centred around $P_{R\parallel} = 0$ and the results of the first Born approximation were found to be close to the experimental data (Wang *et al* 1996a). Reasonable agreement between

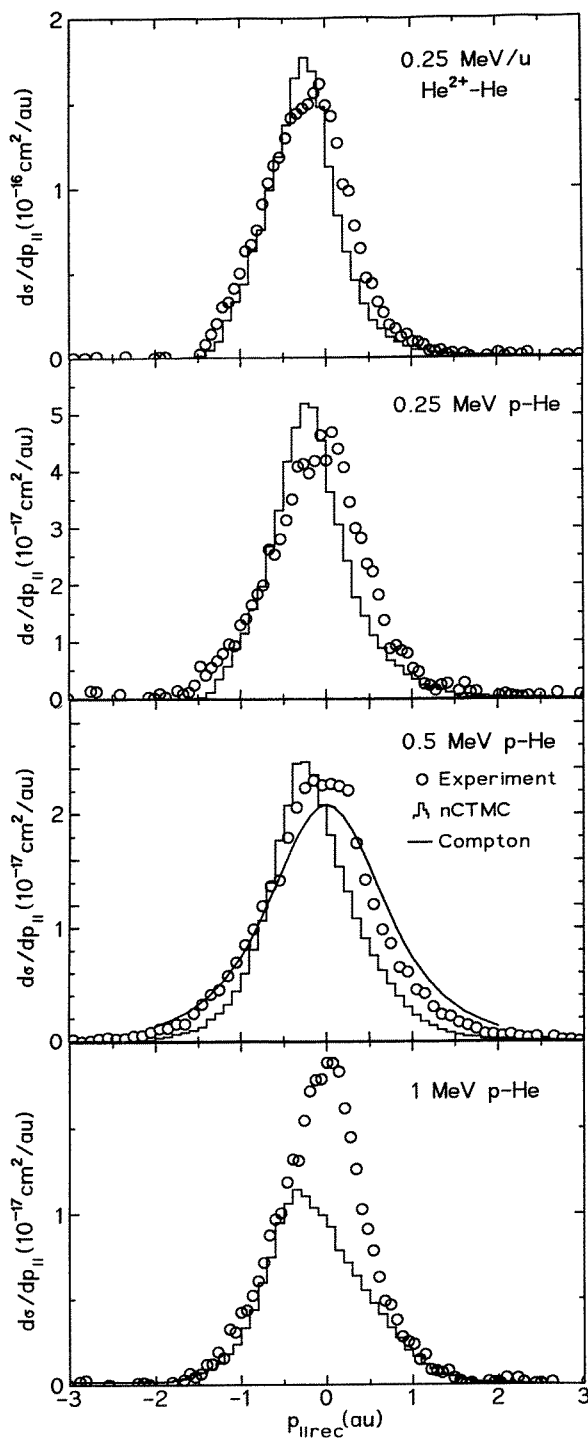


Figure 14. Experimental (open circles) and theoretical (histogram, *n*CTMC) longitudinal momentum distributions (single-differential cross sections $d\sigma^+/dp_{\parallel}$) of the recoil ion for single ionization of He by proton impact (Dörner *et al* 1995a). Full curve, ground-state momentum distribution (Compton profile) of He from Eisenberg (1970) for a qualitative comparison.

experiment and n CTMC as well as CDW-EIS results was obtained for all collision energies investigated (Dörner *et al* 1995a, Wang *et al* 1996a). The $P_{R\parallel}$ -distributions were found to become substantially broader with increasing transverse momentum transfer in qualitative agreement with theoretical predictions of both models. As a possible explanation it was suggested that larger $P_{R\perp}$ correspond, on average, to collisions at smaller impact parameters leading to the preferential removal of electrons with increased initial-state momenta. Thus, an increasingly hot ion is left behind mirroring the fraction of the initial-state electron momentum distribution transferred to continuum states during the collision. It is interesting to compare the $P_{R\parallel}$ distributions at different projectile velocities. At large v_p (figure 13) the longitudinal recoil-ion momentum mainly mirrors the longitudinal momentum(a) of the emitted electron(s) $P_{R\parallel} \approx -\sum P_{e\parallel}^i$, since the other contributions in equation (4) become small. With decreasing v_p (figure 3) on the other hand $\sum P_{e\parallel}^i$ becomes increasingly unimportant resulting in an essential change of character of the $P_{R\parallel}$ spectra, now basically reflecting the energy loss of the projectile $\Delta E_p = (1/v_p)\Delta P_p$ (see also equation (2) in section 3).

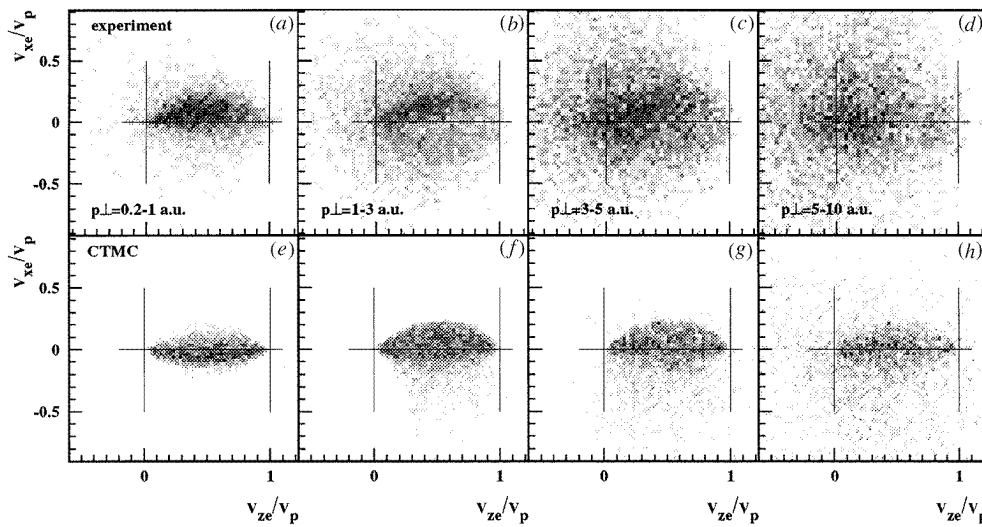


Figure 15. Projection of the velocity distribution of electrons for single ionization in 15 keV p-He collisions onto the scattering plane, defined by the beam axis (z) and the momentum of the target ion, recoiling into the negative x -direction (Dörner *et al* 1996a). The target centre is at $(0, 0)$ and the projectile at $(1, 0)$. Experiment for different transverse momenta, i.e. impact parameter, (a)–(d); n CTMC calculations, (e)–(h).

Very recently, a second set of highly differential experiments on single ionization was performed for 5–15 keV proton impact on helium (Dörner *et al* 1996a). Using an experimental set-up as described in the last paragraph of section 2.4, the two-dimensional momentum distribution of very low-energy continuum electrons ($E_e \leq 13$ eV) was determined for defined impact parameter ($P_{R\perp}$) and orientation of the scattering plane. In figure 15 the measured electron-emission characteristics projected onto the collision plane is shown along with n CTMC results for different transverse momentum transfers to the recoil ion. The coordinate system was chosen such that the projectile initially travels along the positive z -axis and the recoil ions' transverse momentum is along the negative x coordinate. The velocities of the emitted electrons are given in units of the projectile velocity. From the

magnitude of the recoil-ion transverse momenta compared to those of the emitted electrons it was concluded that at these slow collisions $P_{R\perp}$ is mainly compensated by $P_{P\perp}$ being deflected in the direction of the $+x$ -axis (see the discussion by Dörner *et al* (1996a) and figure 3 in this paper). This conclusion was found to be in agreement with the results of classical calculations showing a close relationship between the internuclear impact parameter and the recoil-ion (or projectile) transverse momentum. At low collision energies the heavy particle's transverse deflections are dominated by their internuclear repulsion (therefore an impact parameter as well as the collision plane can be obtained from the recoil-ion scattering).

This feature is substantially different from the situation at larger v_p . At small perturbations and large velocities it was found that the projectile is mainly scattered off the target electron for projectile scattering angles below 0.55 mrad (see the discussions in Kamber *et al* (1988), Dörner *et al* (1989, 1991), Horbatsch (1989a, b), Olson *et al* (1989b), Salin (1989), Fang and Reading (1991), Fukuda *et al* (1991), Gensmantel *et al* (1992), Moshhammer *et al* (1996a), Rodríguez (1996)). Going to large perturbations ($q/v_p > 2$) at large velocities the characteristics of the three-particle dynamics changes again significantly: now the two-body recoil-ion–electron interaction dominates the three-particle interaction which is obvious from figures 13 and 16. The details of the two-centre collision dynamics and its characteristic variation as a function of the perturbation strength and velocity has recently been discussed systematically on the basis of CTMC calculations by Olson *et al* (1997) (see also forthcoming paper by Moshhammer *et al* (1997b)).

In figure 15, a dramatic change in the electron-emission characteristics was observed with varying $P_{R\perp}$. At small transverse momenta the electron-emission mainly proceeds into the forward direction with a broad maximum centred around $v_{ez} = v_{e\parallel} = \frac{1}{2}v_{p\parallel}$, i.e. at the velocity of the saddle point of the internuclear potential (the z -direction is identical to the \parallel -direction). The existence of these 'saddle-point electrons' has been predicted in early and recent classical calculations (Olson 1983, 1986, Bandarage and Parson 1990, Wood and Olson 1996) and has been discussed in various quantum mechanical approaches (see, e.g., Winter and Lin 1984, Solovov 1990, Barany and Ovchinnikov 1993, Janev *et al* 1994, Macek and Ovchinnikov 1994, Pieksma *et al* 1994, Ovchinnikov and Macek 1995). The potential between the projectile and the residual target ion has one point, the saddle point, where no force acts on an electron. As the projectile and target separate the saddle potential rises and electrons moving with the longitudinal velocity of the saddle point during the collision are finally left stranded in the continuum. In terms of quantum mechanical molecular orbital (MO) calculations this process has been described qualitatively and has been termed the T00 or T01 mechanism where the electron is promoted into the continuum via hidden crossings between the molecular orbitals (Macek and Ovchinnikov 1994, Pieksma *et al* 1994, Ovchinnikov and Macek 1995). At intermediate $P_{R\perp}$ a distinct asymmetry was observed in that the electrons are mainly emitted to the side of the emerging projectile, opposite to the recoil ion. At 10 keV a 'horseshoe'-like pattern was found with a minimum at the saddle point changing to an asymmetry in the direction of the recoiling target ion at 5 keV. It was suggested that the strong velocity dependence of the emission characteristics might be explained qualitatively as an interference between T00 and T01 promotion amplitudes. Finally, at large $P_{R\perp}$ and close collisions, the electron-emission essentially becomes target centred with considerably increased electron momenta in the continuum. All the observations at 15 keV were found to be in reasonable agreement with the results of further developed CTMC calculations where the electrons are initialized in a model potential determined from quantal variational calculations (lower part of figure 15). Here, the usual microcanonical initial distribution was improved by applying a Wigner

distribution (see also Eichenauer *et al* 1981) of 10 initial binding energies so that the quantum mechanical radial probability distribution was reproduced over four orders of magnitude. For antiproton collisions at 100 keV a strong backwards emission of the electrons opposite to the direction of the emerging recoil ion was predicted (Wood and Olson 1996). Very recently, the time-dependent Schrödinger equation for the electronic motion in the field of the two nuclei moving on classical trajectories was solved numerically by discretization using a Cartesian mesh (Horbatsch 1996, Chassid and Horbatsch 1995, 1997; see also Schultz *et al* 1996). The calculations were performed for proton on hydrogen collisions at a projectile velocity of 1 au. It was found that the ionization process in this velocity regime populates electron continuum states with small transverse momenta to the beam axis and longitudinal momenta around the saddle-point region.

To summarize, combined high-resolution recoil-ion electron momentum spectrometers have, for the first time, enabled kinematically complete experiments on target single ionization in ion–atom collisions. A rich structure in the emitted electron spectra sensitively depending on the magnitude of the recoil-ion final momenta has been observed in very different regimes of projectile charge states and velocities. The three-particle momentum exchange has been explored in great detail and it was shown that the differential cross section as a function of the recoil-ion longitudinal momentum is directly related to the doubly differential electron-emission cross section. Thus, recoil-ion momentum spectroscopy alone can be understood as being complementary to electron spectroscopy, being ideally suited to investigating the emission characteristics of very low-energy electrons. Certainly, these first experimental investigations will be the starting point for further systematic studies, presently anticipated in different laboratories using positrons, antiprotons or fast heavy ions as projectiles.

Double ionization of the target. Double ionization of helium in collisions with bare projectiles is the simplest charged-particle-induced multiple-ionization reaction. Its investigation is fundamental for the understanding of the role of static and dynamic electron–electron correlation in multi-electron transitions and therefore has been central to many experimental and theoretical ion–atom research activities. Despite its outstanding importance mainly total cross section measurements were performed (for an overview see McGuire (1991), McGuire *et al* (1995), Ullrich *et al* (1993b, 1994b)) and only a few investigations on the differential momentum of one of the emitted particles have been reported in the literature (Giese and Horsdal (1988), Dörner *et al* (1991), Kristensen and Horsdal-Pedersen (1990), Skogvall and Schiwietz (1990, 1992), Salin (1991), Meng *et al* (1993), Schiwietz *et al* (1994a), Ullrich *et al* (1994b), for an overview see Ullrich (1994)). No kinematically complete measurements have been feasible up to now due to the enormous difficulties in analysing the final momenta of three emerging particles in coincidence and applying conventional spectroscopy for the electrons and the ions.

Using the reaction microscope with three independent electron detectors as shown in figure 2 and described in section 2.4, a pioneering kinematically complete experiment on helium double ionization by 3.6 MeV u⁻¹ Se²⁸⁺ impact has been performed recently (Moshhammer *et al* 1996d). In figure 16 the longitudinal momentum balances, along the beam direction, for helium double ionization are shown. Two important features were discussed in close analogy with single ionization by Ni²⁴⁺. First, the momentum transfer by the projectile in each individual ionization reaction was again found (see figures 4 and 13 for single ionization) to be negligibly small compared with the measured final momenta of the recoil-ion ($P_{R\parallel}$) and the electrons ($\sum P_{e\parallel}^i$). These recoil-ion and electron momenta

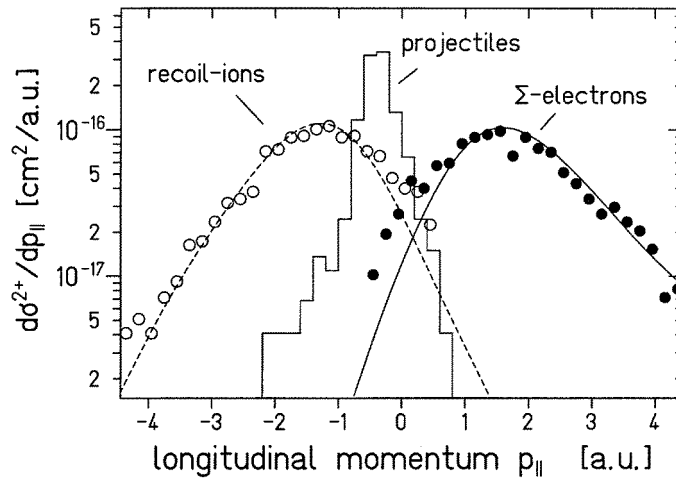


Figure 16. Longitudinal momentum distributions $d\sigma^{2+}/dp_{\parallel}$ for the sum-momentum of the electrons and the He^{2+} ions as well as the momentum change of the $3.6 \text{ MeV u}^{-1} \text{ Se}^{28+}$ projectile for He double ionization (Moshhammer *et al* 1996d). Curves, *n*CTMC calculations on an absolute scale.

consequently have been considered to result from the bound-state electron momentum distribution of the helium atom in the initial state. Both, therefore, should closely reflect the correlated longitudinal sum-momentum distribution of the electrons in the initial state, i.e. the two-electron Compton profile. Since the total momentum of the helium atom is zero in the initial state it follows that $\sum P_{e\parallel}^i \approx -P_{R\parallel}$, a feature which is visible in the data. As for single ionization the fast projectile was observed to deliver energy but only little momentum. Secondly, electrons were found with positive momenta emitted into the forward direction, whereas recoil ions were emerging backwards. Classical calculations demonstrated the PCI between the target fragments and the projectile to be responsible for this behaviour.

Both observations were well described by classical calculations (curves in figure 16) where two independent, distinguishable and classical electrons were initialized on different Kepler orbits bound with the sequential experimental binding energies (*n*CTMC, Olson *et al* 1989a). Surprisingly, explicit quantum mechanical features like the spatial (momentum) correlation of the electrons due to the symmetry of the wavefunction (Fermi statistics) or the direct (e-e) interaction due to the $1/r_{12}$ potential between the two electrons did not have to be included to describe the longitudinal sum-momenta of the emitted electrons. This changed dramatically when the correlated two-electron emission was explored in detail as shown in figure 17 where the longitudinal momenta of both electrons ($P_{e1\parallel}$ versus $P_{e2\parallel}$) are plotted integrated over all recoil-ion transverse and longitudinal momenta (upper left-hand figure). A distinct pattern was found: if one electron is slow the other one will most likely be fast. This feature was even more pronounced for neon double and triple ionization (lower part of the figure). In a series of classical model calculations the authors demonstrated that a reasonable, but still not perfect description of the experimental result was only obtained when the $1/r_{12}$ electron-electron interaction was explicitly included after both electrons had a positive energy relative to the target nucleus (double ionization).

The fact that no substantial momentum is transferred by the projectile during the collision supports the assumption that the observed patterns might be essentially a result of the initial-

state electron correlation. The authors therefore used a correlated helium wavefunction (Regier and Thakkar 1984) to calculate the ground-state probability distribution of the two electrons in the longitudinal momentum space, i.e. in the $P_{e1\parallel}$ versus $P_{e2\parallel}$ plane. For a qualitative comparison with the experimental data the electron–projectile PCI was estimated from the classical calculations and approximately accounted for by shifting the whole distribution by $P_{e1\parallel} + P_{e2\parallel} = 0.6$ au (upper right-hand corner of figure 17). Surprisingly, the shape of the experimental distribution was well reproduced again, supporting the conclusion that the measured patterns strongly reflect the initial-state correlated two-electron wavefunction. For neon double and triple ionization (figure 17) similar, even more

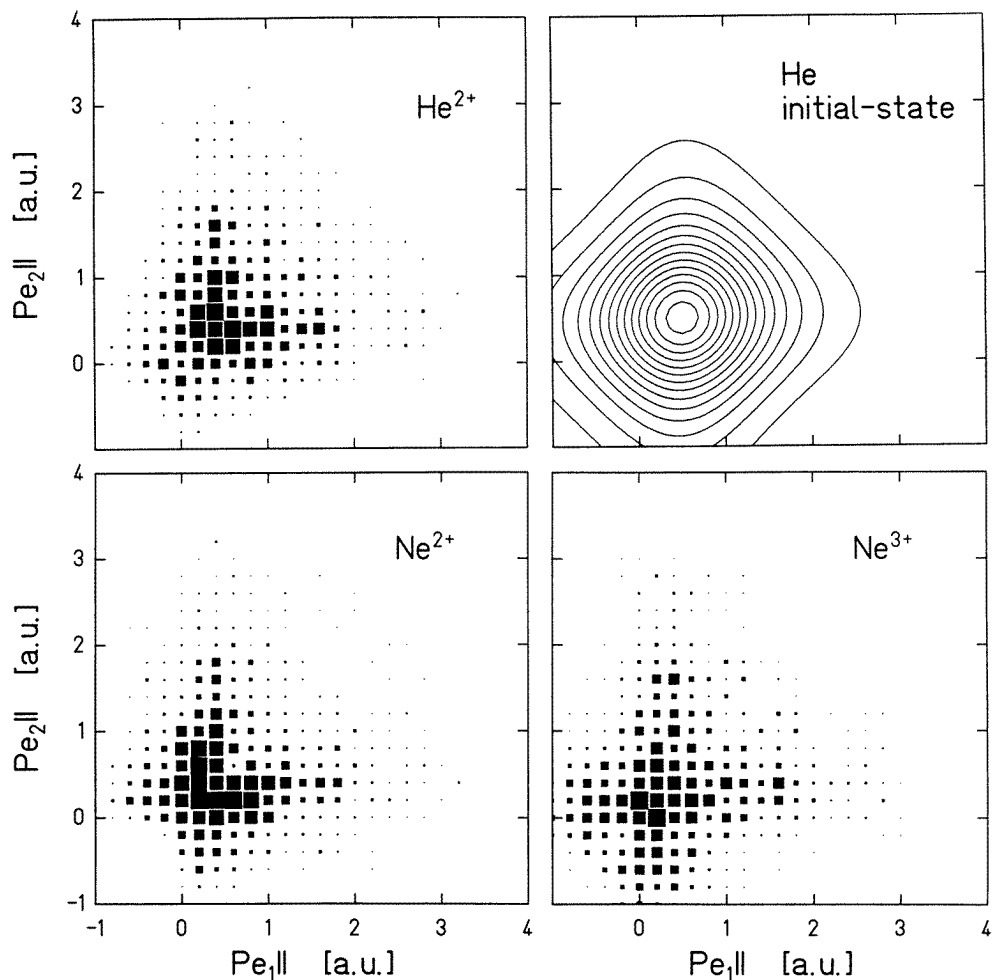


Figure 17. $p_{e1\parallel}$ versus $p_{e2\parallel}$ of the two electrons emitted for double ionization of helium (upper left-hand corner), Ne double (lower left-hand part) and Ne triple ionization (lower right-hand part) for $3.6 \text{ MeV u}^{-1} \text{ Se}^{28+}$ impact (Moshammer *et al* 1996d). Different box sizes represent the cross sections $d^2\sigma^{2+}/dp_{e1\parallel}dp_{e2\parallel}$ in $1.0 \times 10^{-6} \text{ cm}^2 \text{ au}^{-2}$ (largest box) on a linear scale for helium. Results for neon are scaled on the maximum differential cross sections, respectively. Upper right-hand part, projection of a 16-parameter correlated two-electron momentum space wavefunction (Regier and Thakkar 1984) onto the $p_{e1\parallel}$ – $p_{e2\parallel}$ plane (see text). The contour lines are on a linear scale.

pronounced patterns were observed. Since only two out of three electrons are detected for Ne^{3+} production, which means effectively integrating over all momenta of the unobserved electron, it was concluded that such a pattern can only occur if all three electrons in the continuum are strongly correlated.

Finally, these results were interpreted (Moshhammer *et al* 1996a) by viewing the attosecond ($\sim 10^{-18}$ s), extremely intense ($\sim 10^{18}$ W cm $^{-2}$) electromagnetic pulse which is generated by the passing highly charged projectile as a field of virtual quanta (Weizsäcker–Williams formulation for the ionization by relativistic projectiles). In this picture each one of both the (three) He(Ne) electrons is independently ‘photoionized’ by absorbing one virtual photon with an energy corresponding to the individual electron momentum at the instant of ionization. A negligibly small momentum is transferred and no significant momentum exchange between the electrons themselves or between each electron and the helium nucleus may take place since the collision time is short compared with the electron revolution frequency in the bound state. Thus, it was concluded that the initial-state correlation evolves in a dynamically correlated way into the continuum and is finally observed in the strongly correlated two-(three-)electron continuum. Recently, systematic quantum mechanical calculations have been performed on the basis of these considerations (Keller 1997) for He double ionization by 3.6 MeV u $^{-1}$ Se $^{28+}$ and 2 GeV u $^{-1}$ U $^{92+}$ impact.

An interesting parallel can be found in nuclear physics: in recent experiments the ‘equivalent photon method’ (also termed the ‘Heisenberg microscope’) has been exploited to extract information on the short-time angular correlation between the two halo neutrons in the ground state of ^{11}Li (Ieki *et al* 1996). It was concluded that the ground-state n–n correlation is accessible without the need for an elaborate theory if two requirements are met. First, the momentum of the absorbed virtual photon has to be small compared to the momenta of the core and each of the neutrons in the initial state. Secondly, the absorption process should be so fast that the positions of the three constituents are not significantly changed. Both requirements have been fulfilled in both experiments.

Again, these first kinematically complete measurements of double ionization in an ion–atom collision underline the substantial experimental improvement initialized by recoil-ion momentum spectroscopy. In this case, the successful and consequent transfer of techniques being developed to efficiently analyse the recoil-ion momentum, i.e. the projection of reaction products onto position-sensitive detectors by appropriate external fields finally enabled these new generation experiments. Due to the large solid angles reached for all of the particles leading to quadruple detection efficiencies of the order of a few per cent and to coincidence rates for double ionization of up to 100 s $^{-1}$, experiments of this kind are feasible and are presently prepared for a broad range of projectile perturbations and for various projectile species.

Multiple ionization of the target. The experimental investigation of multiple target ionization in ion–atom collisions might be considered to be rudimentary and too complex to yield specific information on the collision dynamics and initial-state correlation of the electrons. Indeed, so far mostly total charge production cross sections or total cross sections for defined final charge states of the projectile and the target have been measured (for an overview see Cocke and Olson (1991)). Data which are differential in the projectile deflection for particular projectile and target charge states (Kelbch *et al* 1988, 1989) or experiments differential in the projectile energy (Schuch *et al* 1988) mostly suffered from the fact that the scattering angles of interest, contributing dominantly to multiple ionization, were barely accessible experimentally. Experiments performed using early

RIM spectrometers with a gas cell target significantly improved this situation. Transverse momenta corresponding to μrad projectile deflection angles became observable (Ullrich 1987, Ullrich and Schmidt-Böcking 1987, Ullrich *et al* 1988a, b, 1989, 1991, 1993a, b) and were partly measured in coincidence with the projectile scattering angle (Dörner *et al* 1989, 1991, Forberich *et al* 1991, Gensmantel *et al* 1992, Lencinas *et al* 1993a, b). Still, however, many interesting questions on the dynamics of many-electron transitions to the continuum, on the energy loss of the projectile, on the deflection of the projectile or the momentum balance of all the particles involved were not yet accessible due to limited resolution. Kinematically complete experiments for multiple ionization were definitely beyond the experimental capabilities.

Again, this situation changed with the development of the newest generation RIM spectrometers and reaction microscopes. The resolution now achieved is generally sufficient to provide conclusive proof of theoretical predictions provided by semiclassical and $n\text{CTMC}$ (n -body CTMC) calculations (Olson *et al* 1987, 1989a, Horbatsch 1989b, 1992, Ullrich *et al* 1989). A strongly collective emission of the electrons for multiple ionization by heavy ion impact was calculated where the electrons are scattered to the side of the incoming projectile into the forward direction and opposite to the recoiling target ion. Accordingly, the recoil ion compensating most of the emitted electron sum-momentum was found to be backward scattered and the projectile should be deflected to ‘negative’ scattering angles, i.e. to the recoil-ion side for most of the ionizing collisions.

Two recent experimental studies on multiple-target ionization for $5.9 \text{ MeV u}^{-1} \text{U}^{65+}$ on Ne (Unverzagt *et al* 1996) and for $6.7 \text{ MeV u}^{-1} \text{Xe}^{44+}$ on Ar collisions (Jardin *et al* 1996) were performed to investigate these features exploiting recoil-ion momentum spectroscopy. The resolutions achieved were around 0.7 au for Ne, 0.25 au for Ar^+ and 9 au for Ar^{7+} corresponding to a projectile scattering angle resolution between 0.1 and $5 \mu\text{rad}$. In both of the experiments the recoiling target ions were found to be scattered into the backward direction with increasingly negative $P_{R\parallel}$ for increasing final charge states as illustrated in figure 18 for Xe on Ar collisions. Due to the large projectile velocities of about 15 and 20 au, respectively, the recoil-ion longitudinal momentum mirrors the longitudinal sum-momentum of the emitted electrons. To a good approximation one obtains $P_{R\parallel} \approx -\sum P_{e\parallel}^i$ (see equation (4) and the discussion in section 3.1). Thus, for the first time two experiments have independently provided information on the collective behaviour of electrons emitted in multiple-ionization events and verified the theoretical prediction that the electrons are emitted predominantly into the forward direction. The resulting electron energy distributions were estimated from the recoil-ion data by Jardin and co-workers. Similar results were found by Unverzagt *et al* who obtained a mean electron longitudinal sum energy for Ne^{6+} production of 1.1 keV which is in quantitative agreement with the estimated value for Ar^{6+} of about 1.4 keV.

Moreover, an excellent agreement in shape and absolute magnitude between the measured differential cross sections as a function of the longitudinal and transverse recoil-ion momenta for the different Ne charge states and the results of $n\text{CTMC}$ calculations was found (Unverzagt *et al* 1996). This is illustrated in figure 19 for $d\sigma^{i+}/dP_{R\perp}$. It has been pointed out by Unverzagt and co-workers that the recoil-ion transverse momenta (which were also measured by Jardin *et al*) are not unambiguously connected with the emission characteristics of the electrons. The balance between the nuclear and the electronic momentum exchange has to be considered which may change with increasing number of electrons emitted. Therefore, the transverse momentum distributions for the different recoil-ion charge states sensitively monitor the full dynamics of the collision where the interplay of all active particles has to be taken into account. The excellent

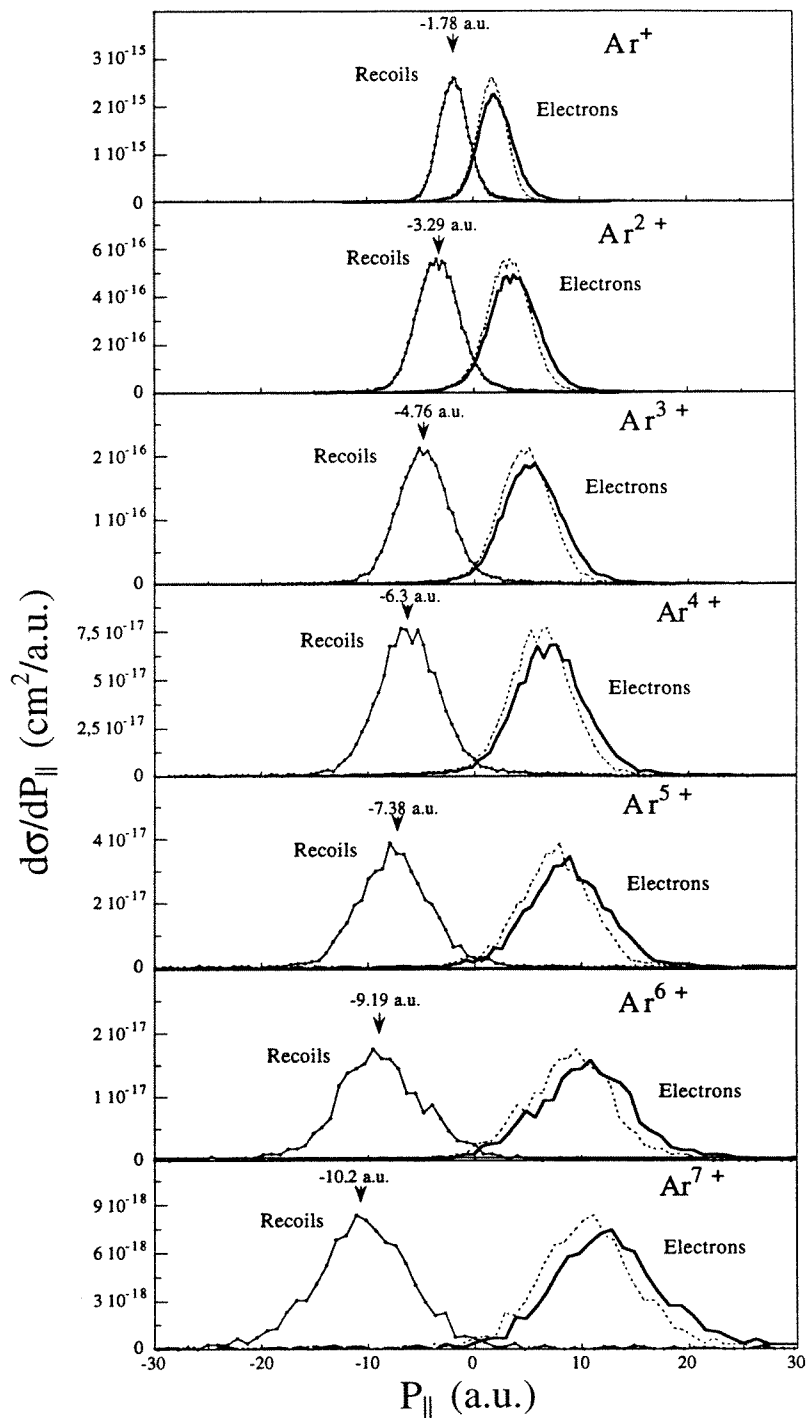


Figure 18. Measured longitudinal recoil-ion momentum distributions for Ar multiple ionization by $6.7 \text{ MeV u}^{-1} \text{ Xe}^{44+}$ impact (Jardin *et al* 1996). The electron momentum distributions are estimated from equation (4) assuming a negligibly small Q -value (broken curve) or taking it approximately into account (full curve).

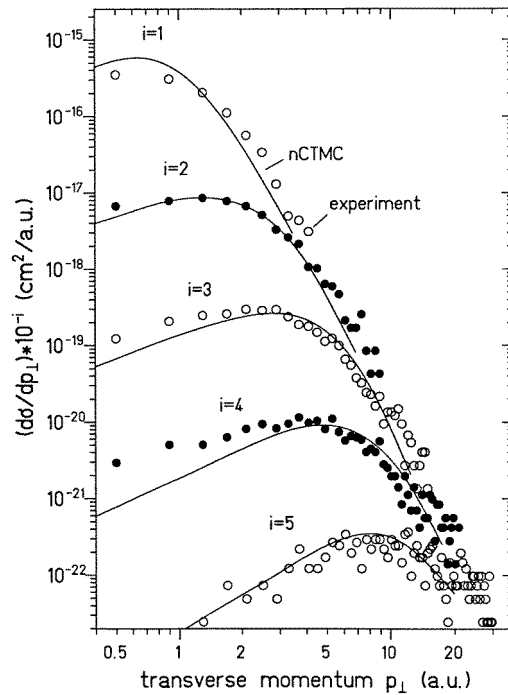


Figure 19. Experimental (full circles) and absolute theoretical (*n*CTMC, curves) transverse momentum distributions of the recoil-ions for *i*-fold ionization of Ne in collisions with $5.9 \text{ MeV u}^{-1} \text{ U}^{65+}$ impact (Unverzagt *et al* 1996).

agreement of the experimental $P_{R\perp}$ distributions with the theoretical results demonstrates the validity of the *n*CTMC approach in the regime of strongly non-perturbative collisions. Moreover, it provides a strong hint that the theoretical prediction of ‘negative’ projectile scattering angles, which could not be verified directly in these initial experiments is correct.

From the discussion of the previous results of He single and double ionization for Ni^{24+} and Se^{28+} impact two other conclusions might be drawn here. First, the forward emission of the electrons can most probably be considered to be due to the PCI not only for single and double but also for multiple ionization. The agreement of the data with theory demonstrates the ability of any classical calculation to accurately treat the many-body Coulomb continuum, still being an unsolved problem of quantum mechanical calculations even for only three particles in final continuum states (see also Rost 1994a, b, 1995). Furthermore, the direct momentum transfer from the projectile to the electrons can be estimated to be much smaller than the width of the observed $P_{R\perp}$ distributions even for multiple ionization. As for He double ionization, this leads to the second important conclusion that the widths of the distributions are then closely related to the many-electron correlated sum-momentum distributions in the bound initial state of the atom. Thus, the many-electron classical ground state modelled in the *n*CTMC approach by initializing the individual independent electrons on Kepler orbits with the sequential experimental ionization potentials seems to correctly account for the bound-state many-electron sum-momentum distribution, a statement which is far from trivial.

It has been emphasized (Kollmus *et al* 1997) that the momenta of at least five electrons

emerging from a single multiple-ionization event will be simultaneously measurable in the near future by exploiting the full capabilities of reaction microscopes. This will provide the first information on the many-electron final- and initial-state correlation along the lines discussed for He double and Ne triple ionization. Furthermore, from the measurement of the longitudinal electron momentum components alone it will be possible to extract the projectile energy loss in a single ion–atom collision with a resolution $\Delta P_p/P_p$ on the order of 10^{-7} – 10^{-9} for relativistic projectiles. This is orders of magnitude better than the precision achievable with conventional energy-loss spectroscopy for single (Schuch *et al* 1988) or multiple collisions at relativistic energies of $\Delta P_p/P_p = 4 \times 10^{-7}$ (Scheidenberger *et al* 1994). Finally, the transverse scattering of the projectile will be directly deducible from the measured transverse momenta of the recoil ion and the electrons with a resolution which can be expected to be sufficient to test the theoretical prediction of negative projectile deflection angles.

4.1.3. Ionization of the projectile. The ionization of a non-bare projectile in an ion–atom collision may proceed via an interaction of the projectile electron with an electron (e–e) or the nucleus (e–n) of the target. This has been pointed out early on and calculated within the first Born approximation by Bates and Griffing (1953, 1954, 1955). In general, the role of (e–e) or (e–n) interactions in various reactions like the resonant (RTE) and radiative (REC) electron capture or the emission of a binary-encounter electron have been studied in great detail as analogous processes to the corresponding free-electron ion interactions, namely dielectronic recombination (DR), radiative recombination (RR) and the elastic scattering of a free electron at an ion. In the past, all of these latter processes were clearly identified in ion–atom collisions due to their unique signatures which are the resonant behaviour (RTE), the emission of photons with a characteristic energy distribution (REC) or the occurrence of a well separated peak in the electron-emission spectra (for a recent review see *Recombination of Atomic Ions* (Graham *et al* 1992)).

Excitation of projectile electrons by an (e–e) interaction with one of the target electrons has been identified using high-resolution zero-degree electron spectroscopy by Zouros *et al* (1989), by Lee *et al* (1992) and by Hvelplund *et al* (1994) (for a recent overview see Zouros (1996)). The experimental signatures unique to the (e–e) interaction in projectile ionization have proved to be much less clear (McGuire *et al* 1981, Anholt 1986, Montenegro and Meyerhof 1991, 1992, Montenegro *et al* 1992). Experimental evidence was reported by Hülskötter *et al* (1989, 1991) who observed a shoulder in the total projectile ionization cross section as a function of the projectile energy just above the threshold for the (e–e) reaction. The threshold was broadened by the target electron Compton profile. Similar studies were performed by Montenegro *et al* (1992) at high projectile velocities where the (e–e) reaction dominates target ionization. Attempts were made to separate both processes kinematically by exploiting predicted differences in the projectile deflection angles, but the results suffered strongly from the limited angular resolution in fast ion–atom collisions (Montenegro *et al* 1993).

Two recent experiments (Dörner *et al* 1994, Wu *et al* 1994a) were able to clearly separate contributions from both processes to projectile ionization by investigating the longitudinal and transverse momentum transfer to the target ion by means of RIMS. As discussed by Dörner *et al* (1994), the momentum loss of the projectile ($\Delta P_{p\parallel} = -Q/v_p - E_e/v_p$) is compensated by the recoil ion in the case of the (e–n) interaction scattering the recoil ion into the forward direction. In contrast, the ion can be considered as a spectator ($\Delta P_{R\parallel} \approx 0$) in the case of the (e–e) interaction where the active, quasi-free target electron balances

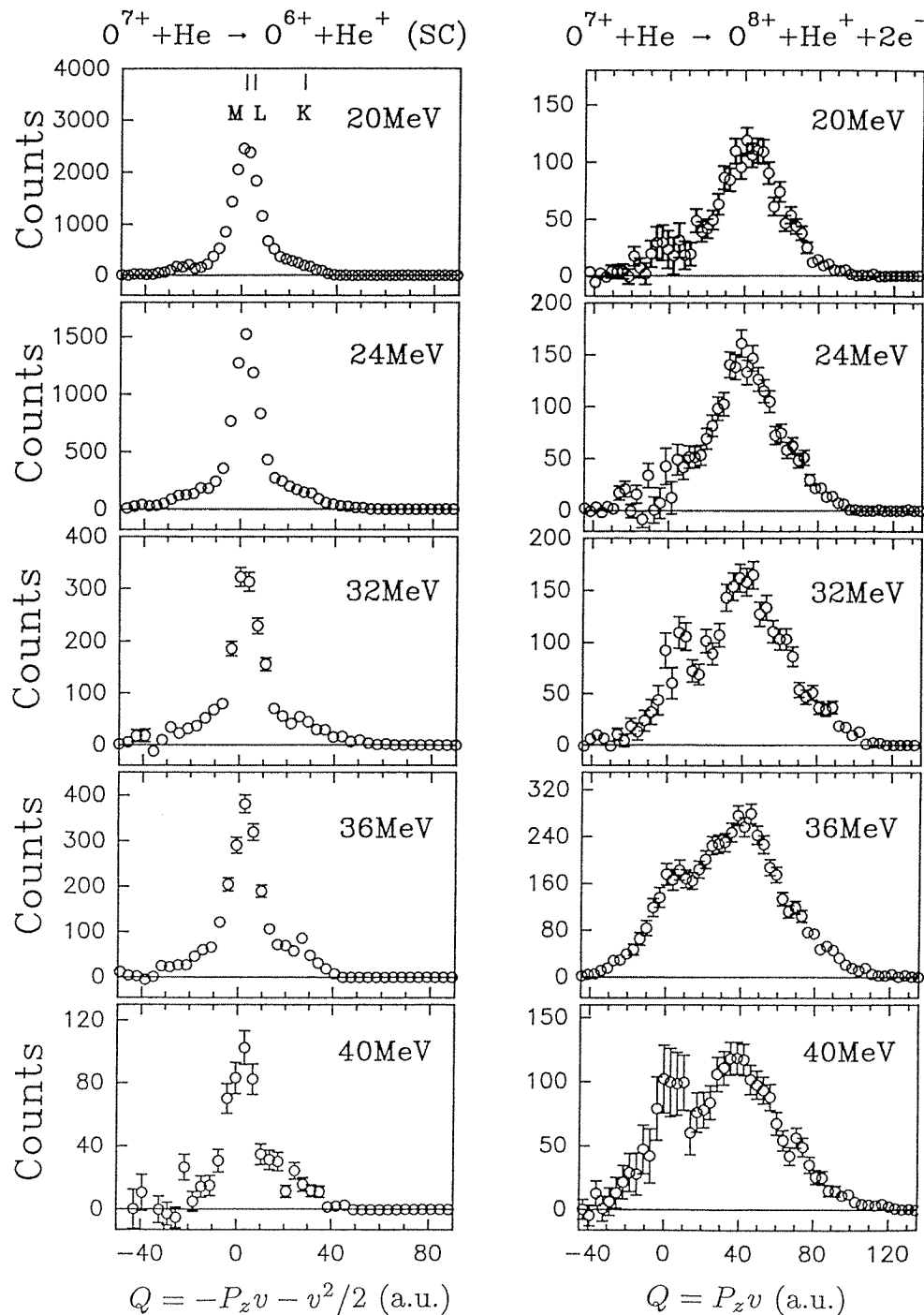


Figure 20. Q -value distributions (calculated from longitudinal momentum distributions of He^+ recoil ions) after single-electron capture (left-hand column) and projectile ionization (right-hand column) for O^{7+} on He collisions at various energies (Wu *et al* 1994a). The structure in the Q -value distribution at $Q \approx 0$ observed for projectile energies $E_p \geq 32$ MeV results from projectile ionization by the interaction with one of the target electrons (see text).

ΔP_{\parallel} . This kinematic difference has been observed in 0.5–2 MeV He^+ on He (Dörner *et al* 1994) as well as in 20–40 MeV O^{7+} on He collisions (Wu *et al* 1994a) and is illustrated in figure 20 for the oxygen projectile. Above threshold for the (e–e) reaction, which is at 25.6 MeV for O^{7+} , a second, well separated peak occurs at $Q \approx 0$. With increasing energy this peak becomes increasingly important and will dominate at high energies since the (e–e) interaction is a first-order process for the target ionization (Montenegro *et al* 1992), whereas the (e–n) mechanism for simultaneous ionization of the projectile and of the target is a second-order process. This was investigated in detail by Wu and collaborators (Wu *et al* 1994a) by plotting the ratio of both cross sections as a function of the projectile energy. Good agreement of the experimental data was obtained with the results of a model calculation where the (e–n) cross section was obtained from a plane-wave Born calculation and the (e–e) contribution was calculated by folding the free-electron ionization cross section (Coulomb–Born exchange calculation) into the Hartree–Fock Compton profile of He using the impulse approximation. In both experiments the transverse recoil-ion momentum was inspected simultaneously and the separation becomes even more evident in the two-dimensional $P_{R\parallel}$ – $P_{R\perp}$ plane. For the He^+ on He collision system the transverse as well as the longitudinal recoil-ion momentum distributions were found to be in good agreement with the results of ‘two-centre n -body CTMC’ calculations. Here, the He target is initialized in the usual n CTMC approach (see, for example, the previous section on ‘multiple ionization of the target’) and the He^+ projectile, i.e. the second centre, is equipped with one electron on a classical Kepler orbit and a binding energy according to the ionization potential of He^+ . During the encounter all mutual interactions between the active particles (both nuclei with each other, both nuclei with all of the electrons, the target electrons with the projectile electron) are taken into account. Replacing the He^+ projectile by an equal velocity electron beam Dörner *et al* (1994) showed that the recoil-ion momentum distribution peaked at the same $P_{R\parallel}$ and $P_{R\perp}$ for free-electron impact as observed before for the bound electron impact of the helium target. This is an other example as pointed out by Wu and co-workers (Wu *et al* 1994a) where ‘the results reveal the power of recoil-ion momentum spectroscopy to separate mechanisms which are difficult to distinguish by other methods’.

4.2. Photon–atom collisions

A further, important and rapidly developing field of atomic collision physics where recoil-ion momentum spectroscopy has enabled a new generation of experiments with respect to completeness, selectivity and energy range that can be covered, is the ionizing interaction of photons with target atoms. Especially at large photon energies or close to multiple-ionization thresholds the ionization cross sections are quite small, for instance, of the order of barns for helium single ionization by keV photon impact. Thus, in these regimes the investigation of multiple photoionization or Compton scattering on gas targets are facing tremendous difficulties if conventional techniques are applied. Even at intermediate photon energies electron–electron coincidence experiments are barely feasible and only a few studies have been reported recently with coincidence rates as small as about 1000/day for electrons being detected under very favourable and, thus, restricted geometrical conditions.

Up to now RIMS has been used to explore double ionization of helium using photons with energies from about the double-ionization threshold at 80 eV to 58 keV, i.e. over the whole energy range available at modern synchrotron radiation facilities. Due to its fundamental nature, as the simplest collision-induced multiple-ionization reaction and the extreme sensitivity of the cross sections to the details of the electron–electron interaction, double photoionization of helium has been the subject of outstanding intense experimental

and theoretical research activities during the last few years. Numerous experimental investigations provided systematic data for the comparison with a large number of theoretical models, many of them being developed very recently.

Mapping the complete momentum vector of the recoiling target ion after photoionization at high γ energies allowed us, for the first time, to separate contributions from Compton scattering and photoabsorption to helium single and double ionization (see section 3.2) which is reviewed in the next subsection. At low and medium energies the complete measurement of the ionization kinematics enabled unprecedented accuracy in measurements of total cross section ratios by integrating over all recoil-ion momenta. Moreover, a kinematically complete ($\gamma, 2e$) experiment on helium double ionization by 80 eV photons was performed recently visualizing the entire final nine-dimensional momentum space without any restrictions in relative emission angles and energies of the emerging three particles. These experiments on photoabsorption at low and medium photon energies are discussed in the second subsection. Only a short, admittedly selective outline on very recent helium photoionization experiments, seen in the light of recoil-ion momentum spectroscopy, can be given in this review. For a detailed overview of the field the reader is referred to the work of Schmidt (1992).

4.2.1. Double ionization of helium by Compton scattering. Compton scattering and photoabsorption are the two fundamental ionizing interactions of a photon with an atom. While Compton scattering can occur at a free electron where the momentum and energy conservation is fulfilled by the emerging photon and electron alone, a third particle is needed in the final channel for photoabsorption to balance the momentum of the emitted electron. Since the mutual Coulomb interaction between all three particles in the initial as well as in the final state are of comparable strength, the ratio of double to single-ionization cross sections $R_\gamma = \sigma^{2+}/\sigma^+$ depends sensitively on the details of the e–e correlation and is a challenging testing ground for theories. Due to the intrinsic differences of Compton scattering and photoabsorption this ratio has been predicted to be different for both mechanisms even in the asymptotic limit of high photon energies.

Experimentally, it has not been possible to separate between both processes having about the same cross sections for a helium target at a photon energy of 6 keV by only detecting the ion charge state (Levin *et al* 1991, 1993, 1996, Sagurton *et al* 1996). As was discussed by Samson *et al* (1994) (see section 3.2) and was demonstrated experimentally (figure 6) large recoil-ion momenta are present in the case of photoabsorption since the emerging electron momentum is compensated by the recoiling target ion whereas small P_R dominate for Compton scattering. In this way Spielberger *et al* (1995) were able for the first time to separate both processes even for double ionization as is illustrated in figure 21, providing the most accurate experimental value so far for the asymptotic high-energy limit for the photoabsorption cross section ratio of $R_{pa} = (1.72 \pm 0.12)\%$ at $E_\gamma \approx 8.8$ keV. This result is in close agreement with various theoretical predictions (Byron and Joachain 1967, Åberg 1970, Ishihara *et al* 1991, Dalgarno and Sadeghpour 1992, Andersson and Burgdörfer 1993, Hino *et al* 1994) and is in accordance with other experimental results which did not separate between both processes (Levin *et al* 1991, 1996).

The theoretical situation is much less clear for R_C , the cross section ratio for double to single ionization after Compton scattering of the photon, which was summarized in figure 22 by Spielberger *et al* (1996). Results of several recent calculations are available in the E_γ regime between 4 and 20 keV (Andersson and Burgdörfer 1994, Suric *et al* 1994, Bergström *et al* 1995) predicting substantially different energy dependencies as well

as absolute values of R_C . Also, the calculations for the asymptotic high-energy value of R_C differ by nearly a factor of two between the predictions of Amusia and Mikhailov (1995a, b) on one side with $R_C = 1.68\%$ and Andersson and Burgdörfer (1994) as well as Suric *et al* (1994) on the other side with about $R_C = 0.8\%$. Experimental data with the smallest error bars in the ratio have again been achieved using RIMS at 7.0 and 58 keV establishing a high-energy value of about $R_C = 0.84\%$ and suggesting an energy dependence supporting the calculations by Andersson and Burgdörfer. It is still unclear whether the asymptotic limit has already been reached at 58 keV energy and experiments are anticipated at E_γ between 50 and 150 keV at the Advanced Photon Source (APS) at the Argonne National Laboratory. Some other experimental data are available at energies between 10 and 20 keV (Levin *et al* 1996, Sagurton *et al* 1996, Samson *et al* 1996, Wehlitz *et al* 1996) which did not actively discriminate against photoabsorption. In principle, this is not crucial for a measurement of R_C in this E_γ regime since the relative contribution of photoabsorption is less than 1% at energies above 15 keV. Due to the extremely small cross sections for He double ionization of about 10 mbarn, however, and the limited photon flux available at present photon sources, the recoil-ion momentum measurement has turned out to be essential for the suppression of the background and the clean identification of the Compton

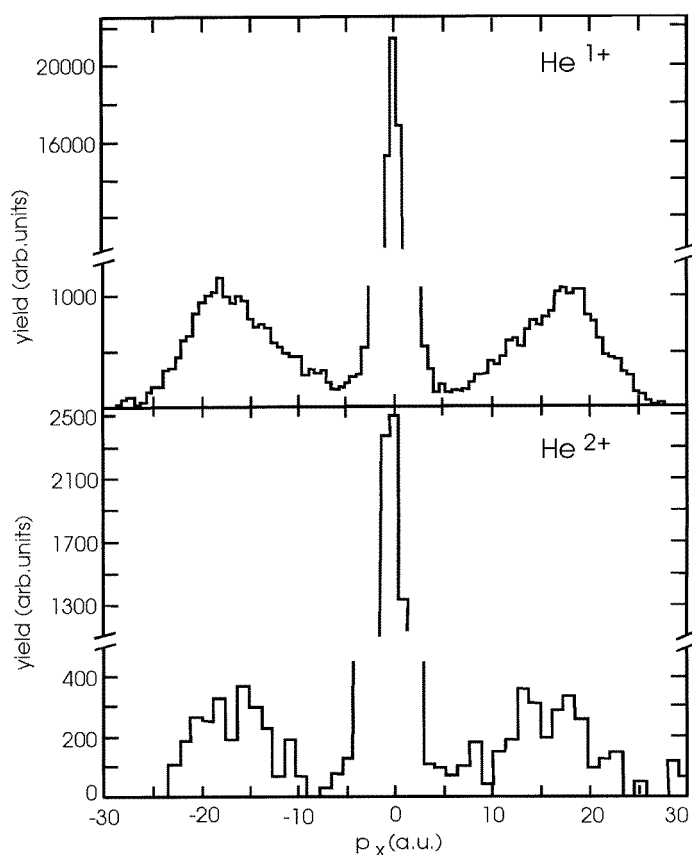


Figure 21. Momentum distributions of He^+ and He^{2+} ions produced by 8.8 keV photons (Spielberger *et al* 1995). The x -axis is the direction of the electric field vector of the linearly polarized light (projection of figure 6 onto the x -direction).

events.

Presently, further measurements are under way in order to establish an experimental energy dependence of the ratio which can decide between the results of the different calculations. The first experiments briefly reviewed here applying RIMS can only be considered as a starting point for more systematic studies. Using reaction microscopes in the near future even kinematically complete measurements of double ionization after Compton scattering of high-energy photons can be envisaged.

4.2.2. Double ionization of helium by photoabsorption. While theoretical predictions on R_{pa} in the high-energy asymptotic limit were shown to be largely in agreement with each other, substantial disagreement on this fundamental number can be observed in figures 23(b) and (c) at lower photon energies where the ratio reaches its maximum at between 150 and 250 eV. Also, the fluctuations in the experimental data available up to now (figure 23(a)) were too large to clearly support either theoretical prediction. In general, it was believed that the data with a maximum value of the ratio of about 5% were the most accurate ones discarding the earliest measurements of Carlson (1967).

Recoil-ion momentum spectroscopy was used by Dörner *et al* (1996c, d) to map the full momentum vector of the recoiling photoionized helium target (see figure 5 for $E_\gamma = 80.1$ eV) in order to eliminate all possible sources of systematic errors discussed in the literature (Levin *et al* 1991, 1993, Berrah *et al* 1993). These are contributions of low-energy stray light or higher-order harmonic light, contributions due to ionization by

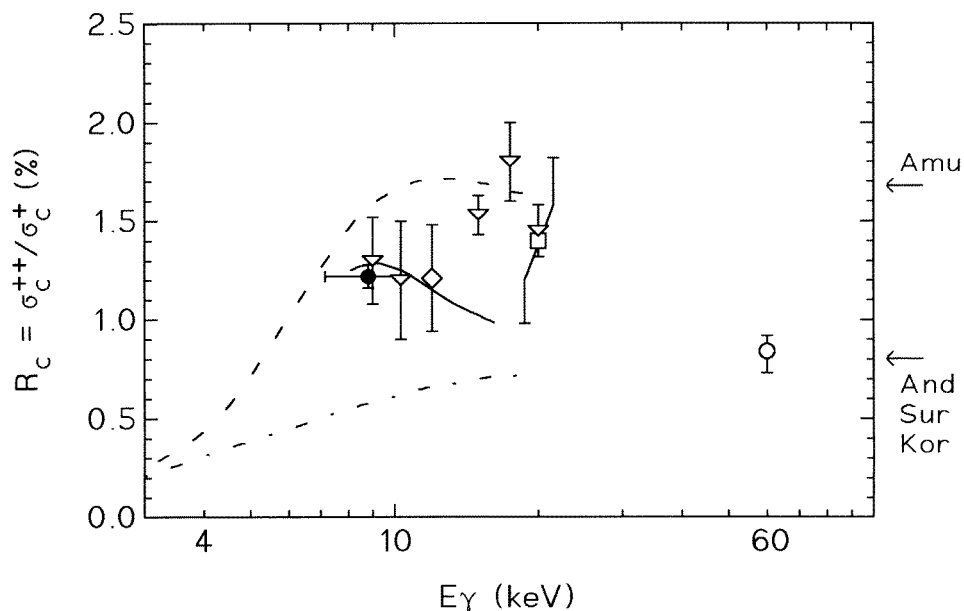


Figure 22. Ratios of double to single ionization, R_C , after Compton scattering as a function of the photon energy (Spielberger *et al* 1996). Experimental data: open circle (RIMS), Spielberger *et al* (1996); full circle (RIMS), Spielberger *et al* (1995); open triangles, Levin *et al* (1996); open diamond, Sagurton *et al* (1996). Theoretical results, broken curve, Bergström *et al* (1995); full curve, Andersson and Burgdörfer (1994); chain curve, Suric *et al* (1994). The arrows indicate the predicted asymptotic ratios $R_C = 1.68\%$ (Amu) of Amusia and Mikhailov (1995a, b) and $R_C = 0.8\%$ (And, Sur) of Andersson and Burgdörfer (1994) and Suric *et al* (1994).

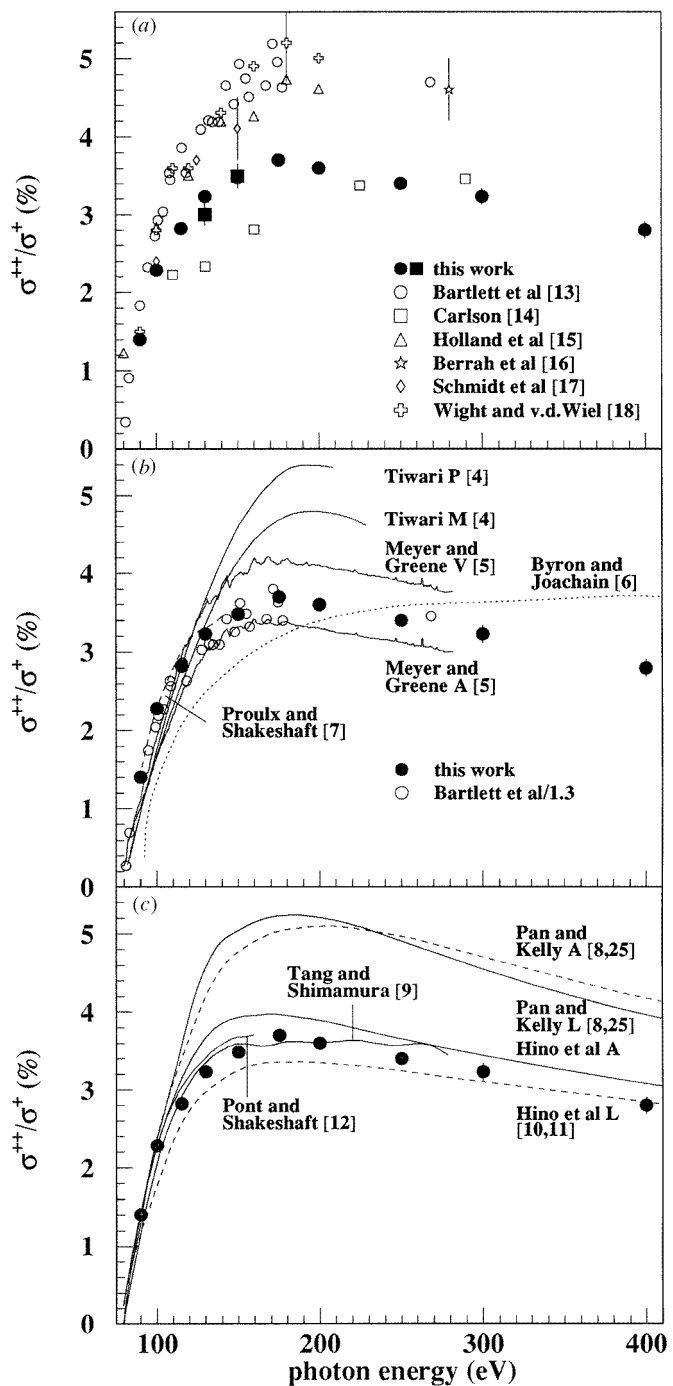


Figure 23. Ratios of double to single ionization, R , after photoabsorption as a function of the photon energy (Dörner *et al* 1996c). Full squares and full circles (RIMS), Dörner *et al* (1996c). Other experimental data and theoretical results as given by Dörner *et al* (1996c). The open circles in (b) are the same data as in (a) but scaled down by a factor of 1.3 (see Dörner *et al* 1996c). V, A and L stand for results obtained in the velocity, acceleration or length form, respectively. P and M denote position and momentum matrix elements, respectively.

photoelectrons created in the vicinity of the reaction volume, contaminations of H_2^+ having the same time of flight as He^{2+} or an enhanced detection solid angle for He^{2+} ions due to an enhanced acceleration in the electrostatic field. Surprisingly the data obtained using RIMS were found to be on average about 20% lower than all the older data except the first measurement of Carlson (1967) which has, however, a very different energy dependence. The data of Dörner *et al* strongly support the theoretical results of Pont and Shakeshaft (1995) and of Tang and Shimamura (1995) the latter representing the wavefunctions in hyperspherical coordinates to represent the bound states and the continuum yielding nearly identical results in the length and acceleration form.

Using a reaction microscope as described at the end of section 2.4, Dörner *et al* (1996d) were able to perform kinematically complete (γ , 2e) experiments at 1–80 eV above threshold to explore the three-body break-up of a bound system, which is one of the most fundamental and still intriguing problems of atomic collision physics (see, e.g., Maulbetsch and Briggs 1993a, b, 1995, Teng and Shakeshaft 1994, Pont and Shakeshaft 1995, Kazanski and Ostrovsky 1995). The vector momenta of all three escaping particles were determined simultaneously thus sampling the entire five-dimensional momentum space. At an excess energy of 1 eV above threshold a 4π solid angle was reached for all possible relative momentum partitions between the emerging two electrons and the He^{2+} ion. This is substantially different from previous experiments applying electron–electron coincidence techniques (Schwarzkopf *et al* 1993, 1994, 1995, Huetz *et al* 1994, Lablanquie *et al* 1995, Dawber *et al* 1995) where only subsets have been measured in coplanar geometry (the momentum vectors of the two electrons $\mathbf{k}_1, \mathbf{k}_2$ are in one plane). The effective data collection efficiency with the recoil-ion technique was orders of magnitude higher than those reached in the latter experiments.

To elucidate the mechanisms of the three-body break-up 1 eV above the double-ionization threshold Dörner and co-workers choose Jacobian momentum coordinates, i.e. $\mathbf{k}_r = \mathbf{k}_1 + \mathbf{k}_2$ and $\mathbf{k}_R = \frac{1}{2}(\mathbf{k}_1 - \mathbf{k}_2)$ of the electron centre-of-mass motion and the electron-pair motion, respectively. Neglecting the incoming photon momentum, the measured recoil-ion momentum is equal to $-\mathbf{k}_r$ and the electrostatic dipole operator is $\boldsymbol{\varepsilon} \cdot \mathbf{r}$ with $\mathbf{r} = \frac{1}{2}(\mathbf{r}_1 + \mathbf{r}_2)$. In figure 24 the momentum distributions for \mathbf{k}_r (the motion of the recoil ion), \mathbf{k}_1 (the motion of either electron) and for \mathbf{k}_R (the relative motion of the two electrons) are projected onto the y - z plane for $-0.1 \text{ au} < k_x < +0.1 \text{ au}$ where z is along the photon polarization vector and y is perpendicular to $\boldsymbol{\varepsilon}$ and to the direction of the incoming photon propagation along x . The He^{2+} recoil-ion distribution qualitatively displayed a dipole distribution, whereas such a behaviour was found to be completely washed out in the momentum distribution of either electron due to the strong interaction of both electrons in the final state. As mentioned by the authors, this feature has been observed before by Wehlitz *et al* (1991) and Dawber *et al* (1995). The relative motion of the two electrons (figure 24(c)), however, showed a distinct pattern indicating that the pair preferentially separates perpendicularly to the photon polarization axis and, thus, to the recoil-ion motion.

The discussion and clear interpretation of the experimental data in terms of Jacobian momentum coordinates highlights a further advantage of experiments performed using reaction microscopes. Since the full solid angle is covered for all of the fragments in kinematically complete experiments this allows, for the first time, a transformation of the experimental data to any set of suitable collective coordinates. Such coordinates quite often elucidate the characteristics of the correlated many-body motion in a much more natural, intuitive and better adapted way as has been demonstrated frequently in nuclear, molecular or solid state physics.

The Jacobi coordinates also illustrate the partition of the excess energy, i.e. the incoming

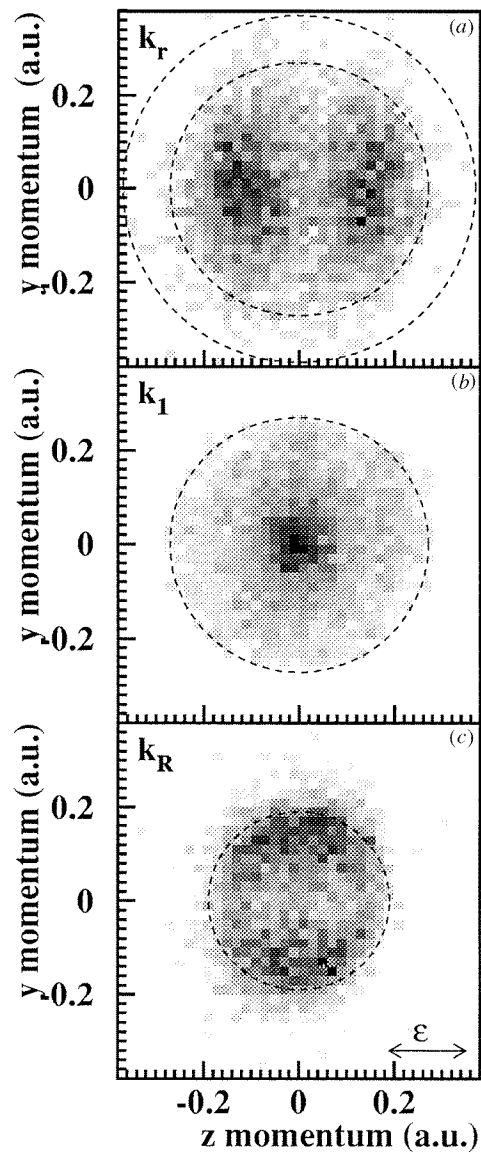


Figure 24. Density plots of projections of the momentum spectra from double ionization of He by 80.1 eV photons (Dörner *et al* 1996d, see text). The z - and y -components of the momentum are plotted on the horizontal and vertical axes, respectively, the polarization vector of the photons is in the z -direction and the photon propagates in the x -direction. Only events with $-0.1 \text{ au} < k_x < 0.1 \text{ au}$ are projected onto the plane. (a) The He^{2+} recoil-ion (or $-\mathbf{k}_r$) momentum distribution. The outer circle indicates the maximum possible recoil-ion momentum and the inner circle is the locus of events for which the \mathbf{k}_r motion has half of the excess energy. (b) The distribution of single-electron momenta (\mathbf{k}_1 or \mathbf{k}_2). The circle locates the momentum of an electron which carries the full excess energy. (c) The relative electron momentum (or $\mathbf{k}_R = \frac{1}{2}(\mathbf{k}_1 - \mathbf{k}_2)$) distribution. The circle identifies the maximum possible value for \mathbf{k}_R .

photon energy minus the He double-ionization threshold energy, between the electronic motion along \mathbf{k}_r (motion the electron centre of mass) and along \mathbf{k}_R (relative motion between

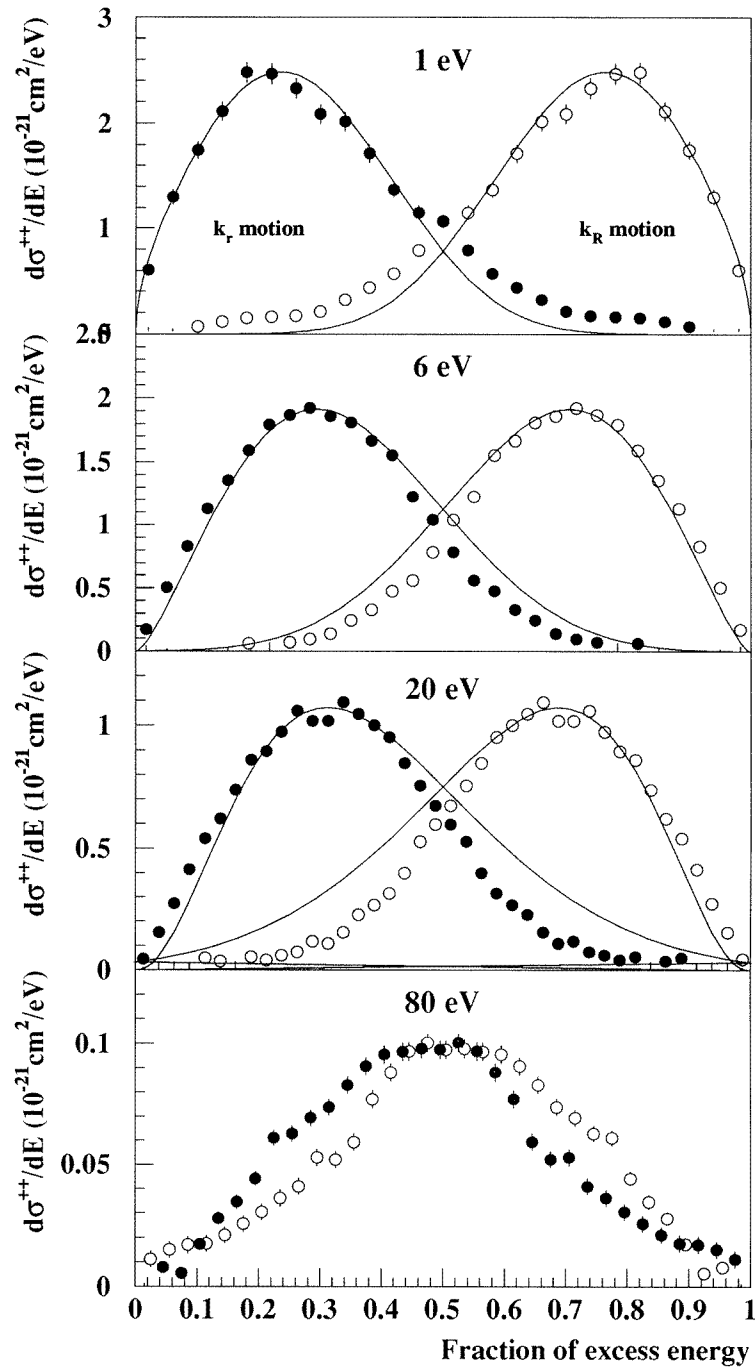


Figure 25. Cross sections differential in energy plotted as a function of the fraction of the excess energy in the k_r (full circles) or k_R (open circles) motion (Dörner *et al* 1996d). The full curve in the upper three figures is from a fourth-order Wannier calculation (see Feagin 1995, 1996). The theoretical curves are normalized at the maximum of the experiment, which is on an absolute scale.

the two electrons). This is shown in figure 25, where the fraction of the excess energy is plotted versus energy-differential double-ionization cross sections for both motions at different incoming photon energies above threshold. At threshold most of the excess energy drives the k_R motion whereas at 80 eV above threshold the energy partition between both motions was found to be about identical in good agreement with the results of a fourth-order Wannier theory (Feagin 1995, 1996). A close inspection of the recoil-ion emission characteristics revealed a substantial deviation from an exact dipole-like characteristics at 1 eV above threshold approaching such a pattern with increasing photon energy. The most recent *ab initio* calculations on the He^{2+} ion momentum and angular distribution by Pont and Shakeshaft (1995) show almost perfect agreement with the experiment at 20 eV above threshold in shape and absolute magnitude. These authors discuss in detail the connection of the ion momentum with the traditional fivefold differential cross sections emerging from electron coincidence studies.

In conclusion, applying recoil-ion momentum spectroscopy for the investigation of ionizing photon-atom interactions has provided the most precise data on the ratio of double to single-ionization cross sections for helium and, in addition, enabled the first separate measurement of this ratio for photoabsorption and Compton scattering at high photon energies. These data serve as benchmarks for recent theories. Moreover, a first set of kinematically complete experiments on helium double-ionization close to threshold have been reviewed delivering experimental information with unprecedented completeness on the full nine-dimensional momentum space for the three-body Coulomb break-up of helium. Experiments to extend such investigations to higher photon energies and to other target species are presently being performed at the Advanced Light Source (ALS) of the Lawrence Berkeley National Laboratory (LBNL).

4.3. Electron-atom collisions

A tremendous amount of experimental data has been collected on collisions of electrons with atoms, among them for a long time the most precise and complete measurements on single-target ionization in atomic collision physics. In these so-called (e, 2e) experiments the momenta of two outgoing electrons were measured simultaneously sometimes even using spin-polarized electrons as projectiles (for reviews see, e.g., Erhardt *et al* (1986), Weigold and McCarthy (1978), Lahmam-Bennani (1991)). However, due to experimental difficulties mostly coplanar final electron momenta have been investigated and only two (e, 3e) measurements, i.e. kinematically complete studies on double ionization of Ar by electron impact, have been reported in literature to the best of our knowledge (Lahmam-Bennani *et al* 1989, 1992). (e, 3e) experiments are extremely difficult to perform if conventional spectrometers are used to detect the three outgoing electrons and no such investigation on the fundamental He target, where the cross sections are considerably smaller, has been feasible up to now.

Using high-resolution recoil-ion momentum spectroscopy one experiment has been reported recently (Jagutzki *et al* 1996) on single and double ionization of He for 270–3200 eV electron impact. In the study of Jagutzki and co-workers differential, but still not kinematically complete, information on He double ionization was obtained. In figure 26 differential cross sections $d\sigma/dP_R$ as a function of the recoil-ion momentum ($P_R = (P_{R_x}^2 + P_{R_y}^2 + P_{R_z}^2)^{1/2}$) are shown for two different impact energies in comparison with experimental data from (e, 2e) experiments (Opal *et al* 1972, Oda 1975) and classical calculations (broken curve). Similarly to single ionization of He by 3.6 MeV u^{-1} Ni^{24+} impact the *n*CTMC result does not correctly predict the total cross section and was

multiplied by a factor of 2.9 by the authors for a better comparison with the shape of the experimental data. From the (e, 2e) results, derived from absolute $d\sigma/dE_e$ it can be concluded that the momentum transfer from the projectile to the ionized electron $k = |\mathbf{P}_o^f - \mathbf{P}_o^i|$ is typically very small with $k < 0.3$ au for more than 90% of the singly ionizing collisions ($\mathbf{P}_o^{f,i}$ are the final and initial electron momentum vectors, respectively). Under these conditions it was shown by the authors that $\mathbf{P}_R \approx -\mathbf{P}_e^{\text{slow}}$, i.e. the final recoil-ion momentum mirrors the momentum of the slowly emerging ionized electron, a behaviour that was found for single ionization in fast ion-atom collisions. Since the experimental recoil-ion momentum distributions were observed to be in good agreement with the low-energy part (representing the momentum distribution of the slowly emitted electron) of the results derived from (e, 2e) data for 500 and 2000 eV it was concluded by Jagutzki and co-workers that the above assumption was correct. Moreover, for fast collisions, where the final state interaction between the two emerging electrons is typically small it can be expected that the measured recoil-ion momentum distribution should directly reflect the emitted electron bound-state Compton profile if \mathbf{P}_R is projected

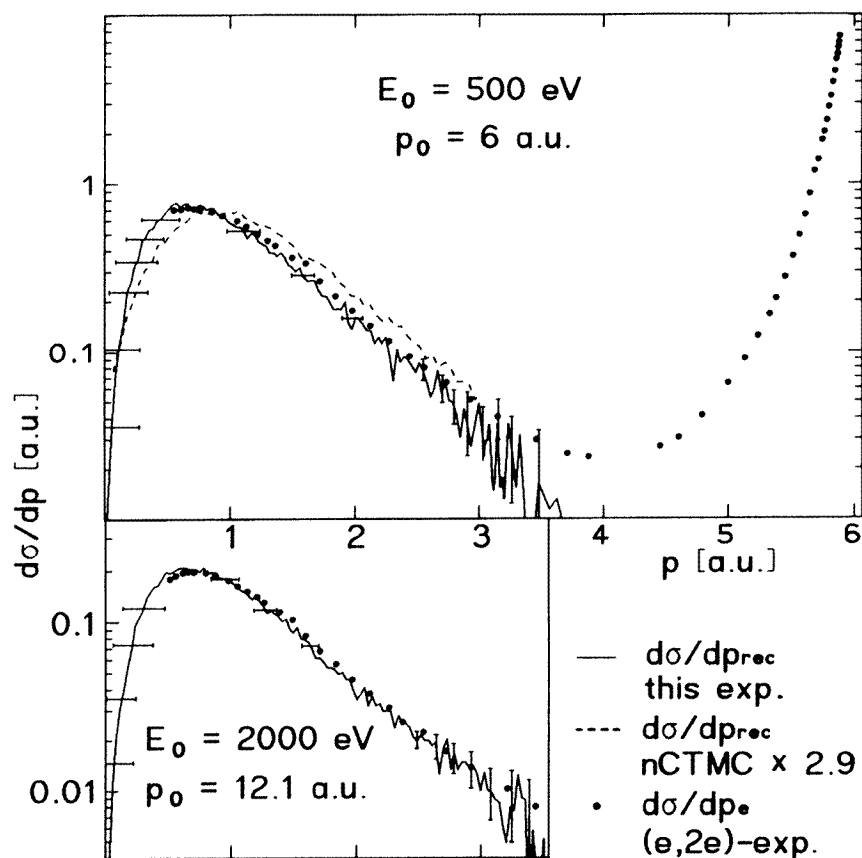


Figure 26. Single-differential ionization cross section $d\sigma/dp_{\text{He}}$ for the recoil ion (full curve, Jagutzki *et al* (1996); broken curve, nCTMC calculations) for 500 eV (2000 eV) electrons on He. The dots show electron-emission cross sections $d\sigma/dp_e$ calculated from (e, 2e) data of Opal *et al* (1972) and Oda (1975).

onto one axis. Jagutzki *et al* were able to show that the projected $d\sigma/dP_{R_x}$ were indeed in good agreement with the He Compton profile with some deviation at small momenta.

In figure 27 experimental (lower part) as well as theoretical (upper part) two-dimensional momentum distributions in the $P_{R\perp}-P_{R\parallel}$ plane are shown for the He($e, 3e$)He $^{2+}$ reaction at an incoming electron energy of 500 eV. The curves in the figures indicate the kinematic circles for a pure inelastic collision between the electron and the He nucleus. A much broader distribution in both directions was observed for He $^{2+}$ recoil ions in agreement with the *n*CTMC results. This was attributed in the first instance to the broader two-electron Compton profile. The maximum of this distribution is essentially following the kinematic circle which has been interpreted to be a clear signature of the incoming electron–nucleus scattering (Ullrich *et al* 1994a). Since the kinematics of the three-electron continuum is much more complex no detailed further conclusions could be extracted from the present doubly differential data.

The authors emphasized, that these first recoil-ion experiments for electron impact can only be considered as a first step in the direction of complete ($e, 3e$) investigations which are in preparation. It was realized that such measurements will become feasible if two electrons are observed in coincidence with the recoiling target ion which can be achieved using reaction microscopes of the type described in section 2.4.

5. Summary

Recoil-ion momentum spectroscopy, the determination of the charge state and of the momentum of a recoiling target ion emerging from an ionizing collision of an atom with any kind of radiation, is a technique that has been developed over more than a decade from the first successful experiments to present high-resolution ‘reaction microscopes’. A decisive breakthrough was marked by the implementation of (pre-cooled) supersonic jet

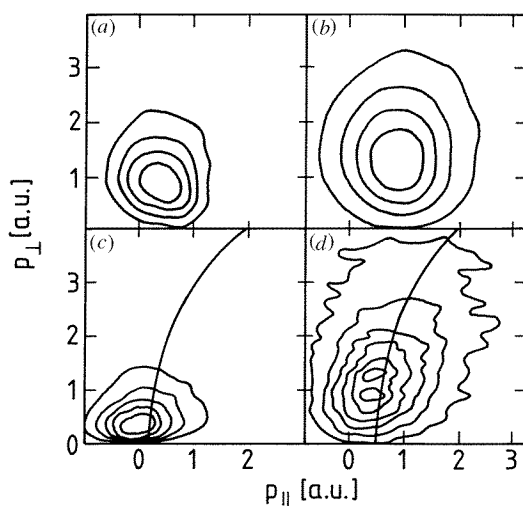


Figure 27. Double-differential cross sections $d^2\sigma/dp_{\parallel}dp_{\perp}$ for recoil ions emerging from 500 eV e^{-} on He collisions (Jagutzki *et al* 1996). The spacing of the contour lines is linear. (a) *n*CTMC single ionization. (b) *n*CTMC double ionization. (c) and (d) experimental data for single and double ionization, respectively. The full curves represent the pure two-body collision kinematics.

targets yielding superior recoil-ion momentum resolution at a 4π detection solid angle for target ions emerging from a large variety of collision-induced atomic reactions. Recently, a further substantial improvement was achieved by the invention of rigorously new projection techniques for the detection of electrons and the implementation of such analysers into high-resolution RIM spectrometers. The newest instruments of this kind, termed 'reaction microscopes' enable us to determine the momentum vectors of up to four reaction products (the recoil ion and three emitted electrons) with solid angles exceeding those of conventional methods by many orders of magnitude.

In essence, these two technical innovations have initiated a new generation of atomic collision experiments which are unprecedented in resolution, completeness and broadness, covering the entire range of different projectiles (ions, photons, electrons and antiparticles) and collision velocities available at advanced accelerator and synchrotron radiation facilities. Outstanding examples are: (i) The first kinematically complete experiments for single and double ionization of atoms by ion impact at GeV energies. (ii) The mapping of the two-dimensional final electron momentum space in low-energy (5–15 keV) proton–helium collisions for a defined internuclear impact parameter and collision plane. (iii) The imaging of the complete nine-dimensional momentum space after double photoionization of helium at energies close to threshold. (iv) The first experimental separation of the contributions of Compton scattering and photoabsorption to helium double ionization at keV photon energies.

As the most advanced reaction microscopes have only been in operation for about two years, the experimental results reviewed in this paper can certainly be considered as just being the fascinating starting point of a large series of kinematically complete experiments to be performed in the near future. One might envisage a variety of exciting results on the dynamics of many-electron transitions and of the electron–electron correlation in atomic collisions, and also its impact on neighbouring fields like atomic structure investigations for heavy few-electron systems, multi-photon ionization in strong laser fields or the collision-induced disintegration of molecules. It has been pointed out (Ullrich *et al* 1994a, Moshhammer *et al* 1996c) that the technique might even be profitable for the investigation of the electroweak interaction: kinematically complete, β -decay experiments should enable high-precision electron–neutrino angular correlation measurements and, in the far future, a precise neutrino mass determination.

Acknowledgments

The experimental methods and physical interpretations described in this paper have evolved over more than 10 years from continuous discussions with many colleagues who are too numerous to acknowledge individually. We are deeply indebted to our friend Ron Olson who steadily accompanied us with his calculations and insight into dynamical processes in ion–atom collisions. The guidance from his theoretical results was decisive in efficiently developing the experimental methods. Our deepest thanks go to Lew Cocke, who has been one of the 'promoters' of this technique over many years. His constructive criticism, rigorous analysis of experimental results and ingenious ideas for solving technical problems have always pushed us tremendously. Many generations of students brought in their ideas and worked hard to design, develop and build up the spectrometers. The continuous collaboration with Rainer Dreizler, Bob DuBois, Udo Buck, Jean Pierre Grandin, Siegbert Hagmann, Marko Horbatsch, Paul Mokler, John Reading, Pat Richard, Antoine Salin, Dieter Schneider, Reinhold Schuch and Michael Schulz, is gratefully acknowledged. We are grateful for numerous discussions with Miron Amusia, Jörg Ast, Anders Barany, John Briggs, Amine Cassimi, Henrik Cederquist, Pablo Fainstein, Don Gemmell, Pascal Jardin,

Stefan Keller, Berthold Krässig, Scott Kravis, Azzedine Lahmam-Bennani, Chidong Lin, Hans-Jürgen Lüdde, Rido Mann, Reinhard Morgenstern, Tadashi Kambara, Helge Knudsen, Don Madison, Walter Meyerhof, Mike Prior, Carlos Reinhold, Jan-Michael Rost, Gregor Schiwietz, Volker Schmidt, Bernd Sonntag, Thomas Stöhlker, Nico Stolterfoht and Theo Zouros.

References

- Abdallah M, Cocke C L, Kravis S, Montenegro E C, Moshammer R, Salesh L, Ullrich J, Varghese S L, Wolff W and Wolff H 1997 *Proc. 14th Int. Conf. on the Application of Accelerators in Research and Industry (AIP Conference Proceedings)* (New York AIP) at press
- Åberg T 1970 *Phys. Rev. A* **2** 1726
- Abrines R and Percival I C 1996 *Proc. Phys. Soc.* **88** 861
- Ali R, Frohne V, Cocke C L, Stöckli M, Cheng S and Raphaelian L A 1992 *Phys. Rev. Lett.* **69** 2491
- Amusia M Ya and Mikhailov A I 1995a *J. Phys. B: At. Mol. Opt. Phys.* **28** 1723
- 1995b *Phys. Lett.* **199A** 201
- Andersson L R and Burgdörfer J 1993 *Phys. Rev. Lett.* **71** 50
- 1994 *Phys. Rev. A* **50** R2810
- Anholt R 1986 *Phys. Lett.* **114A** 126
- Bandarage G and Parson R 1990 *Phys. Rev. A* **41** 5878
- Bates D R and Griffing G 1953 *Proc. Phys. Soc. A* **66** 961
- 1954 *Proc. Phys. Soc. A* **67** 663
- 1955 *Proc. Phys. Soc. A* **68** 90
- Barany A and Ovchinnikov S 1993 *Phys. Scr. T* **46** 243
- Barat M and Roncin P 1992 *J. Phys. B: At. Mol. Opt. Phys.* **25** 2205
- Belkic Dz and Gayet R 1977 *J. Phys. B: At. Mol. Phys.* **10** 1923
- Bergström P M, Hino K and Macek J H 1995 *Phys. Rev. A* **51** 3044
- Berrah N, Heiser F, Wehlitz R, Levin J, Whitfield S B, Viehhaus J, Sellin I A and Becker U 1993 *Phys. Rev. A* **48** R1733
- Bosch F 1993 *The Physics of Electronic and Atomic Collisions (AIP Conf. Proc. 295)* p 3
- Breinig M *et al* 1982 *Phys. Rev. A* **25** 3015
- Buchenau H, Knuth E L, Northby J, Toennies J P and Winkler C 1990 *J. Chem. Phys.* **92** 6875
- Byron F W and Joachain C J 1967 *Phys. Rev.* **164** 1
- Cassimi A, Duponchel S, Flechard X, Jardin P, Sortais P, Hennecart D and Olson R E 1996 *Phys. Rev. Lett.* **76** 3679
- Carlson T A 1967 *Phys. Rev.* **156** 142
- Cederquist H, Liljeby L, Biedermann C, Levin J C, Rothard H, Groeneveld K O, Vane C R and Sellin A 1989 *Phys. Rev. A* **39** 4308
- Cederquist H *et al* 1995 *Phys. Rev. A* **51** 2169
- Chassid M and Horbatsch M 1995 *J. Phys. B: At. Mol. Opt. Phys.* **28** L621
- 1997 *J. Phys. B: At. Mol. Opt. Phys.* submitted
- Cocke C L 1994 Private communication
- Cocke C L and Olson R E 1991 *Phys. Rep.* **205** 155
- Colavecchia F D, Cravero W and Garibotti C R 1995 *Phys. Rev. A* **52** 3737
- Dalgarno A and Sadeghpour 1992 *Phys. Rev. A* **46** R3591
- Dawber G, Avaldi L, McConkey A G, Rojas H, MacDonald M A and King G C 1995 *J. Phys. B: At. Mol. Opt. Phys.* **28** L271
- Deco G R, Maidagan J M and Rivarola R D 1984 *J. Phys. B: At. Mol. Phys.* **17** L707
- Dörner R, Khemliche H, Prior M H, Cocke C L, Gary J A, Olson R E, Mergel V, Ullrich J and Schmidt-Böcking H 1996a *Phys. Rev. Lett.* **77** 4520
- Dörner R 1996b Private communication
- Dörner R, Mergel V, Zaoyuan L, Ullrich J, Spielberger L, Olson R E and Schmidt-Böcking H 1995a *J. Phys. B: At. Mol. Opt. Phys.* **28** 435
- Dörner R, Ullrich J, Olson R E, Jagutzki O and Schmidt-Böcking H 1993 *Phys. Rev. A* **47** 3845
- Dörner R, Ullrich J and Schmidt-Böcking H 1991 *GSI-REPORT GSI-91-28* (in German)
- Dörner R, Ullrich J, Schmidt-Böcking H and Olson R E 1989 *Phys. Rev. Lett.* **63** 147
- Dörner R *et al* 1994 *Phys. Rev. Lett.* **72** 3166

- Dörner R *et al* 1995b *The Physics of Electronic and Atomic Collisions (AIP Conf. Proc.* **360**) p 495
- Dörner R *et al* 1996c *Phys. Rev. Lett.* **76** 2654
- Dörner R *et al* 1996d *Phys. Rev. Lett.* **77** 1024
- Dörner R *et al* 1997 *Nucl. Instrum. Method. B* **124** 225
- DuBois R D 1987 *Phys. Rev. A* **36** 2585
- Eichenauer D, Grün N and Scheid W 1981 *J. Phys. B: At. Mol. Phys.* **14** 3929
- Eisenberg P 1970 *Phys. Rev. A* **2** 1678
- Ehrhardt H, Jung K, Knoth G and Schlemmer P 1986 *Z. Phys. D* **1** 3
- Ermolaev A M 1990 *Phys. Lett.* **149A** 151
- Everhart E and Kessel Q C 1965 *Phys. Rev. Lett.* **14** 247
- Fang X and Reading J F 1991 *Nucl. Instrum. Method. B* **53** 453
- Fainstein P D, Ponce V H and Rivarola R D 1991 *J. Phys. B: At. Mol. Opt. Phys.* **24** 3091
- Federenko N V and Afrosimov V V 1956 *Sov. Phys.—Tech. Phys.* **1** 1872
- Fastrup B 1980 *Methods of Experimental Physics: Atomic Physics* ed P Richard (New York: Academic) ch 4
- Folkerts H O, Hoekstra R, Meng L, Olson R E, Fritsch W, Morgenstern R and Summers H P 1993 *J. Phys. B: At. Mol. Opt. Phys.* **26** L619–24
- Feagin J M 1995 *J. Phys. B: At. Mol. Opt. Phys.* **28** 1495
- 1996 *J. Phys. B: At. Mol. Opt. Phys.* **29** L551–9
- Forberich E, Dörner R, Ullrich J, Olson R E, Ullmann K, Gensmantel A, Lencinas S, Jagutzki O and Schmidt-Böcking H 1991 *J. Phys. B: At. Mol. Opt. Phys.* **24** 3613
- Frohne V, Cheng S, Ali R, Raphaëlian M, Cocke C L and Olson R E 1993 *Phys. Rev. Lett.* **71** 696
- 1996 *Phys. Rev. A* **53** 2407
- Fukuda H, Shimamura I, Vegh L and Watanabe T 1991 *Phys. Rev. A* **44** 1565
- Gensmantel A, Ullrich J, Dörner R, Olson R E, Ullmann K, Forberich E, Lencinas S and Schmidt-Böcking H 1992 *Phys. Rev. A* **45** 4572
- Giese J P and Horsdal E 1988 *Phys. Rev. A* **60** 2018
- Graham W G, Fritsch W, Hahn Y and Tanis J A (eds) 1992 *Recombination of Atomic Ions (NATO ASI Series B* **296**) (New York: Plenum)
- Gramlich K, Grün N and Scheid W 1989 *J. Phys. B: At. Mol. Opt. Phys.* **22** 2567
- Grandin J P, Hennecart D, Husson X, Lecler D, Lesteven-Vaisse I and Lisfi D 1988 *Europhys. Lett.* **6** 683
- Gryzinski M 1959 *Phys. Rev.* **115** 374
- Hino K I, Bergström P M and Macek J H 1994 *Phys. Rev. Lett.* **72** 1620
- Hoekstra R, Sauraud M G, de Heer F J and Morgenstern R 1989 *J. Phys. C: Solid State Phys.* **50** 387
- Horbatsch M 1989a *J. Phys. B: At. Mol. Opt. Phys.* **22** L639
- 1989b *Phys. Lett.* **137A** 466
- 1992 *J. Phys. B: At. Mol. Opt. Phys.* **25** 3797
- Horsdal E, Jensen B and Nielsen K O 1986 *Phys. Rev. Lett.* **57** 1414
- Hülskötter H-P, Meyerhof W E, Dillard E and Guardala N 1989 *Phys. Rev. Lett.* **63** 1938
- Hülskötter H-P *et al* 1991 *Phys. Rev. A* **44** 1712
- Htwe W T, Vajnai T, Barnhart M, Gaus A D and Schulz M 1994 *Phys. Rev. Lett.* **73** 1348
- Huetz A, Lablanquie P, Andric L, Selles P and Mazeau J 1994 *J. Phys. B: At. Mol. Opt. Phys.* **27** L13
- Hvelplund P, González A D, Dahl P and Bhalla C P 1994 *Phys. Rev. A* **49** 2535
- Ieki K *et al* 1996 Michigan State University MSUCL-1036
- Ishihara T, Hino K and McGuire J H 1991 *Phys. Rev. A* **44** R6980
- Janev R K, Ivanovski G and Solovev E A 1994 *Phys. Rev. A* **49** R645
- Jagutzki O 1995 *PhD Thesis* Johann-Wolfgang-Goethe Universität Frankfurt, published in Edition Wissenschaft, Reihe Physik, Bd. 1 Tectum Verlag, Marburg
- Jagutzki O, Spielberger L, Dörner R, Nüttgens S, Mergel V, Schmidt-Böcking H, Ullrich J, Olson R E and Buck U 1996 *Z. Phys. D* **36** 5–10
- Jardin P, Cassimi A, Grandin J P, Rothard H, Lemoigne J P, Hennecart D, Husson X and Lepontre A 1996 *Nucl. Instrum. Method. B* **107** 41
- Jardin P, Grandin J P, Cassimi A, Lemoigne J P, Gosselin A, Husson X, Hennecart D and Lepontre A 1993 *5th Conf. on Atomic Physics of Highly Charged Ions (AIP Conf. Proc.* **274**) p 291
- Kambara T *et al* 1995 *J. Phys. B: At. Mol. Opt. Phys.* **28** 4593–606
- Kambara T, Igarashi A, Watanabe N, Nakai Y, Kojima T M and Awaya Y 1997 *J. Phys. B: At. Mol. Opt. Phys.* **30** 1251–60
- Kamber E Y, Cocke C L, Cheng S and Varghese J 1988 *Phys. Rev. Lett.* **60** 2026
- Kazanski A K and Ostrobsky V N 1995 *Phys. Rev. A* **51** 3698

- Kelbch S, Cocke C L, Hagmann S, Horbatsch M, Kelbch D, Koch R and Schmidt-Böcking H 1988 *Phys. Lett.* **127A** 92
- Kelbch S, Cocke C L, Hagmann S, Horbatsch M, Kelbch D, Koch R, Schmidt-Böcking H and Ullrich J 1989 *J. Phys. B: At. Mol. Opt. Phys.* **22** 1277
- Keller S, Lüdde H J and Dreizler R M 1997 *Phys. Rev. A* **55** 4215
- Kessel Q C and Everhart E 1966 *Phys. Rev.* **146** 16
- Khemliche H, Prior M H and Schneider D 1995 *Phys. Rev. Lett.* **74** 5013
- Kimura M 1988 *J. Phys. B: At. Mol. Opt. Phys.* **21** L19
- Kimura M and Lane N F 1989 *Advances in Atomic, Molecular and Optical Physics* vol 26 (San Diego, CA: Academic) p 79
- Kinoshita T 1990 *Quantum Electrodynamics, Advanced Series on Directions in High Energy Physics* vol 7 (Singapore: World Scientific)
- Knudsen H, Mikkelsen U, Paludan K, Kirsebom K, Moller S P, Uggerhoj E, Slevin J, Charlton M and Morenzoni E 1995 *Phys. Rev. Lett.* **74** 4627
- Kollmus H, Schmitt W, Moshhammer R, Unverzagt M and Ullrich J 1997 *Nucl. Instrum. Method. B* **124** 377
- Kravis S *et al* 1996 *Phys. Rev. A* **54** 1394
- Kristensen F G and Horsdal-Pedersen E 1990 *J. Phys. B: At. Mol. Opt. Phys.* **23** 4129
- Lablanquie P, Mazeau J, Andric L, Selles P and Huetz A 1995 *Phys. Rev. Lett.* **74** 2192
- Lahmam-Bennani A 1991 *J. Phys. B: At. Mol. Opt. Phys.* **24** 2401
- Lahmam-Bennani A, Duguet A, Grisogono A M and Lecas M 1992 *J. Phys. B: At. Mol. Opt. Phys.* **25** 2873
- Lahmam-Bennani A, Dupré C and Duguet A 1989 *Phys. Rev. Lett.* **63** 1582
- Lee D H, Zouros T J M, Sanders J M, Richard P, Anthony J M, Wang Y D and McGuire J H 1992 *Phys. Rev. A* **46** 1374
- Lebius H and Huber B A 1992 *Z. Phys. D* **23** 61
- Lencinas S *et al* 1993 *J. Phys. B: At. Mol. Opt. Phys.* **26** 287
- Levin J C, Armen G B and Sellin I A 1996 *Phys. Rev. Lett.* **76** 1220
- Levin J C, Lindle D W, Keller N, Miller R D, Azuma Y, Berrah-Mansour N, Berry H G and Sellin I A 1991 *Phys. Rev. Lett.* **67** 968
- Levin J C, Sellin I A, Johnson B M, Lindle D W, Miller R D, Berrah N, Azuma Y, Berry G H and Lee D-H 1993 *Phys. Rev. A* **47** R16
- Levin J C, Short R T, O C S, Elston S B, Gibbons J P, Sellin I A and Schmidt-Böcking H 1987 *Phys. Rev. A* **36** 1649
- Macek J H and Ovchinnikov S Yu 1994 *Phys. Rev. A* **50** 468
- Mann R, Cocke C L, Schlachter A S, Prior M and Marrus M 1982 *Phys. Rev. Lett.* **49** 1329
- Martin C, Jelinsky P, Lampton M, Malina R F and Anger H O 1981 *Rev. Sci. Instrum.* **52** 1067
- Maulbetsch R and Briggs J S 1993a *J. Phys. B: At. Mol. Opt. Phys.* **26** 1679
- 1993b *J. Phys. B: At. Mol. Opt. Phys.* **26** L647
- 1995 *J. Phys. B: At. Mol. Opt. Phys.* **28** 551
- McConkey J W, Crowe A and Hender M A 1972 *Phys. Rev. Lett.* **29** 1
- McGuire J H 1991 *Adv. At. Phys.* **29** 217
- McGuire J H, Berrah N, Bartlett R J, Samson J A R, Tanis J A, Cocke C L and Schlachter A S 1995 *J. Phys. B: At. Mol. Opt. Phys.* **28** 913
- McGuire J H, Stolterfoht N and Simony P R 1981 *Phys. Rev. A* **24** 97
- Meng L, Olson R E, Dörner R, Ullrich J and Schmidt-Böcking H 1993 *J. Phys. B: At. Mol. Opt. Phys.* **26** 3387
- Mergel V 1994 *Diploma Thesis* Johann-Wolfgang-Goethe Universität Frankfurt
- 1997 *PhD thesis* Johann-Wolfgang-Goethe Universität Frankfurt (Berichte aus der Physik) (Aachen: Shaker) ISBN 3-8265-2067-X
- Mergel V *et al* 1995a *Phys. Rev. Lett.* **74** 2200
- Mergel V *et al* 1995b *Nucl. Instrum. Method. B* **96** 593
- Mergel V *et al* 1995c *Annual Report* vol 56 Institut für Kernphysik, Universität Frankfurt p 12
- Mergel V *et al* 1995d *19th Int. Conf. the Physics of Electronic and Atomic Collisions* ed J B A Mitchell, J W McConkey and C E Brion *Abstracts of Contributed Papers* p 755
- Mohr P J and Soff G 1993 *Phys. Rev. Lett.* **70** 158
- Montemayor V J and Schiwietz G 1989 *J. Phys. B: At. Mol. Opt. Phys.* **22** 2555
- Montenegro E C, Belkacem A, Spooner D W, Meyerhof W E and Shah M B 1993 *Phys. Rev. A* **47** 1045
- Montenegro E C and Meyerhof W E 1991 *Phys. Rev. A* **44** 7229
- 1992 *Phys. Rev. A* **46** 5506
- Montenegro E C, Sigaud G M and Meyerhof W E 1992 *Phys. Rev. A* **45** 1575

- Moshhammer R, Ullrich J, Kollmus H, Schmitt W, Unverzagt M and Schmidt-Böcking H 1997a *Proc. 17th Int. Conf. on X-ray and Inner-Shell Processes* ed R L Johnson, H Schmidt-Böcking and B F Sonntag (*AIP Conference Proceedings* vol 389, p 153)
- Moshhammer R, Ullrich J, Kollmus H, Schmitt W, Unverzagt M, Schmidt-Böcking H, Wood C J and Olson R E 1997b *Phys. Rev. A* **56** at press
- Moshhammer R, Ullrich J, Unverzagt M, Schmitt W, Jardin P, Olson R E, Dörner R, Mergel V and Schmidt-Böcking H 1996a *Nucl. Instrum. Method. B* **107** 62–6
- Moshhammer R, Unverzagt M, Schmitt W, Ullrich J and Schmidt-Böcking H 1996b *Nucl. Instrum. Method. B* **108** 425–45
- Moshhammer R *et al* 1994 *Phys. Rev. Lett.* **73** 3371
- Moshhammer R *et al* 1996c *Phys. Rev. Lett.* **77** 1242
- Nüttgens S 1994 *Diploma Thesis* Johann-Wolfgang-Goethe Universität Frankfurt
- Oda N 1975 *Radiat. Res.* **64** 80
- Ohtani S, Kaneko Y, Kimura M, Kobayashi N, Iwai T, Matsumoto A, Okuno K, Tagaki S, Tawara H and Tsurubuchi S 1982 *J. Phys. B: At. Mol. Phys.* **15** L533
- Olson R E 1983 *Phys. Rev. A* **27** 1871
- 1986 *Phys. Rev. A* **33** 4398
- Olson R E, Feeler C R, Wood C J, Cocke C L, Dörner R, Mergel V, Schmidt-Böcking H, Moshhammer R and Ullrich J 1997 *Nucl. Instrum. Method. B* **124** 249
- Olson R E and Salop A 1977 *Phys. Rev. A* **16** 531
- Olson R E, Ullrich J, Dörner R and Schmidt-Böcking H 1989a *Phys. Rev. A* **40** 2843
- Olson R E, Ullrich J and Schmidt-Böcking H 1987 *J. Phys. B: At. Mol. Phys.* **20** L809
- 1989b *Phys. Rev. A* **39** 5572
- Opal C D, Beatty E C and Peterson W K 1972 *At. Data* **4** 209
- Ovchinnikov S Yu and Macek J H 1995 *Phys. Rev. Lett.* **75** 2474
- O'Rourke S F C and Crothers D S F 1997a *Physica Scripta* in press
- 1997b *J. Phys. B: At. Mol. Opt. Phys.* **30** 2443
- Pálinkás J, Schuch R, Cederquist H and Gustafsson O 1989 *Phys. Rev. Lett.* **63** 2464–7
- Park J T 1978 *Collision Spectroscopy* ed R G Cook (New York: Plenum) p 19
- Pedersen J O P, Hvelplund P, Petersen A G and Fainstein P D 1990 *J. Phys. B: At. Mol. Opt. Phys.* **23** L597–603
- Pieksma M, Ovchinnikov S Y, van Eck J, Westerveld W B and Niehaus A 1994 *Phys. Rev. Lett.* **73** 46
- Pivovarov L I, Tubavaev A and Novikov M T 1962 *Sov. Phys.—JETP* **15** 1035
- Platten H, Schiwietz G, Schneider T, Schneider D, Zeitz W, Musiol K, Zouros T, Kowallik R and Stolterfoht N 1987 *Proc. 15th Int. Conf. on the Physics of Electronic and Atomic Collisions (Brighton)* ed J Geddes *et al* (Amsterdam: North-Holland) p 437
- Pont M and Shakeshaft R 1995 *Phys. Rev. A* **51** 494
- Puckett L J and Martin D W 1976 *Phys. Rev. A* **5** 1432
- Raphaelian M L A, Stöckli M P, Wu W and Cocke C L 1995 *Phys. Rev. A* **51** 1304
- Regier P E and Thakkar A J 1984 *Phys. Rev. A* **30** 30
- Rodríguez V D 1996 *J. Phys. B: At. Mol. Opt. Phys.* **29** 275–86
- Rodríguez V D, Wang Y D and Lin C D 1995a *Phys. Rev. A* **52** R9
- 1995b *J. Phys. B: At. Mol. Opt. Phys.* **28** L471–6
- Roncín P, Adjouri C, Andersen N, Barat M, DuBois A, Gaboriaud M N, Hansen J P, Nielsen S E and Szilagy S Z 1994 *J. Phys. B: At. Mol. Opt. Phys.* **27** L93
- Roncín P, Gaboriaud M N and Barat M 1991 *Europhys. Lett.* **16** 551
- Rost J-M 1994a *Phys. Rev. Lett.* **72** 1998
- 1994b *J. Phys. B: At. Mol. Opt. Phys.* **27** 5923
- 1995 *J. Phys. B: At. Mol. Opt. Phys.* **28** 3003
- Rudd M E, Kim Y K, Madison D H and Gay T J 1992 *Rev. Mod. Phys.* **64** 441
- Rudd M E and Macek J H 1972 *Case Studies At. Phys.* **3** 47
- Rudd M E, Toburen L H and Stolterfoht N 1976 *At. Data Nucl. Data Tables* **18** 413
- Ryufuku H, Sasaki K and Watanabe T 1980 *Phys. Rev. A* **21** 745
- Sagurton M, Morgan D and Bartlett R J 1996 Private communication from Spielberger *et al* (1996)
- Salin A 1989 *J. Phys. B: At. Mol. Opt. Phys.* **22** 3901
- 1991 *J. Phys. B: At. Mol. Opt. Phys.* **24** 3211
- Samson J A R, He Z X, Bartlett R J and Sagurton M 1994 *Phys. Rev. Lett.* **72** 3329
- Scheidenberger C *et al* 1994 *Phys. Rev. Lett.* **73** 50
- Schiwietz G 1988 *Phys. Rev. Lett.* **37** 370

- Schiwietz G, Grande P L, Auth C, Winter H and Salin A 1994a *Phys. Rev. Lett.* **72** 2159
- Schiwietz G, Skogvall B, Tanis J and Schneider D 1988 *Phys. Rev. A* **38** 5552
- Schiwietz G, Stettner U, Zouros T J M and Stolterfoht N 1987 *Phys. Rev. Lett.* **35** 598
- Schiwietz G, Xiao G, Grande P L, Skogvall B, Köhrbrück R, Sulik B, Sommer K, Schmoldt A, Stettner U and Salin A 1994b *Europhys. Lett.* **27** 341–6
- Schmeisser C, Cocke C L, Mann R and Meyerhof W 1984 *Phys. Rev. A* **30** 1661
- Schmidt H T *et al* 1997 *Hyperfine Interactions* **108** 339
- Schmidt V 1992 *Rep. Prog. Phys.* **55** 1483
- Schmidt-Böcking H *et al* 1990 *Lecture Notes in Physics* vol 376 (Berlin: Springer) p 268
- Schuch R, Schöne H, Miller P D, Krause H F, Dittner P F, Datz S and Olson R E 1988 *Phys. Rev. Lett.* **60** 925
- Schultz D R, Krstic, Reinhold C O and Wells J C 1996 *Phys. Rev. Lett.* **76** 2882
- Schwarzkopf O, Krässig B, Elminger J and Schmidt V 1993 *Phys. Rev. Lett.* **70** 3008
- Schwarzkopf O, Krässig B, Schmidt V, Maulbetsch F and Briggs J S 1994 *J. Phys. B: At. Mol. Opt. Phys.* **27** L347
- Schwarzkopf O and Schmidt V 1995 *J. Phys. B: At. Mol. Opt. Phys.* **28** 2847–62
- Shah M B and Gilbody H B 1985 *J. Phys. B: At. Mol. Phys.* **18** 899
- Shingal R and Lin C D 1991 *J. Phys. B: At. Mol. Opt. Phys.* **24** 251
- Skogvall B and Schiwietz G 1990 *Phys. Rev. Lett.* **65** 3265
- 1992 *Phys. Rev. A* **46** 5687
- Spielberger L *et al* 1995 *Phys. Rev. Lett.* **74** 4615
- 1996 *Phys. Rev. Lett.* **76** 4685
- Sobotka S E and Williams M B 1988 *IEEE Trans. Nucl. Sci.* **NS-35** 348
- Solovev E A 1990 *Phys. Rev. A* **42** 1331
- Stöhlker Th *et al* 1993 *Phys. Rev. Lett.* **71** 2184
- 1997 *Hyperfine Interactions* **108** 29
- Stolterfoht N 1978 *Structure and Collisions of Ions and Atoms (Topics in Current Physics 5)* ed I A Sellin (Berlin: Springer) p 155
- 1987 *Phys. Rep.* **146** 315
- Stolterfoht N, DuBois R D and Rivarola R D 1997 *Rev. Mod. Phys.* in preparation
- Stolterfoht N, Platten H, Schiwietz G, Schneider D, Gulyàs L, Fainstein P D and Salin A 1995 *Phys. Rev. A* **52** 3796
- Stolterfoht N, Sommer K, Swenson J K, Havener C C and Meyer F W 1990 *Phys. Rev. A* **42** 5396
- Suárez S, Garibotti C, Bernardi G, Focke P and Meckbach W 1993 *Phys. Rev. A* **48** 4339
- Suric T, Pisk K, Logan B A and Pratt R H 1994 *Phys. Rev. Lett.* **73** 790
- Tang J Z and Shimamura I 1995 *Phys. Rev. A* **52** 1
- Teng Z J and Shakeshaft R 1994 *Phys. Rev. A* **49** 3591
- Toshima N 1993 *Phys. Lett.* **175A** 133
- Thomas L H 1927 *Proc. R. Soc. A* **114** 561–76
- Tökési K and Hock G 1996 *J. Phys. B: At. Mol. Opt. Phys.* **29** L119–25
- Ullrich J 1987 *PhD Thesis* Johann-Wolfgang-Goethe Universität Frankfurt
- Ullrich J 1994 *GSI-REPORT* GSI-94-08 (in German)
- Ullrich J, Dörner R, Jagutzki O, Lencinas S, Gensmantel A, Forberich E, Ullmann K, Olson R E and Schmidt-Böcking H 1993a *Radiation Effects Defects Solids* **126** 77
- Ullrich J, Dörner R, Jagutzki O, Mergel V, Moshhammer R, Schmidt-Böcking H, Schmitt W, Spielberger L, Unverzagt M and Vogt T 1996 *Ann. Meeting of the Optical Society of America and the Society for Imaging Science and Technology Conf. Proc.* accepted
- Ullrich J, Dörner R, Lencinas S, Jagutzki O and Schmidt-Böcking H 1991 *Nucl. Instrum. Method. B* **61** 415
- Ullrich J, Dörner R, Mergel V, Jagutzki O, Spielberger L and Schmidt-Böcking H 1994a *Comments At. Mol. Phys.* **30** 285
- Ullrich J, Horbatsch M, Dangendorf V, Kelbch S and Schmidt-Böcking H 1988a *J. Phys. B: At. Mol. Opt. Phys.* **21** 611
- Ullrich J, Moshhammer R, Unverzagt M, Schmitt W, Jardin P, Olson R E, Dörner R, Mergel V and Schmidt-Böcking H 1995 *Nucl. Instrum. Method. B* **98** 375–9
- Ullrich J, Olson R E, Dörner R, Kelbch S, Berg H and Schmidt-Böcking H 1989 *J. Phys. B: At. Mol. Opt. Phys.* **22** 627
- Ullrich J and Schmidt-Böcking H 1987 *Phys. Lett.* **125A** 193
- Ullrich J, Schmidt-Böcking H and Kelbch C 1988b *Nucl. Instrum. Method. A* **268** 216
- Ullrich J *et al* 1993b *Phys. Rev. Lett.* **71** 1697
- Ullrich J *et al* 1994b *Nucl. Instrum. Method. B* **87** 70–5

- Unverzagt M, Moshhammer R, Schmitt W, Olson R E, Jardin P, Mergel V, Ullrich J and Schmidt-Böcking H 1996 *Phys. Rev. Lett.* **76** 1043
- Vogt T 1996 *Diploma Thesis* Johann-Wolfgang-Goethe Universität Frankfurt
- Wang Y D, Rodríguez V D, Lin C D, Cocke C L, Kravis S, Abdallah M and Dörner R 1996a *Phys. Rev. A* **53** 3278
- Wang Y D, Tribedi L C, Richard P, Cocke C L, Rodríguez V D and Lin C D 1996b *J. Phys. B: At. Mol. Opt. Phys.* **29** L203–8
- Wehlitz R, Heiser F, Hemmers O, Langer B, Menzel A and Becker U 1991 *Phys. Rev. Lett.* **67** 3764
- Wehlitz R *et al* 1996 Private communication from Spielberger *et al* (1996)
- Weigold E and McCarthy I E 1978 *Adv. At. Mol. Phys.* **14** 127
- Weitz M, Huber A, Schmidt-Kaler F, Leibfried D and Hänsch T W 1994 *Phys. Rev. Lett.* **72** 328
- Werth G 1987 *Phys. Scr.* T **22** 191
- Winter T G and Lin C D 1984 *Phys. Rev. A* **29** 3071
- Wood C J and Olson R E 1996 *J. Phys. B: At. Mol. Opt. Phys.* **29** L257–62
- Wu W, Giese J P, Ben-Itzhak I, Cocke C L, Richard P, Stöckli M, Ali R and Schöne H 1993 *Phys. Rev. A* **48** 3617
- Wu W, Giese J P, Chen Z, Ali R, Cocke C L, Richard P and Stöckli M 1994a *Phys. Rev. A* **50** 502
- Wu W, Wong K L, Cocke C L, Giese J P and Montenegro E C 1995 *Phys. Rev. A* **51** 3718
- Wu W *et al* 1994b *Phys. Rev. Lett.* **72** 3170
- Zouros T J M 1996 *Comments At. Mol. Phys.* **32** 291–313
- Zouros T J M, Lee D H and Richard P 1989 *Phys. Rev. Lett.* **62** 2261
- Zouros T J M, Schneider D and Stolterfoht N 1987 *Phys. Rev. A* **35** 1963